Long-Baseline Neutrino Experiment (LBNE) Project

Conceptual Design Report

Volume 1: The LBNE Project

October 2012

Contents

Acronyms, Abbreviations and Units

3D	3 dimensional
ALICE	A Large Ion Collider Experiment (at CERN)
BR	branching ratio
C.L.	confidence level
CC	charged current (interaction)
CCQE	charged current quasi-elastic (interaction)
CDR	Conceptual Design Report
CF	Conventional Facilities
CP	product of charge and parity transformations
CPT	product of charge, parity and time-reversal transformations
DAQ	data acquisition
DocDB	document database application used by LBNE and other Fermilab experiments
DOE	Department of Energy
DUSEL	Deep Underground Science and Engineering Laboratory
ESH	Environment, Safety and Health
eV	electron-Volt, unit of energy (also keV, MeV, GeV, etc.)
FGT	Fine-Grained Tracker
GENIE	Generates Events for Neutrino Interaction Experiments (an object-oriented neutrino Monte Carlo generator)
GUT	grand unified theory

ICARUS	Imaging Cosmic And Rare Underground Signals (experiment at LNGS)
L	level, indicates depth in feet underground at the far site, e.g., 4850L
L/E	length to energy ratio
L1, L2, ...	WBS level within the LBNE Project, where the overall Project is L1
LAr-FD	LBNE's liquid argon Far Detector; also refers to the associated L2 Project
LArTPC	liquid argon time projection chamber
LBNE	Long-Baseline Neutrino Experiment
LNGS	Laboratorio Nazionale (National Laboratory) del Gran Sasso
MaVaNs	mass varying neutrinos
MI	Main Injector (at Fermilab)
NC	neutral current (interaction)
ND	(Near Site) neutrino detector
NDC	Near Detector Complex; refers to the L2 Project
NSI	nonstandard interactions
OPERA	Oscillation Project with Emulsion-Racking Apparatus (experiment at LNGS)
POT	protons on target
QA	quality assurance
QE	quasi-elastic (interaction)
SDSTA	South Dakota Science and Technology Authority
SURF	Sanford Underground Research Facility (in Lead, SD, the LBNE Far Site)
SUSY	supersymmetry
T	Tesla
t	ton
TPC	time projection chamber (not used as 'total project cost' in the CDR except in Section 4.3)
W	watt (also mW, kW, MW)
WBS	Work Breakdown Structure

List of Figures

List of Tables

1 About the LBNE Conceptual Design Report

The Long-Baseline Neutrino Experiment (LBNE) Project will provide facilities to enable a world-class program in neutrino physics that can measure fundamental physical parameters, explore physics beyond the Standard Model and better elucidate the nature of matter and anti-matter.

The LBNE Conceptual Design Report (CDR) describes the scope and design of the technical and conventional facilities that the LBNE Project plans to build. The scope comprises

- an intense neutrino beam aimed at a far site
- detectors located downstream of the neutrino source
- a massive neutrino detector located at the far site
- construction of conventional facilities at both the near and far sites

Specifically, LBNE will build a new high-intensity neutrino beam at the Fermi National Accelerator Laboratory (Fermilab) aimed at the Sanford Underground Research Facility (SURF), 1,300 km away, where a massive neutrino detector will be built. The experiment will be optimized for precision measurement of $\nu_\mu \rightarrow \nu_e$ oscillations with the goal of searching for CP violation in the neutrino sector, as well as carrying out precision measurements of neutrino-oscillation parameters.

This CDR is organized into six volumes, one to describe the overall LBNE Project (designated *Level-1* or *L1*) and one for each of its major elements (designated *Level-2* or *L2* Projects):

1. The LBNE Project
2. The Beamline at the Near Site
3. Detectors at the Near Site

4. The Liquid Argon Detector at the Far Site
5. Conventional Facilities at the Near Site
6. Conventional Facilities at the Far Site

Volume 1 provides an introduction to LBNE and to the following volumes of this CDR. It contains high-level information and refers the reader to L2-specific volumes and supporting documents. It also outlines the physics program that LBNE is designed to carry out. More detailed information about the physics program and the experimental capabilities are presented in [1] and [2]. A list of supporting documents providing information on risk analysis and mitigation, value engineering, costing, project management and other topics not directly in the design scope are listed in Chapter 7.

Each Volume 2 through 6 contains a common, brief introduction to the overall LBNE Project, an introduction to the individual L2 Project and a detailed description of its conceptual design.

2 Executive Summary

2.1 Introduction to the LBNE Project

The Long-Baseline Neutrino Experiment (LBNE) Project team has prepared this Conceptual Design Report (CDR), which describes a world-class facility that will enable the scientific community to carry out a compelling research program in neutrino physics. The ultimate goal in the operation of the facility and experimental program is to measure fundamental physical parameters, explore physics beyond the Standard Model and better elucidate the nature of matter and antimatter.

It is planned to implement LBNE as a phased program, with increased scientific capabilities at each phase. The LBNE Project is defined to be the design and construction of the first phase, which will consist of a new neutrino beamline at Fermi National Accelerator Laboratory (Fermilab), tertiary muon detectors to monitor the beam, and a 10-kton liquid argon TPC far detector located at the Sanford Underground Research Facility (SURF), placed at the surface under several meters of shielding. Subsequent phases, which are not part of the LBNE Project, could include the construction of a near neutrino detector on the Fermilab site and construction of a larger detector underground at SURF.

2.1.1 Scientific Motivation

Although the Standard Model of particle physics presents a remarkably accurate description of the elementary particles and their interactions, it is known that the current model is incomplete and that a more fundamental underlying theory must exist. Results from the last decade, that the three known types of neutrinos have nonzero mass, mix with one another and oscillate between generations, implies physics beyond the Standard Model [3].

The three-flavor-mixing scenario for neutrinos can be described by three mixing angles (θ_{12}, θ_{23} and θ_{13}) and one CP-violating phase (δ_{CP}). The frequency of neutrino oscillation also depends on the difference in the squares of the neutrino masses, $\Delta m^2_{ij} = m^2_i - m^2_j$; three neutrinos implies two independent mass-squared differences (Δm^2_{21} and Δm^2_{32}).

The entire complement of neutrino experiments to date has measured five of the mixing parameters: three angles, θ_{12}, θ_{23}, and recently θ_{13}, and two mass differences, Δm^2_{21} and Δm^2_{32}. The sign of Δm^2_{21} is known, but not that of Δm^2_{32}. The value of θ_{13} has been determined to be much smaller than the other two mixing angles [4], implying that mixing is quantitatively different in the neutrino and quark sectors.

Observations of $\nu_\mu \rightarrow \nu_e$ oscillations (from a beam composed initially of muon neutrinos, ν_μ) over a long baseline are the key to unambiguously determining the mass hierarchy (the sign of Δm^2_{32}), and the unknown CP-violating phase δ_{cp}. The signature of CP violation is a difference in the probabilities for $\nu_\mu \rightarrow \nu_e$ and $\overline{\nu}_\mu \rightarrow \overline{\nu}_e$ transitions. The study of the disappearance of ν_μ probes θ_{23} and $|\Delta m^2_{32}|$. Non-standard physics can manifest itself in differences observed in higher-precision measurements of ν_μ and $\bar{\nu}_\mu$ disappearance over long baselines. The precision with which the current set of neutrino-oscillation parameters are known ensures that the compelling physics program outlined for LBNE is feasible with the proposed combination of baseline, detector mass and beam.

2.1.2 LBNE and the U.S. Neutrino-Physics Program

In its 2008 report, the Particle Physics Project Prioritization Panel (P5) recommended a world-class neutrino-physics program as a core component of the U.S. particle-physics program [5]. Included in the report is the long-term vision of a large detector at the formerly proposed Deep Underground Science and Engineering Laboratory (DUSEL) in Lead, SD (now SURF), and a high-intensity neutrino source at Fermilab.

On January 8, 2010, the Department of Energy approved the Mission Need [6] for a new long-baseline neutrino experiment that would enable this world-class program and firmly establish the U.S. as the leader in neutrino science. The LBNE Project is designed to meet this Mission Need.

With the facilities provided by the LBNE Project and the unique features of the experiment – in particular the long baseline, the broad-band beam and the high resolution of the detector – the LBNE Science Collaboration proposes to mount a broad attack on the science of neutrinos with sensitivity to all known parameters in a single experiment. The focus of the program will be the explicit demonstration of leptonic CP violation, if it exists, by precisely measuring the asymmetric oscillations of muon-type neutrinos and antineutrinos into electron-type neutrinos and antineutrinos. The experiment will enable precise measurements of the neutrino-oscillation parameters, in particular, the CP-violating phase in the three-flavor framework, and the search for new physics that would show up as deviations from this model.

A configuration of the LBNE facility in which the Far Detector is located deep underground would also provide opportunities for research in other areas of physics, such as nucleon

decay and neutrino astrophysics, including studies of neutrino bursts from locally occurring supernovae. A deep-underground site is not part of the LBNE Project; it could be pursued as a future phase of the LBNE program or as part of the initial phase of LBNE if adequate resources can be secured from non-DOE sources by CD-2.

The scientific goals and capabilities of LBNE are summarized in Chapter 6. The physics capabilities of the full implementation of the LBNE program is fully described in the 2010 Interim Report of the Long-Baseline Neutrino Experiment Collaboration Physics Working Groups [1]. The physics capabilities enabled by the LBNE Project, which represents the first phase of this program, are presented in [7].

2.1.3 Overview of Project Organization

The LBNE Project Office at Fermilab is headed by the Project Director and assisted by the Project Manager, Project Scientist and Systems Engineer. Project Office support staff include a Project Controls Manager and supporting staff, a Financial Manager, an Environment, Safety and Health (ES&H) Manager, a Computing Coordinator, Quality Assurance, Procurement and Risk Managers, a documentation team and administrative support. The construction of LBNE is supported by the laboratories and universities of the LBNE Science Collaboration, which provides scientific, engineering and technical expertise.

More information on Project organization can be found in Chapter 4, and a full description of LBNE Project Management is contained in The LBNE Project Management Plan [8].

2.2 Overview of the LBNE Science Objectives

The primary science objectives of the LBNE Project are the following experiments [9] (those that can be addressed by the LBNE **Project** appear in normal font and those can only be addressed by a subsequent phase of the LBNE ***Program*** in which the Far Detector can be placed deep underground appear in *italics*):

1. search for, and precision measurements of, the parameters that govern $\nu_\mu \rightarrow \nu_e$ oscillations, as discussed above in Section 2.1.1; this includes precision measurements of the third mixing angle, θ_{13}, for whose value only an upper bound is currently known, and if θ_{13} is large enough, measurement of the CP violating phase δ_{CP} and determination of the mass ordering (the sign of Δm^2_{32})
2. precision measurements of θ_{23} and $|\Delta m^2_{32}|$ in the ν_μ-disappearance channel
3. *search for proton decay, yielding measurement of the partial lifetime of the proton (τ/BR) in one or more important candidate decay modes, $p \rightarrow e^+\pi^0$ or $p \rightarrow K^+\nu$.*

4. *detection and measurement of the neutrino flux from a core-collapse supernova within our galaxy, should one occur during the operating life of LBNE*

A high-level discussion of these objectives as well as a list of additional objectives that LBNE may pursue can be found in Chapter 3.

2.3 Principal Parameters of the LBNE Project

The individual CDR volumes provide detail on the designs that LBNE has developed, based on a carefully constructed set of requirements that are organized in a traceable flow-down structure. Scientific requirements for LBNE, provided by the LBNE Collaboration, follow from the science objectives. Design of individual L2 projects, systems and components are based on mid- and low-level requirements, respectively, that trace all the way back either to the science or programmatic requirements.

The experimental capabilities and expected performance of the Far Detector technology are documented thoroughly in the LBNE Case Study Report for a Liquid Argon TPC [10] and summarized in Chapter 6.

Table 2–1 summarizes the principal parameters of the experiment.

Table 2–1: LBNE Principal Parameters

Project Element Parameter	**Value**
Near- to Far-Site Baseline	1,300 km
Primary Proton Beam Power	708 kW, upgradable to 2.3 MW
Protons on Target per Year	6.5×10^{20}
Primary Beam Energy	60 – 120 GeV (tunable)
Neutrino Beam Type	Horn-focused with decay volume
Neutrino Beam Energy Range	0.5 – 5 GeV
Neutrino Beam Decay Pipe Diameter × Length	4 m × 200 m
Far Detector Type	LArTPC
Far Detector Active (Fiducial) Mass	13.5 (10) ktons

3 LBNE Science Objectives

Prior to the realization that LBNE could be implemented only as a phased program, the LBNE Science Collaboration, working with LBNE Project Management, developed a prioritized set of research goals for the full implementation of LBNE which was approved by the then LBNE Project Manager (now Project Director), the LBNE Collaboration Co-Spokespersons, the Fermilab Director, and the LBNE Federal Project Director. This set of goals is presented in Version 1.0 of "Physics Research Goals of the LBNE Project" [11].

The goals for the full LBNE program have not changed as a result of a phased implementation of the program. However, not all of the goals of the full program can be achieved in the first phase. This chapter presents the full set of research goals, and specifies which goals will be addressed by the LBNE **Project** (in normal font) and which ones can only be addressed by subsequent phases of the LBNE ***Program*** (*in italics*). This same information is presented in the current version of the "Physics Research Goals of the LBNE Project" [9].

The **primary objectives** of LBNE, in priority order are the following experiments:

1. precision measurements of, the parameters that govern $\nu_\mu \rightarrow \nu_e$ oscillations; this includes precision measurement of the third mixing angle, measurement of the CP violating phase δ_{CP}, and determination of the mass ordering (the sign of Δm^2_{32}).

2. precision measurements of θ_{23} and $|\Delta m^2_{32}|$ in the ν_μ-disappearance channel.

3. *search for proton decay, yielding significant improvement in the current limits on the partial lifetime of the proton (τ/BR) in one or more important candidate decay modes, e.g. $p \rightarrow e^+\pi^0$ or $p \rightarrow K^+\nu$.*

4. *detection and measurement of the neutrino flux from a core-collapse supernova within our galaxy, should one occur during the lifetime of LBNE.*

Of these, the first two can be addressed by the LBNE Project, and the configuration of the LBNE Project is set to maximize the effectiveness of the facility to achieve them. *The second*

two require a deep underground location for the Far Detector, and can only be addressed in a subsequent phase of LBNE.

Secondary objectives, which may be enabled by the facility that is designed to achieve the primary objectives include:

1. other accelerator-based neutrino-oscillation measurements.
2. *measurements of neutrino-oscillation phenomena using atmospheric neutrinos.*
3. *measurement of other astrophysical phenomena using medium-energy neutrinos.*

The first of these can be addressed by the LBNE Project, and will be considered in determining the configuration of LBNE only if investment to enable these measurements does not compromise the ability to achieve the primary objectives. *Secondary objectives 2 and 3 require a deep underground location for the far Detector, and can only be addressed in a subsequent phase of LBNE.*

Additional secondary objectives, the achievement of which may require upgrades to the facility that is designed to achieve the primary physics objectives, include:

1. *detection and measurement of the diffuse supernova-neutrino flux.*
2. *measurements of neutrino-oscillation phenomena and of solar physics using solar neutrinos.*
3. *measurements of astrophysical and geophysical neutrinos of low energy.*

All of the additional secondary objectives require a deep underground location for the Far Detector, and can only be addressed in a subsequent phase of LBNE.

4 Project Organization

4.1 Overview

The LBNE Project consists of a set of subprojects (referred to throughout this CDR as "level-2 (L2) projects" relative the the overall level-1 (L1) project), coordinated by a central Project Office located at Fermilab; they include:

1. Project Management
2. Beamline
3. Near Detector Complex
4. Liquid Argon Far Detector
5. Conventional Facilities

The LBNE Project Office at Fermilab is headed by the Project Director and assisted by the Project Manager, Project Scientist and Systems Engineer. Project Office support staff include a Project Controls Manager and supporting staff, a Financial Manager, an Environment, Safety and Health (ES&H) Manager, a Computing Coordinator, Quality Assurance, Procurement and Risk Managers, a documentation team and administrative support.

The construction of LBNE is supported by the laboratories and universities of the LBNE Science Collaboration, which provides scientific, engineering and technical expertise. A Project organization chart is shown in Figure 4–1.

4.2 Work Breakdown Structure

The LBNE Work Breakdown Structure (WBS) is a means of organizing the work scope of the Project. A WBS decomposes the Project's tasks and deliverables into smaller, manageable

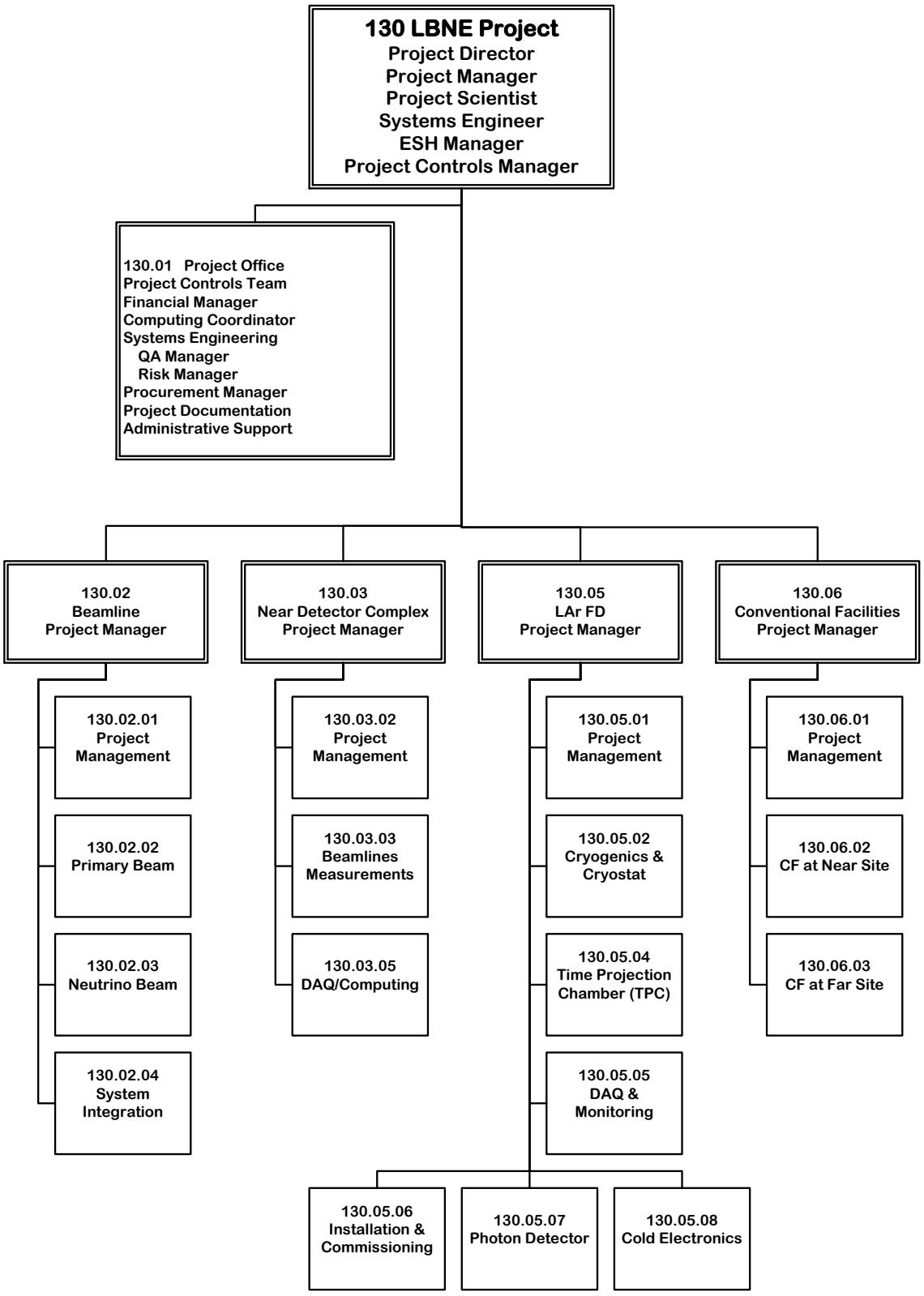

Figure 4–1: LBNE Project L2-L3 Organization Chart

components. The overall LBNE Project ("Project 130" within the Fermilab-wide WBS) is defined as WBS Level 1 (L1), and each of its component projects, listed above, is defined as Level 2 (L2). The L2 projects, in turn, get broken out into lower, component levels. Table 4–1 shows the LBNE WBS down to Level 3. WBS 130.04, the water Cherenkov detector (not listed above), has been discontinued. It appears in the table below since LBNE bears the costs for its development through the conceptual design stage.

Table 4–1: WBS Chart (WBS Element Numbers and Names) to Level 3

Number	Name
130	**LBNE**
130.01	**Project Management Office**
130.01.01	Conceptual Design Phase Management (CD-0 to CD-1)
130.01.02	Preliminary & Final Design Phase Management (CD-1 to CD-3)
130.01.03	Construction Phase Management (CD-3 to CD-4)
130.01.04	Closeout Phase Management
130.02	**Beamline**
130.02.01	Beamline Project Management
130.02.02	Primary Beam
130.02.03	Neutrino Beam
130.02.04	System Integration
130.03	**Near Detector Complex (NDC)**
130.03.01	Near Detector Complex Conceptual Design (CD-0 to CD-1)
130.03.02	Near Detector Complex Management
130.03.03	Near Detector Beamline Measurements
130.03.04	NDC Global DAQ and Computing Systems
130.04	**Water Cherenkov Detector - Conceptual Design**
130.04.01	Project Management - Conceptual Design
130.04.02	Water Containment - Conceptual Design
130.04.03	Photon Detectors - Conceptual Design
130.04.04	Electronics/Readout - Conceptual Design
130.04.05	Calibration - Conceptual Design
130.04.06	Water System - Conceptual Design
130.04.07	Computing - Conceptual Design
130.04.08	Integration, Installation and Safety Systems - Conceptual Design
130.05	**Liquid Argon Far Detector (LAr-FD)**
130.05.01	LAr Project Management
130.05.02	LAr Cryogenics & Cryostat
130.05.04	LAr Time Projection Chamber (TPC)
130.05.05	LAr DAQ & Monitoring
130.05.06	LAr Installation & Commissioning
130.05.07	LAr Photon Detector
130.05.08	LAr Cold Electronics

130.06	Conventional Facilities (CF)
130.06.01	CF Project Management
130.06.02	CF Near Site (Fermilab)
130.06.03	CF Far Site (SURF)

4.3 Project Cost and Schedule

The initial cost range for the LBNE Project is $805M to $1,110M, with a target Total Project Cost (TPC) of $867M, including 40% contingency on the remaining work. The Project Schedule is 14 years from CD-0 to CD-4, beginning with CD-0 in January 2010 and completion in third Quarter 2025, which includes two years of schedule contingency.

Table 4–2: Target Budget Cost Estimates at WBS Level 2

WBS L2	Description	TPC (in $k)	TPC % Contingency on Cost Estimate to Completion
130.01	Project Management Office	103,113	92%
130.02	Beamline	164,680	29%
130.03	Near Detector Complex	22,557	148%
130.04	Water Cherenkov Far Detector	11,178	0%
130.05	LAr 10-kton Surface Far Detector	253,114	41%
130.06	Conventional Facilities	312,790	31%
Estimated Total Project Cost (TPC)		867,432	40%

5 Project Scope

5.1 Overview

The DOE Mission Need [6] for the LBNE Project proposes the following major elements:

- an intense neutrino beam aimed at a far site
- detectors located at the near site just downstream of the neutrino source
- a massive neutrino detector located at the far site

The LBNE Project scope includes construction of experimental systems and facilities at two separate geographical locations. The LBNE reference design is intended to achieve the Project's mission. A proton beam extracted from the Fermilab Main Injector (MI) is used to produce a neutrino beam that travels through the Earth's mantle to a detector located 1,300 km away at SURF, the site of the former Homestake Mine in Lead, South Dakota. The Far Detector will be installed near the surface with an embankment constructed above it. The 1,300-km separation between the sites presents an optimal baseline [2] for LBNE's neutrino-oscillation physics goals.

The main scope elements on the Fermilab site, also referred to as the Near Site, include:

- a primary beamline (consisting of magnets and support equipment) to extract protons from a proton synchrotron and transport the resulting proton beam to a target (where approximately 85% of the protons interact, producing pions and kaons)
- a target and target hall complex
- magnetic focusing horns to direct pions and kaons into a decay pipe
- a decay pipe in which these particles decay into neutrinos

- a beam absorber at the end of the decay pipe to absorb both the residual secondary particles and the primary protons that did not interact in the target
- an array of muon detectors downstream of the absorber to provide information about the neutrino-beam production
- conventional facilities to support the technical components of the primary proton beam, the neutrino beam and the muon detector system

The main scope elements at SURF, the Far Site, include:

- a 10 kton fiducial-mass liquid argon TPC far detector
- conventional facilities to house and support the technical components of the Far Detector

5.2 Beamline at the Near Site

The LBNE Beamline at Fermilab, a conventional, horn-focused neutrino beamline, will be designed to provide a neutrino beam of sufficient intensity and energy to meet the goals of the LBNE experiment with respect to long-baseline neutrino-oscillation physics. The components of the beamline will be designed to extract a proton beam from the Fermilab Main Injector (MI) and transport it to a target area where the collisions generate a beam of charged secondary particles. This secondary beam, aimed toward the Far Detector, is followed by a decay pipe where the particles of the secondary beam decay to generate the neutrino beam. At the end of the decay pipe, an absorber pile removes the residual hadrons. The beam layout is shown in Figures 5–1 and 5–2.

The facility is designed for initial operation at a proton-beam power of 708 kW, with the capability to support an upgrade to 2.3 MW. The beam is extracted from a new extraction point on the Main Injector, MI-10. After extraction, the beam is bent to the right and up to an apex, then back down at an angle of 101 milliradians (5.79°) toward the target, thus establishing the needed trajectory for the neutrino beam towards the far detector at SURF (see Figure 5–2).

The primary beam will be above-grade for about 550 feet; this design minimizes expensive underground construction and significantly enhances capability for groundwater radiological protection. However, the design requires construction of an earthen embankment, or hill, whose dimensions are commensurate with the bending strength of the dipole magnets required for the beamline. The embankment will need to be approximately 950 feet long and 58 feet above grade at its apex.

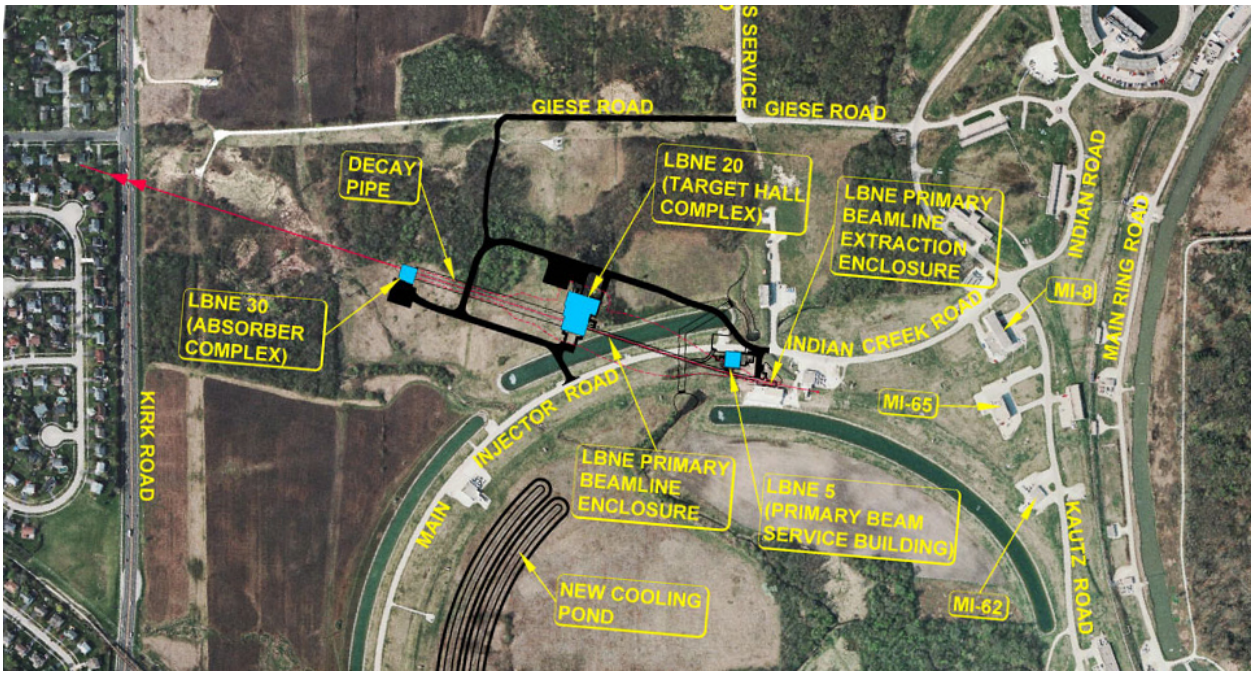

Figure 5–1: Plan view of the overall Near Site Project layout showing the LBNE Beamline extraction point from the Main Injector, the primary beamline, target hall, decay pipe and absorber.

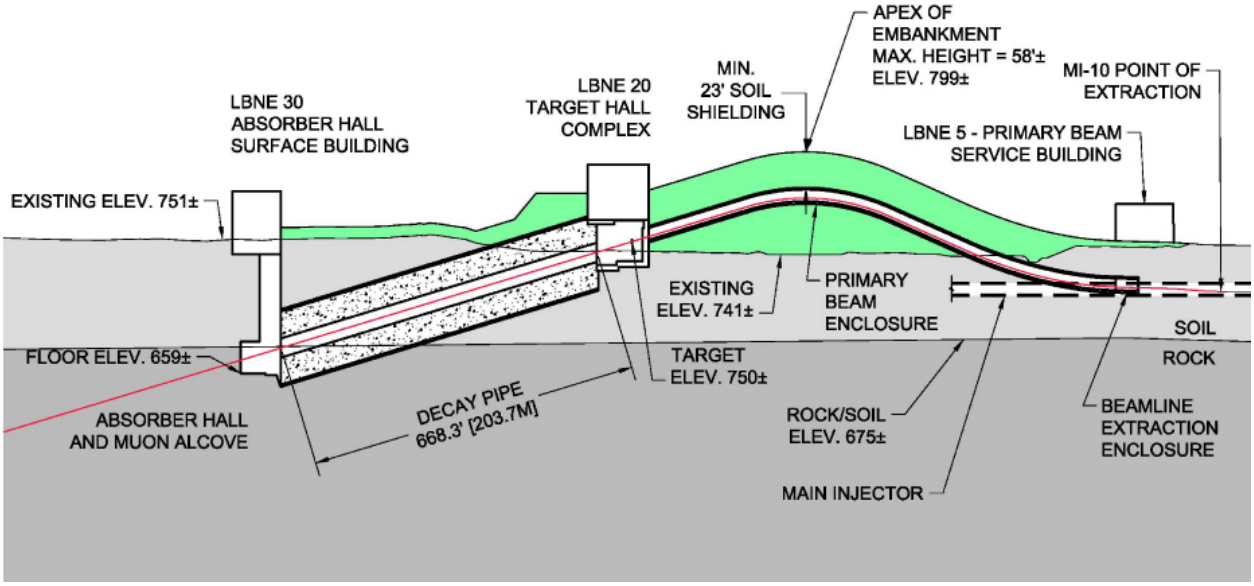

Figure 5–2: LBNE Near Site schematic longitudinal section view; the vertical scale is exaggerated 3 to 1 with respect to the horizontal scale

The proton beam strikes a thin graphite target, two nuclear interaction lengths long (96 cm), with which about 85% of the protons interact to produce a shower of secondary particles, mainly pions with a small admixture of kaons. The charged secondaries are focused in the forward direction by two toroidal focusing horns as shown in Figure 5–3. The horn current polarity can be selected to preferentially focus positive or negative secondaries, which then enter a 204-m long, 4-m diameter air-filled pipe in which they are allowed to decay, predominantly into muon-type neutrinos (anti-neutrinos in the case of negative polarity) and muons. At the end of the decay pipe an absorber stops both the secondaries that did not decay and the protons that did not interact in the target. The decay pipe dimensions have been chosen such that decays of the pions and kaons result in neutrinos in the energy range useful for the experiment (0.5-5 GeV). Kaon and muon decays also produce electron-neutrinos that are considered irreducible background to $\nu_\mu \rightarrow \nu_e$ oscillation physics.

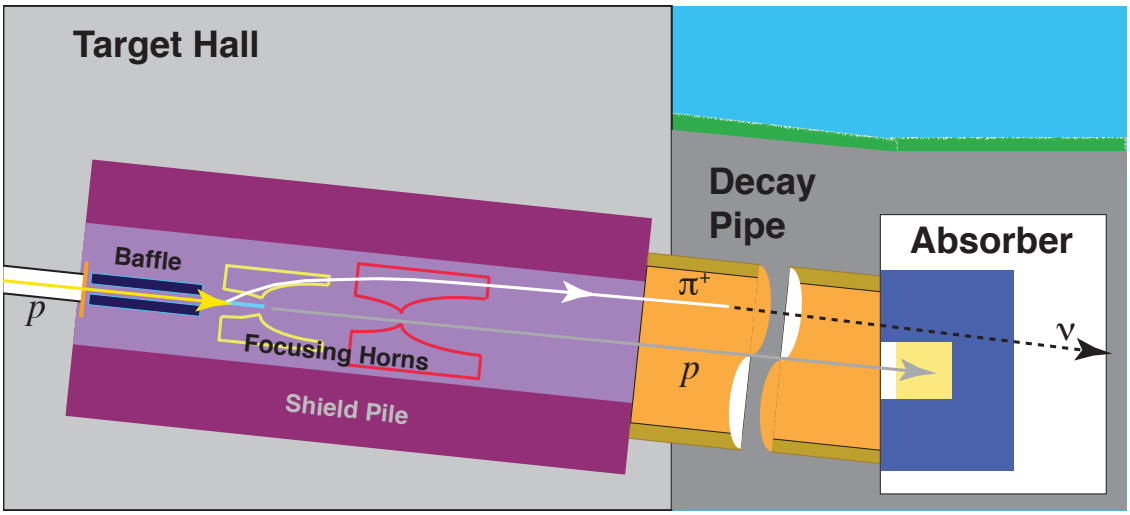

Figure 5–3: A cartoon of the LBNE neutrino beamline showing the major components of the neutrino beam. From left to right (the direction of the beam): the beam window, horn-protection baffle, target, the two toroidal focusing horns, decay pipe and absorber.

5.3 Near Detector Complex

The role of the LBNE Near Detector Complex (NDC) is to characterize the neutrino beam at its source, in order to provide a an accurate description of the unoscillated flux spectrum for the analysis of muon to electron neutrino and muon to muon neutrino oscillations. Ideally, the NDC would comprise both a beamline measurement system to determine absolute neutrino fluxes and spectra, as well as a near neutrino detector located sufficiently downstream of the absorber to accurately measure the unoscillated neutrino interaction spectrum. The NDC would also help characterize the response of the Far Detector to neutrino interactions, by measuring neutrino cross sections and event topologies off of the same target nucleus as in the Far Detector.

Due to financial constraints, a near neutrino detector is not included in the LBNE Project, although building one in a later phase of the LBNE program is planned. The NDC is therefore limited to an array of muon detectors, called the Beamline Measurements (BLM) system and the associated data acquisition (DAQ) system. The BLM system, located downstream of the absorber at the end of the decay region, is designed to measure the flux of muons produced from the decays of pions and kaons to muons and muon-neutrinos. These measurements constrain the absolute beam-neutrino flux. The BLM system includes three detectors intended to measure (1) the muon-beam profile (with a grid of ion chambers), (2) the muon-beam energy spectrum (using variable-pressure threshold gas Cherenkov detectors), and (3) the muon flux by counting the number of muon-decay Michel electrons in "stopped-muon" detectors. The BLM will be located in the region of the Absorber Complex at the downstream end of the decay region. Figure 5–4 shows the downstream side of the absorber and a conceptual layout of the BLM muon systems.

The LBNE measurement of the unoscillated neutrino spectrum also relies on measurements made outside the scope of LBNE to calibrate the muon detector response, and utilizes common simulation code tuned using measurements of the unoscillated NuMI beam spectrum in the MINOS near-detector and the MINERνA detector. The LBNE beam is of very similar design to the NuMI beam, and utilizes identical targetry and focusing elements.

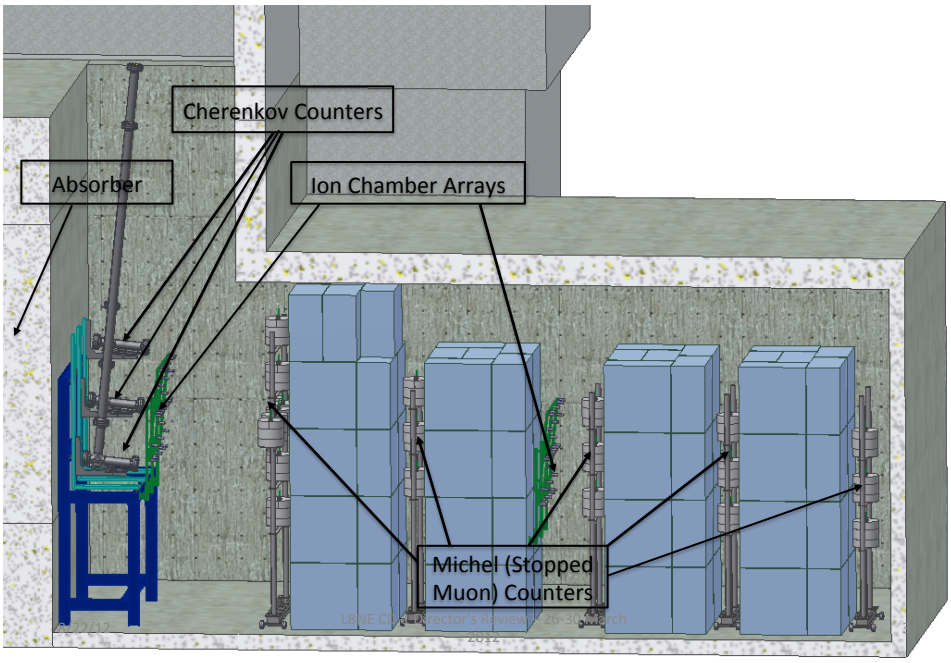

Figure 5–4: Layout of Near Detector beamline measurement system placed downstream of the absorber

5.4 Conventional Facilities at the Near Site

The baseline design for the LBNE Project extracts a proton beam from the MI-10 point of the Main Injector. This design choice, in conjunction with the Far Detector location and hence the beamline orientation, determines the location and layout of the Near Site Conventional Facilities. The Near Site Conventional Facilities provide the support buildings for the underground facilities as well as the infrastructure to house the Beamline technical systems, from the extraction point through the target and absorber. See Figure 5–1 for a schematic of the experimental and conventional Near Site facilities.

After the proton beam is extracted at MI-10, about 30 ft below grade, the Beamline will continue along the Primary Beam Enclosure at an incline into and through an embankment constructed of engineered fill that reaches a maximum height of about 58 ft above existing grade. After reaching the apex of the embankment the Beamline declines back toward existing grade and through the Target Hall, a 668-ft (203.7-m) long decay pipe, and the Absorber Hall. Downstream of the Absorber Hall, the Beamline is directed through bedrock, allowing muons to range out before the beam reaches the Far Detector. Figure 5–2 shows a schematic longitudinal section of the entire Near Site, with an exaggerated vertical scale of 3 to 1 to show the entire Project alignment in one illustration.

The Near Site Conventional Facilities LBNE Project layout at Fermilab, the "Near Site", is shown in Figure 5–1. Following the beam from east to west, or from right to left in this figure, is the underground Primary Beamline Extraction Enclosure, the underground Primary Beamline Enclosure/Pre-target Tunnel and its accompanying surface based Service Building (LBNE 5), the in-the-berm Target Hall Complex (LBNE 20), the decay pipe and the underground Absorber Hall and its surface Service Building (LBNE 30). The Project limits are bounded by Giese Road to the north, Kautz Road to the east, Main Injector Road to the south, and Kirk Road to the west.

5.5 Liquid Argon Far Detector

The LBNE Far Detector is a liquid argon time projection chamber (LArTPC). This type of detector combines fine-grain tracking with total absorption calorimetry to enable precision neutrino-event detection in scalable neutrino detectors. The millimeter-scale spatial resolution combined with recordable dE/dx provides excellent signal efficiency and background rejection for both beam and non-beam physics.

The signal in liquid argon is generated by a well known electromagnetic process, the generation of ionization electrons by the passage of particles through liquid argon. The electrons drift in a uniform electric field to a sense plane that measures the position of the ionization in two dimensions. The drift time provides the third dimension, providing a full 3D image

of the particle interaction.

The LBNE LArTPC, referred to as the LAr-FD, consists of two massive rectangular box-shaped cryostats in a single pit excavated just below grade, above which an embankment will be constructed, primarily to absorb the hadronic and electromagnetic components of cosmic-ray showers. The two cryostats, each with its long axis parallel to the beam direction, will sit in a side-by-side configuration orthogonal to the beam. The cryostats are separated by a wall, which is effectively the center of the detector and thus coincident with the center of the beam. Each cryostat is 13.9 m wide by 14 m high by 25.3 m long.

The fiducial mass of each cryostat, as defined for neutrino-oscillation studies, is 5 kton and the active (instrumented) mass is 6.7 kton, resulting in a total active mass of 13.5 kton. The detector's configuration is illustrated in Figure 5–5.

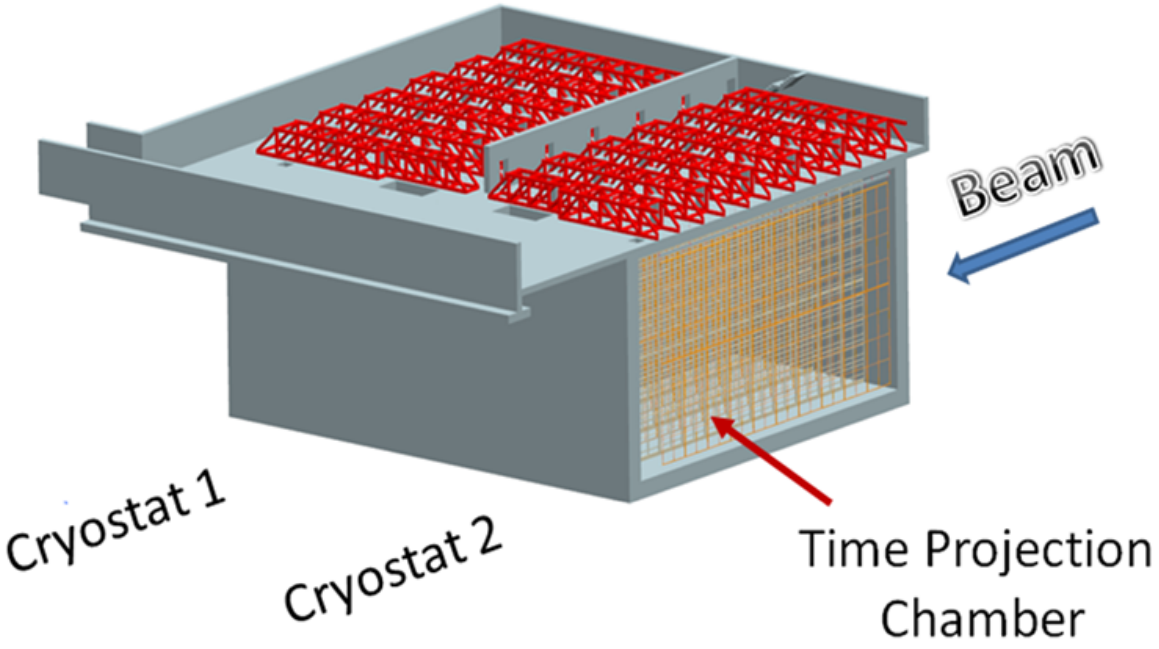

Figure 5–5: LAr-FD configuration

The detector includes a cryogenic system that keeps the liquid argon at a temperature of 87 K and maintains the required purity using a pump and filter system.

The proposed location of the LAr-FD on the SURF site is shown in Figure 5–6.

Figure 5–7 shows the placement of the installation with respect to the surrounding topography. The detector is placed at the base of a hill to the east, which provides $\geq$ 300 m of rock shielding against cosmic rays coming within 25° of the neutrino beam directions. Figure 5–8 provides a detailed view of the configuration of the detector and ancillary buildings.

Figure 5–6: Location of LAr-FD on the SURF site in Lead, SD.

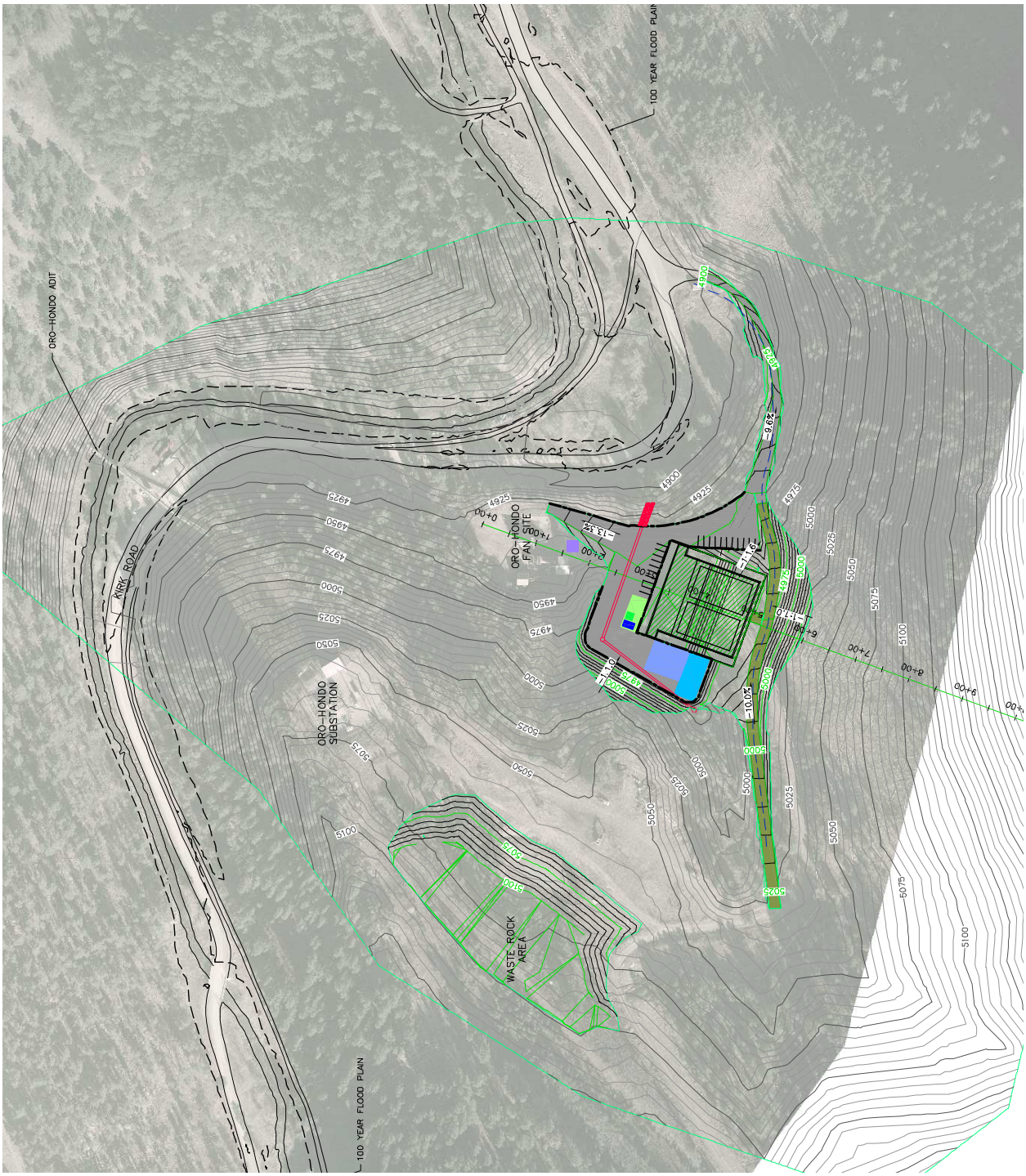

Figure 5–7: LAr-FD configuration with respect to the site (North points up)

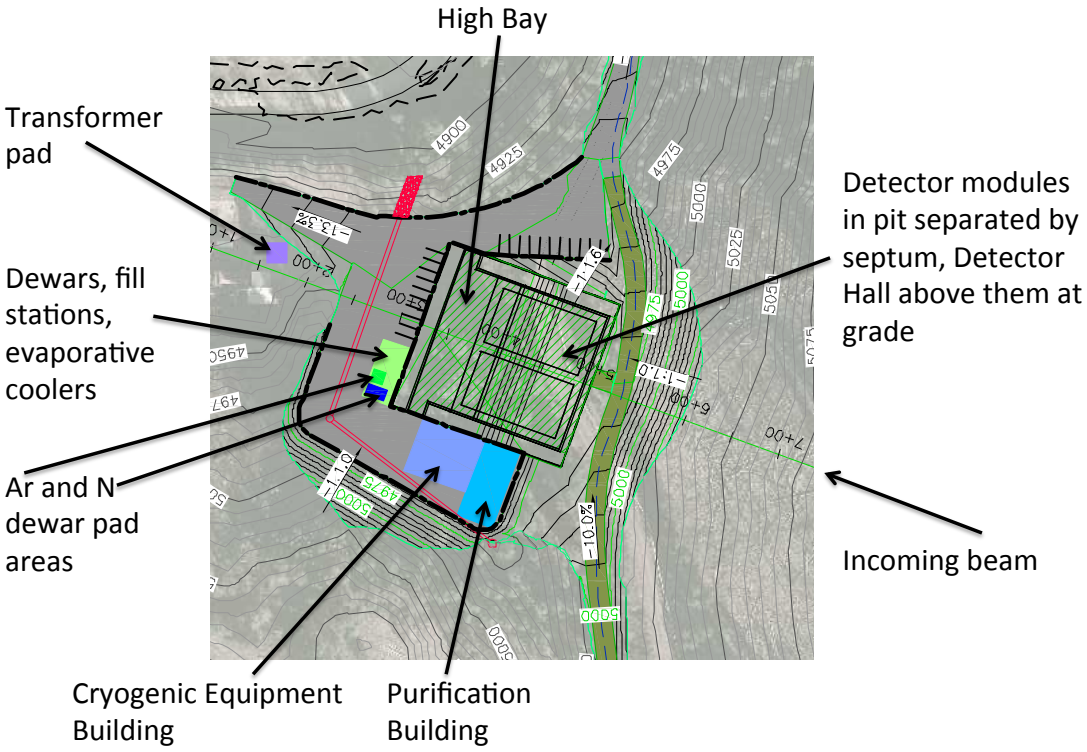

Figure 5–8: LAf-FD configuration and ancillary buildings (North points up)

The detection system in each cryostat consists of a time projection chamber (TPC) and readout electronics. A TPC consists of rows of cathode planes interleaved with rows of anode planes between sets of which uniform electric fields are created. See Figure 5–9. Charged particles passing through the TPC release ionization electrons that drift along the field to the anode planes. The bias voltage is set on the anode wires (of which there are four layers) such that ionization electrons drift between the first several layers (called *induction* layers) and are collected on the last layer (the *collection* layer).

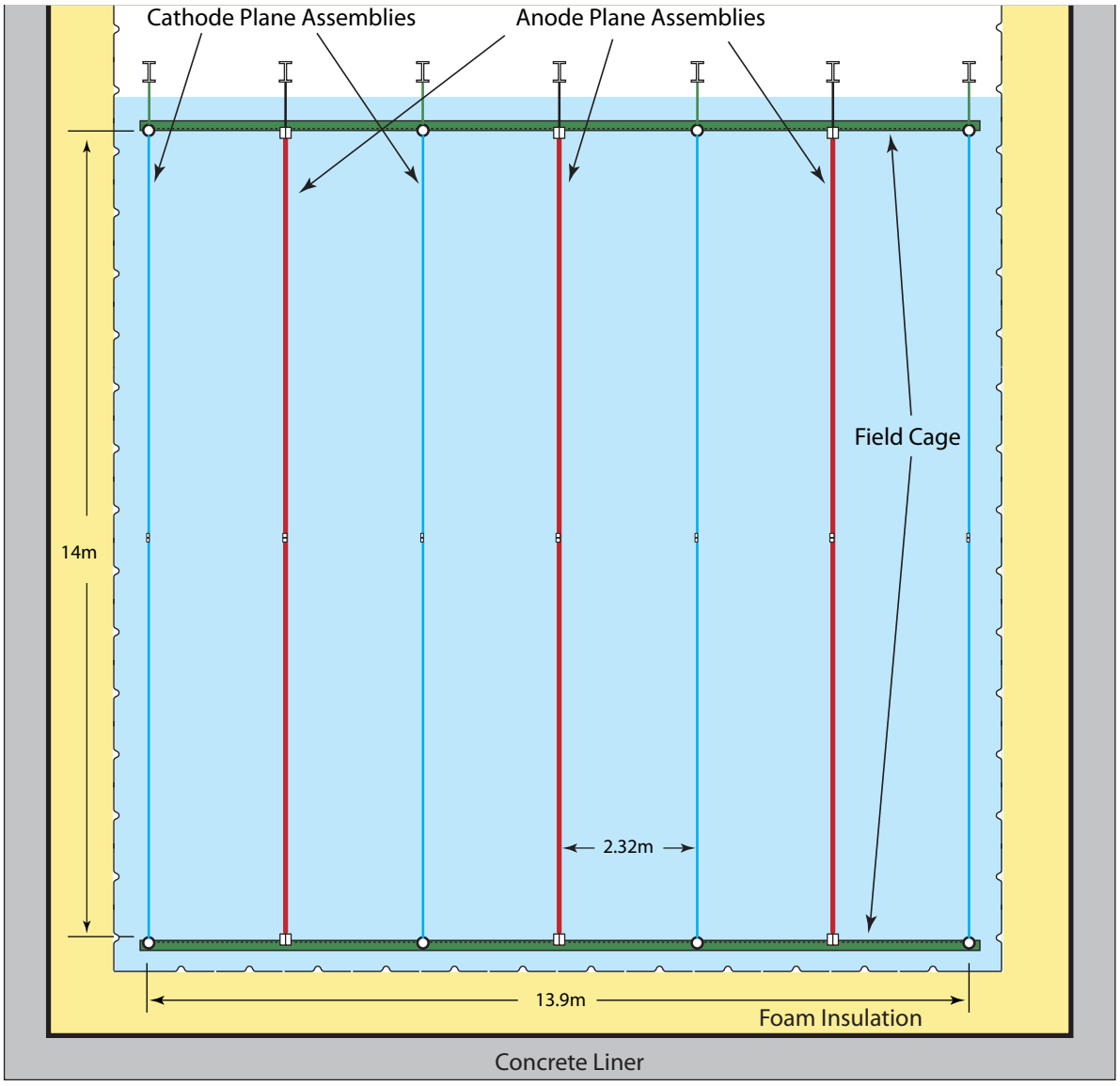

Figure 5–9: TPC cross section view

Readout electronics amplify and continuously digitize the induced waveforms on the sensing wires at several MHz, and transmit these data to the data acquisition (DAQ) system. The

wire layers are oriented at different angles relative to each other allowing 3D reconstruction of the particle trajectories with the drift time providing the third dimension. The drift time is measured relative to a trigger provided by the timing of the Main Injector beam extraction (for beam events) and by an array of photon detectors that measure scintillation light (for non-beam events).

5.6 Far Detector Depth

In 2008, the LBNE Science Collaboration undertook a detailed study of the depth requirements for the main physics topics of interest with large detectors. This work is referred to as "The Depth Document" [12]. The topics considered were accelerator-generated neutrinos; supernova, solar and atmospheric neutrinos; and nucleon decay. The requirement on the depth of the detector is guided by the rate of the desired signals and the rate of backgrounds from cosmic rays over a very wide range of energies (from solar-neutrino energies of 5 MeV to high energies in the hundreds of GeV.)

In the current scope of the LBNE Project, the overburden is sufficient to achieve the accelerator-based science objectives. If a future opportunity arises that would allow placement of the Far Detector deep underground, the additional topics can be explored. Table 5–1 lists the depth requirements for this detector to accomplish LBNE's goals for each physics measurement.

Table 5–1: Minimum depth requirement (in meters-water-equivalent) by physics topic for the Liquid Argon TPC Far Detector

Physics Topic	Minimum Depth (mwe)
Long-baseline accelerator	0 – 1,000
$p \rightarrow K^{+}\nu$	3,000
Day/Night ^{8}B Solar ν	4,300
Supernova burst	3,500
Relic supernova ν	2,500
Atmospheric ν	2,400

5.7 Conventional Facilities at the Far Site

The Far Site used in our reference design is the Sanford Underground Research Facility (SURF) in Lead, SD.

The scope of the facilities required for the LAr-FD includes a new excavated space just below grade for the detector itself of dimensions 38.5 m wide × 31.2 m long × 18.1 m, utility spaces

for experimental equipment and utility spaces for facility equipment. A cross sectional view of the facilities is given in Figure 5–10.

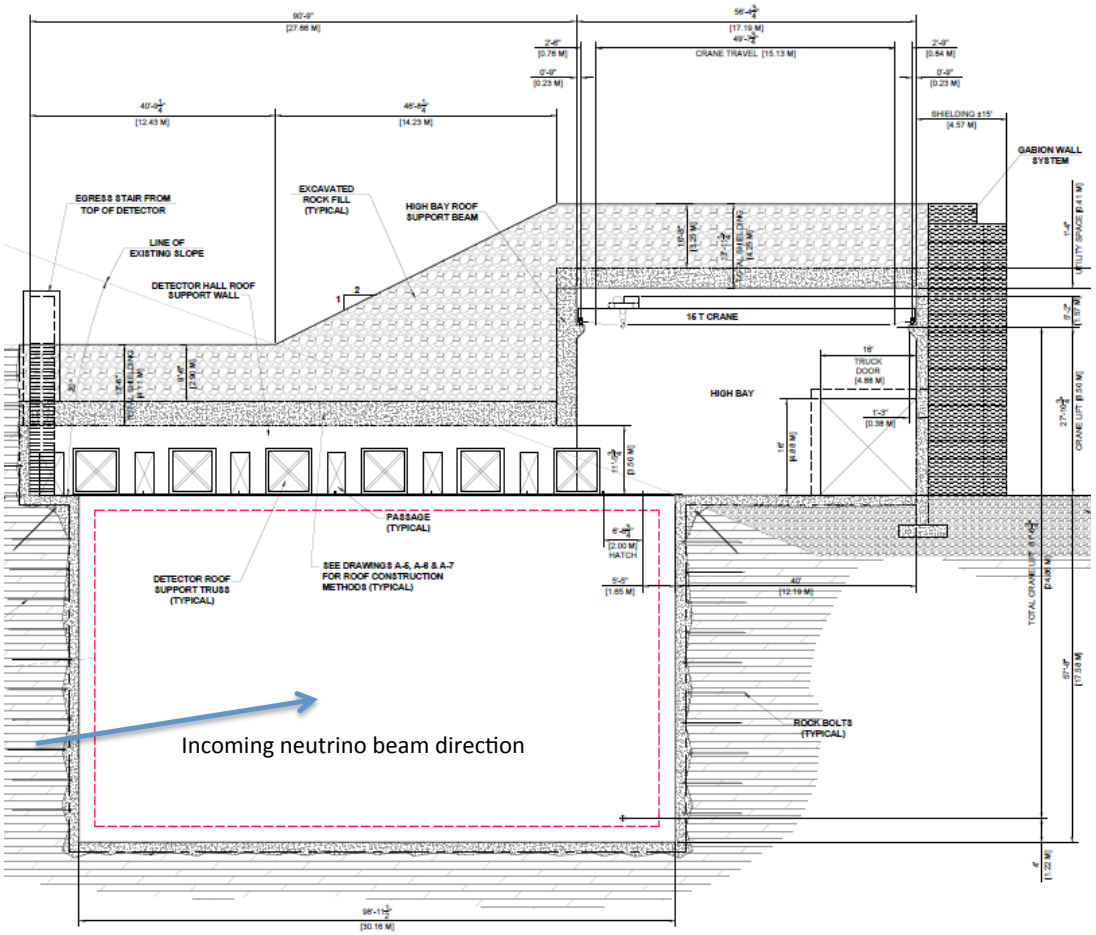

Figure 5–10: Cross section of the 10-kton LAr-FD taken parallel to the beamline

Infrastructure for the facility includes power to experimental equipment, domestic water, industrial water for process and fire suppression, fire detection and alarm, normal and standby power systems, and cyberinfrastructure for communications and security.

6 Experimental Capabilities

6.1 Overview

Pursuit of the primary science objectives for LBNE as described in Chapter 3 dictates the need for very large mass (10-100 kiloton-scale) neutrino detectors located at a distance of > 1000 km from the neutrino source [7]. A large mass coupled with a powerful beam and long exposures is required to accumulate enough neutrino interactions – $\mathcal{O}(1000)$ events – to make precision measurements of the parameters that govern the sub-dominant $\nu_\mu \rightarrow \nu_e$ oscillations. The LBNE reconfiguration study [2] determined that the Far Detector location at SURF provides an optimal baseline (1,300 km) for precision measurement of neutrino oscillations using a conventional neutrino beam from Fermilab, and offers the best sensitivity to CP violation, as shown in Figure 6–1.

The large cosmic-ray background in the Far Detector, due to its location at the surface, limits the physics capabilities of LBNE to measurements done with the neutrino beam from Fermilab. The constraints of beam timing (10 μsec proton pulse every 1.33 seconds), the beam direction, as well as the relatively high-energy (> 1 GeV) specific signatures of the beam neutrino events, which permit powerful rejection of cosmic ray backgrounds, are not available for the non-beam physics that could be enabled by a large LArTPC detector.

This chapter discusses the long-baseline neutrino oscillation measurements that the ten-kiloton surface Far Detector will make using the neutrino beam from Fermilab (also described in [7]). Additional information is also provided regarding the research capabilities (nucleon decay searches, supernova-neutrino and atmospheric-neutrino measurements), that would be enabled if it became possible to place the Far Detector underground, either by obtaining additional resources beyond those assumed in developing the conceptual design presented in this CDR, or in a later stage of the LBNE program. The "Fall 2010 Report from the Physics Working Group" [1] presents a detailed study of the more extensive physics capabilities of an LBNE implementation in which a 34-kiloton Far Detector is placed 4,580 feet underground and a near neutrino detector is deployed.

To meet the physics objectives of LBNE, the detector is required to have excellent particle

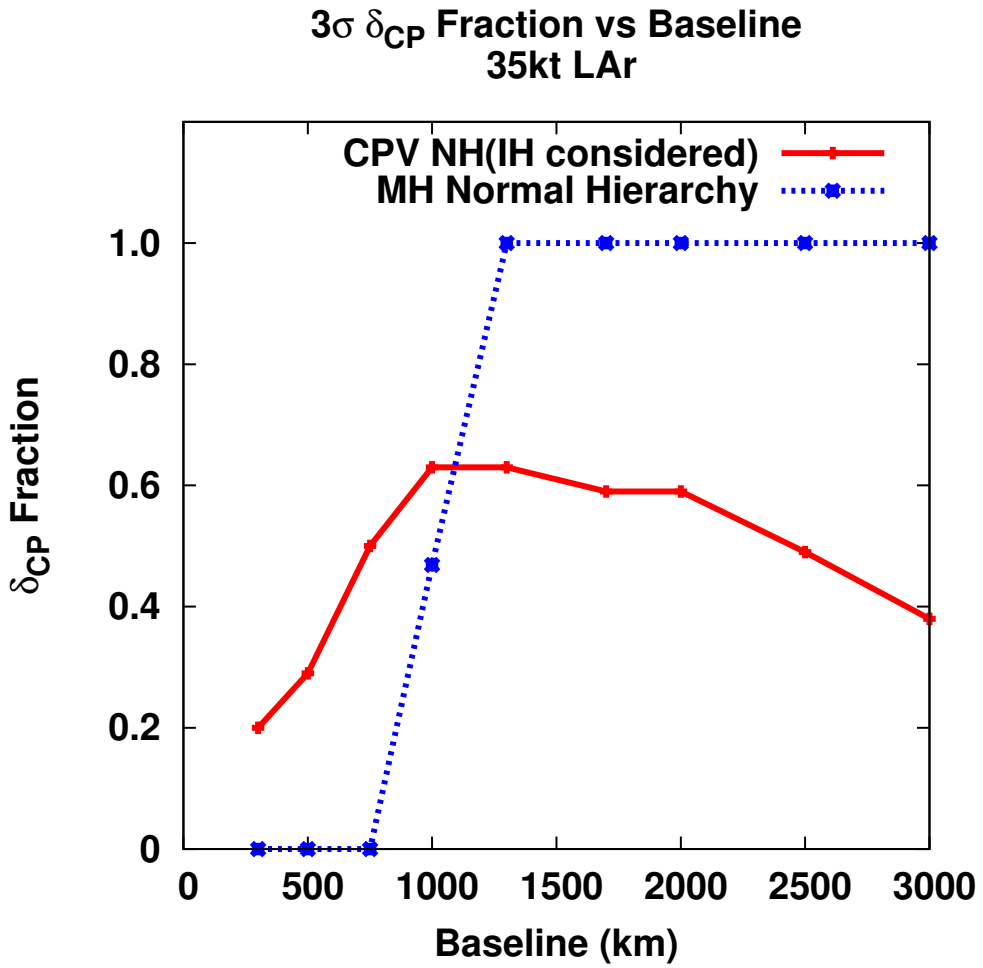

Figure 6–1: The fraction of δ_{cp} values for which CP violation and the mass hierarchy can be determined at the 3σ level or greater as a function of baseline. The LBNE beam design was optimized for each baseline. Projections assume $\sin^2 2\theta_{13} = 0.09$ and a 35-kton LArTPC as the Far Detector [7].

identification capability over a wide range of particle energies from a few MeV to tens of GeV, corresponding to the energy range of particles that must be measured to fully reconstruct beam-neutrino events. To enable precision measurements of the parameters that govern $\nu_\mu \rightarrow \nu_e$ oscillations at the LAr-FD surface location, the Far Detector design and reconstruction techniques will need to reduce the cosmic-ray background to a level comparable to or below that of the beam backgrounds.

A substantial component of the background for ν_e charged-current (CC) interactions comes from neutral-current (NC) interactions where a π^0 is produced. The π^0 decays to two γs which shower electromagnetically and can thus fake the electron signal from a ν_e interaction. NC interactions in which a charged pion is produced are the predominant background for ν_μ CC interactions in which the pion mimics a muon. Therefore, to study neutrino-flavor oscillations with high precision, the LBNE Far Detector must be capable of high-efficiency, high-purity $e/\mu/\gamma$ and $\pi/K/p$ separation.

Time Projection Chambers (TPCs) are the detectors of choice for low-rate, large-volume, high-precision particle physics experiments due to their excellent 3D position resolution and particle identification in large volumes. In addition to detailed event topologies and measurements of particle kinematics, dE/dx measurements allow TPCs to unambiguously distinguish electrons, muons, photons, kaons, pions and protons over a wide range of energies (see Figure 6–2).

The 10-kton LArTPC Far Detector, the LAr-FD, fulfills the high-mass requirement and provides excellent particle identification over a wide range of energies, as expected. The LAr-FD photon-detection system is integrated with the TPC to detect scintillation light from particle interactions in order to (1) determine the exact start time of the drift, and (2) enable the localization of cosmic-ray muons to reduce backgrounds within the neutrino-beam spill window. The "LBNE Case Study Report for a Liquid Argon TPC" [10] has further details on the performance metrics of the LAr-FD.

In addition to identifying the flavor of neutrino interactions, measurements of the spectra of the oscillated neutrino signals over a wide energy range are required to enable precision measurements of the oscillation parameters. The best neutrino energy resolutions are obtained using charged-current quasi-elastic (CCQE) events in which the scattering of the neutrino is almost elastic; only a charged lepton and one or more nucleons emerge from the target nucleus. The charged lepton in CCQE events carries most of the energy of the neutrino. Final State Interactions (FSI) inside the nucleus will alter the expected nucleon types and spectrum. Measurements of this effect in a detector with an argon target nucleus, would help improve the neutrino energy resolution for all CC events in the LAr-FD. Information on FSI in neutrino interactions on argon will be available from the ArgoNeuT and MicroBooNE [13] experiments, and, if sufficient resources are found to construct a near neutrino detector for LBNE, this detector would be able to make these measurements over precisely the energy regime of LBNE.

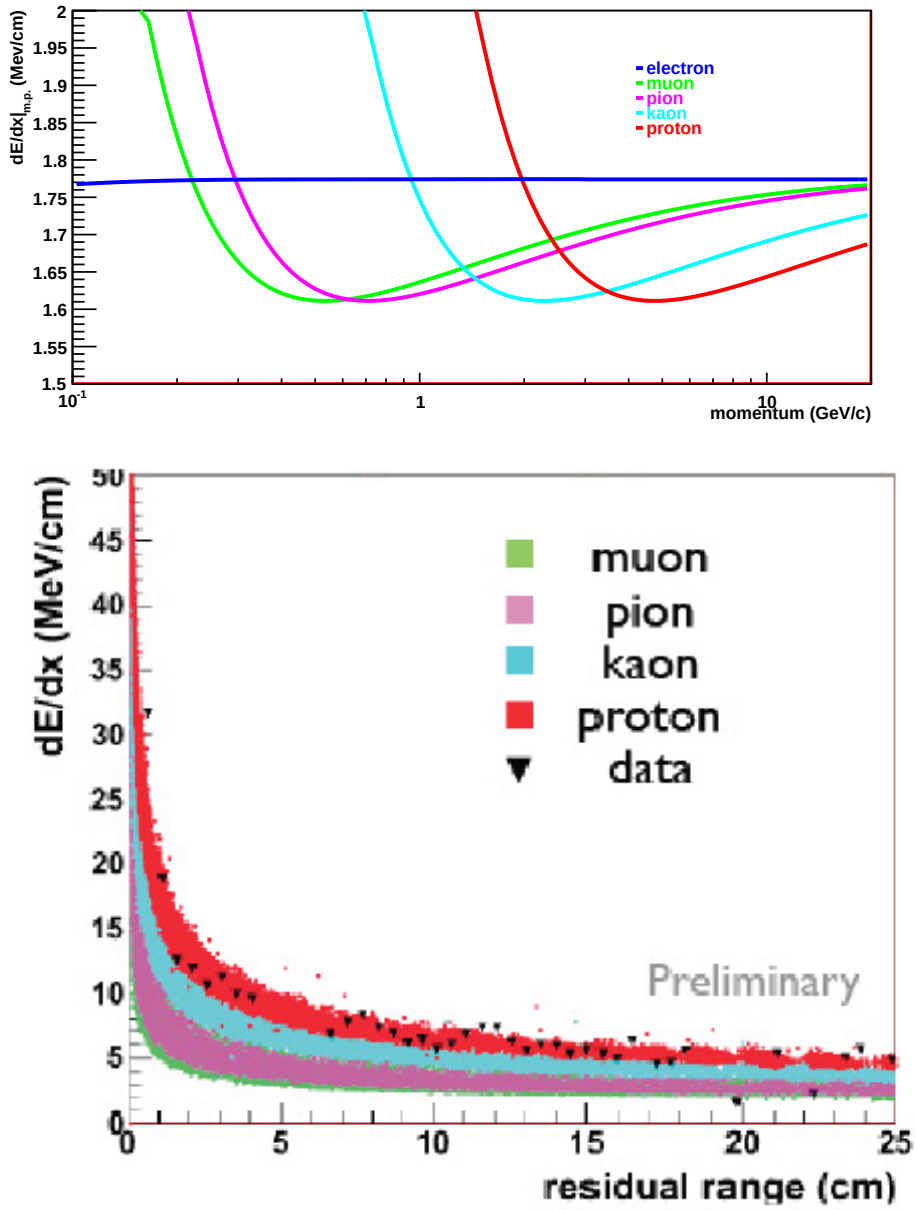

Figure 6–2: Distributions of dE/dx values for different charged particle species from a GEANT4 simulation of a liquid Argon TPC. The top plot is the most probable value of dE/dX vs particle momentum. The bottom plot is the value of dE/dx versus residual range from a GEANT4 simulation. The points are proton dE/dx measurements obtained from ArgoNEUT.

6.2 Accelerator-based Long-Baseline Neutrino Oscillations

The primary scientific objective for LBNE is the precision measurement of the parameters that govern neutrino oscillations over a long baseline, exceeding 1,000 km. Neutrino oscillations are described by the Pontecorvo-Maki-Nakagawa-Sakata (PMNS) leptonic mixing matrix [14]. Table 6–1 summarizes the current values of the neutrino oscillation parameters obtained from a global fit to experimental data [15]. A comparison to the equivalent mixing-parameter values in the quark CKM mixing matrix is also shown [14]. Clearly, the neutrino mixing parameters are not known nearly as precisely as are those in the quark sector.

Table 6–1: Best fit values of the neutrino mixing parameters in the PMNS matrix (assumes normal hierarchy) and comparison to the equivalent values in the CKM matrix from [15,14]. Δm^2 is defined as $m_3^2 - (m_1^2 + m_2^2)/2$.

Parameter	Value (neutrino PMNS matrix)	Value (quark CKM matrix)
θ_{12}	$34 \pm 1^\circ$	$13.04 \pm 0.05^\circ$
θ_{23}	$38 \pm 1^\circ$	$2.38 \pm 0.06^\circ$
θ_{13}	$8.9 \pm 0.5^\circ$	$0.201 \pm 0.011^\circ$
δm^2	$+(7.54 \pm 0.22) \times 10^{-5}$ eV^2	
$\lvert\Delta m^2\rvert$	$(2.43^{+0.10}_{-0.06}) \times 10^{-3}$ eV^2	$m_3 >> m_2$
δ_{CP}	$-170 \pm 54^\circ$	$67 \pm 5^\circ$

The observation of $\nu_\mu/\bar{\nu}_\mu \rightarrow \nu_e/\bar{\nu}_e$ oscillations in the neutrino-energy region from 0.5 to 5 GeV at 1,300 km, and measurement of their characteristics, would enable the unambiguous determination of the neutrino mass hierarchy and the measurement of δ_{cp}, the CP phase. Figure 6–3 shows the $\nu_\mu \rightarrow \nu_e$ oscillation probability (colored curves) at 1,300 km for $\sin^2 2\theta_{13} = 0.1$ and various values of the unknown CP violating phase, δ_{cp}. A detailed GEANT4 [16] simulation (see Figure 6–4) of the LBNE beamline, described in Volume 2 of this CDR, is used to estimate the neutrino flux at the far detector.

Table 6–2 lists the neutrino-interaction rates for all three known species of neutrinos as expected at the LBNE Far Detector site. A tunable beam spectrum, obtained by varying the distance between the target and the first focusing horn (Horn 1), is assumed. The concept is illustrated in Figure 6–5, and examples of three possible beam tunes are shown in Figure 6–6.

6.2.1 Measurement of the Unoscillated Neutrino Flux at the Near Detector Complex

Precise measurement of the parameters governing beam-neutrino oscillations at the Far Detector depends on comparison of the observed ν_μ or ν_e spectra with accurate predictions of the unoscillated spectra (flux and cross-section). The science and strategy for a long-baseline neutrino experiment near detector is detailed in [17].

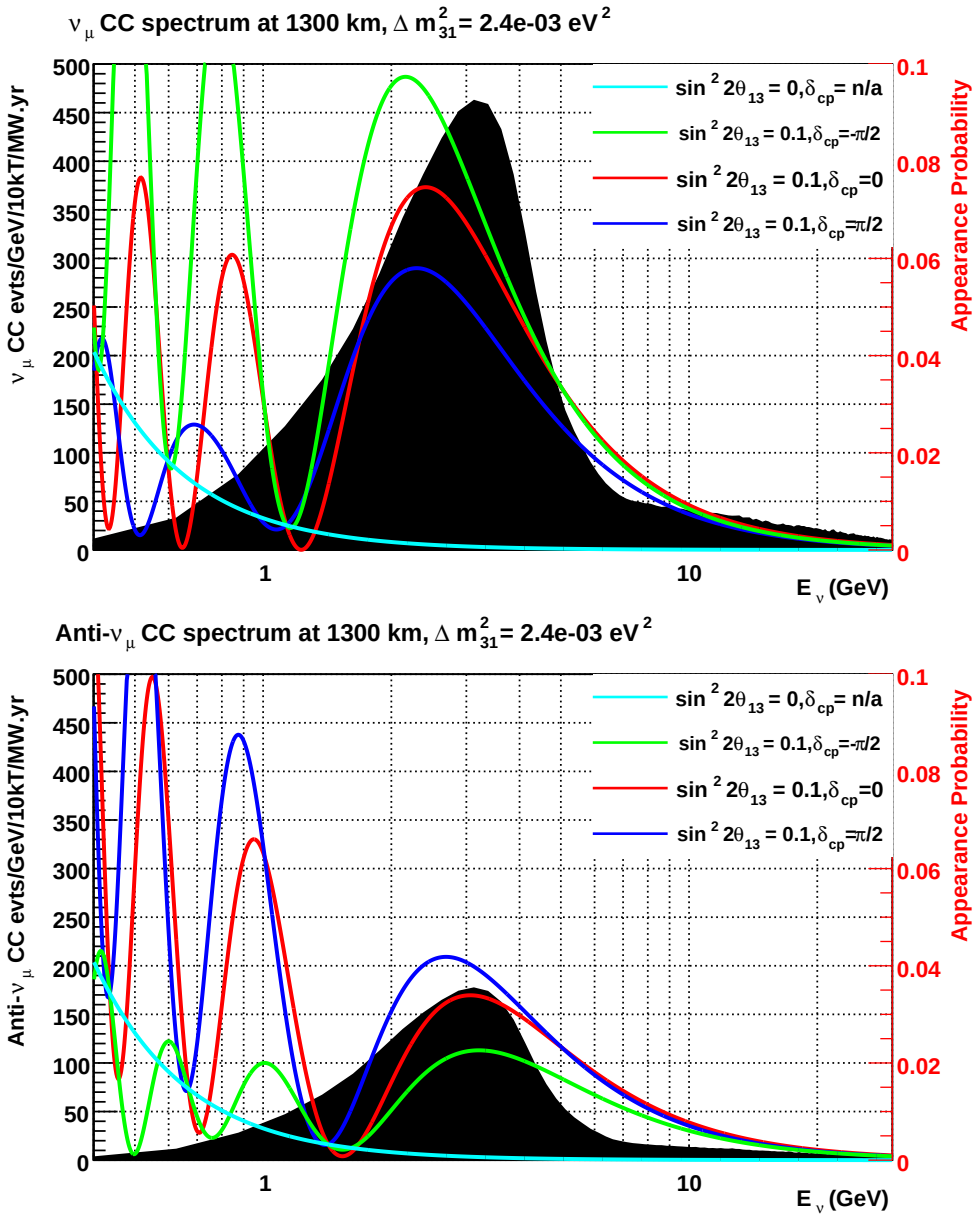

Figure 6–3: The $\nu_\mu \to \nu_e$ (top) and $\bar{\nu}_\mu \to \bar{\nu}_e$ (bottom) oscillation probabilities at 1,300 km for $\sin^2 2\theta_{13} = 0.1$ and normal hierarchy. The colored curves are for various values of the CP-violating phase δ_{cp}. The cyan curve shows the ν_e appearance probability from the solar oscillation term only. The black histograms are the unoscillated ν_μ and $\bar{\nu}_\mu$ CC spectrum at 1300km from the low-energy (LE) beam tune.

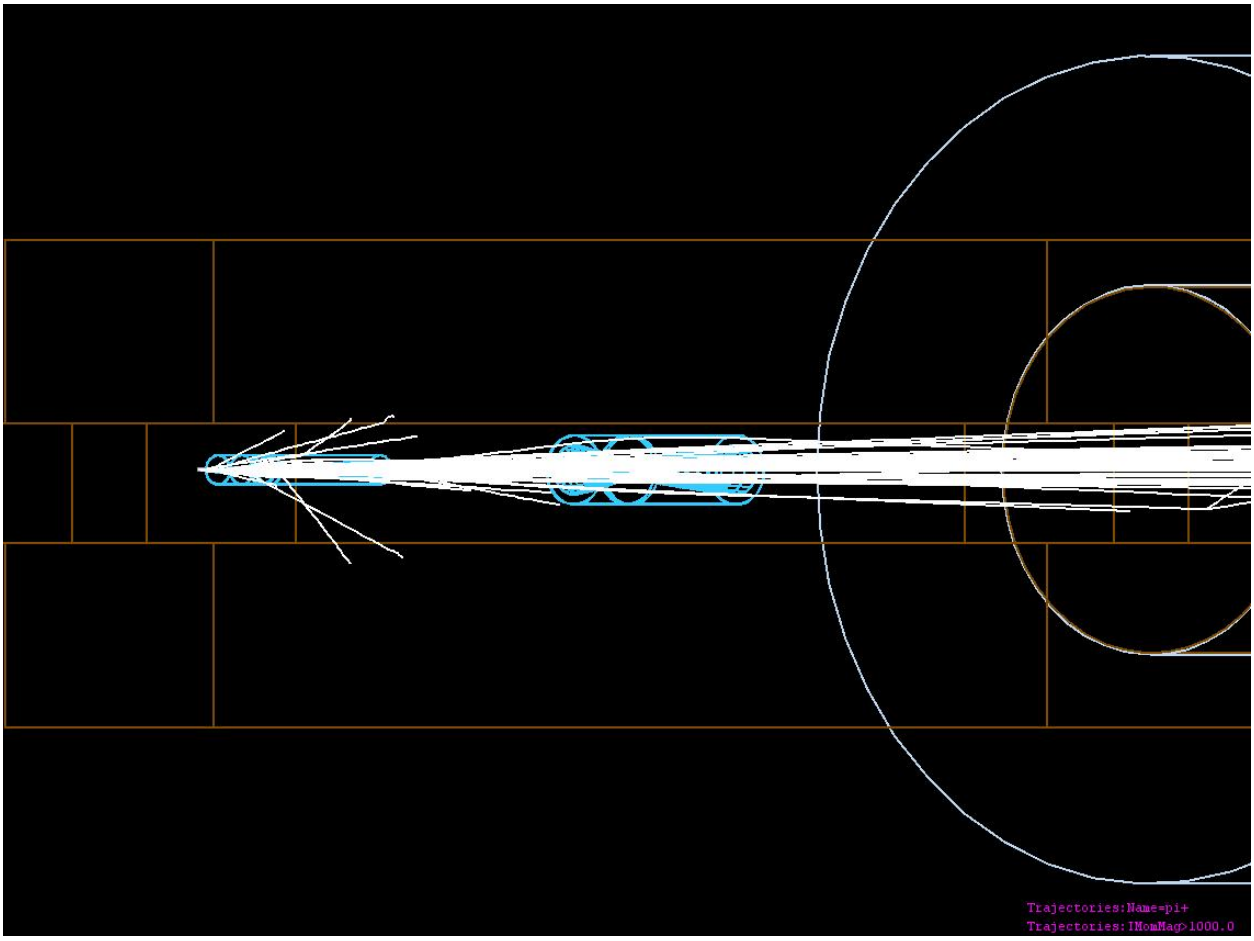

Figure 6–4: The GEANT4 simulation of the LBNE beamline. The 120 GeV proton beam is incident from the left. The NuMI horns are drawn in blue. The white lines are π^+ tracks with momenta > 1 GeV emerging from the target and entering the decay pipe at right.

Table 6–2: ν_μ, ν_τ, ν_e interaction rates per 10 kton.MW.yr (10^{21} protons-on-target) at the Far Detector site in LBNE for different beam tunes obtained by moving the target w.r.t. horn 1. Normal hierarchy, $\sin^2 2\theta_{13} = 0.1,\ \delta_{cp} = 0$. The rates are integrated in the region 0.5-20 GeV. The first column of numbers is the unoscillated ν_μ total charge-current interaction rate. The second column of numbers is the rate of ν_μ CC interactions expected given $\nu_\mu \to \nu_\mu$ oscillations.

Target Position	ν_μ CC	ν_μ CC osc	ν_μ NC	ν_e CC beam	$\nu_\mu \to \nu_e$ CC	$\nu_\mu \to \nu_\tau$ CC
-0.35 m (LE tune)	1.9K	720	420	29	80	9
-1.5 m (ME tune)	3.4K	2.2K	764	35	97	44
-2.5 m (HE tune)	4.1K	3.2K	940	28	79	65

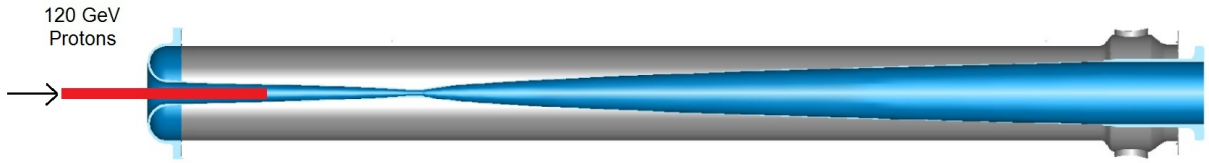

Figure 6–5: Configuration of movable target in Horn 1 to enable tuning of the beam. The horn has a double parabolic inner conductor (gray). The graphite target (red) is shown here partially inserted into Horn 1 in the Low-Energy (LE) beam tune position.

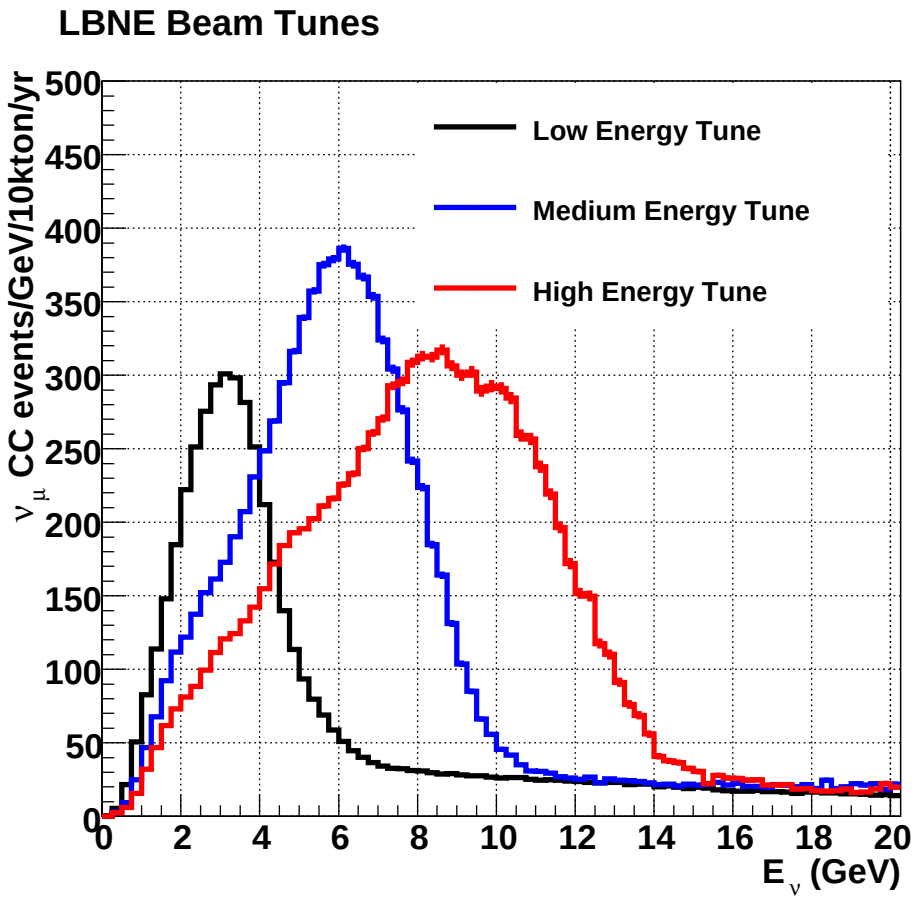

Figure 6–6: LBNE beam tunes produced by moving the target with respect to Horn 1. The default low-energy beam tune (black)is with the target partially inserted into Horn 1 as shown in Figure 6–5. Higher energy beam tunes can be obtained by moving the target out of Horn 1. For example, the medium energy tune (blue) is obtained by moving the target 1.5 m upstream of Horn 1. The highest energy tune available (red) is produced when the target is moved 2.5m upstream of Horn 1 - which is the maximum displacement of the target possible with the current carrier design. The beam is assumed to be 708 kW with 6.5×10^{20} protons-on-target/year

Modern long-baseline experiments with near neutrino detectors, such as MINOS [18], are able to predict the unoscillated spectra and backgrounds at the Far Detector with a precision of 5% or better. The LBNE conceptual design does not include a high precision near neutrino detector. An overview of previous $\nu_\mu \rightarrow \nu_e$ experiments lacking near neutrino measurements [17] indicates that the beam systematic uncertainty on the ν_e appearance signal varies from 5% (NOMAD) to 14% (BNL E776). The MiniBooNE experiment [19], for example, achieved a systematic uncertainty on the unoscillated flux of 9% using target hadron-production data to constrain the beamline simulation. The LBNE NDC comprises a beamline-measurements system (BLM) that will be used to extract a measurement of the LBNE unoscillated neutrino flux using the same technique that was used in NuMI [20]. The BLM system measures the flux of muons emerging from the neutrino beamline downstream of the absorber. Since the muons originate from the same hadron decays that produce ν_μ, the ν_μ flux can be extrapolated from measurements of the associated muons. The BLM is designed to measure the muon flux from the decays of $\pi^\pm \rightarrow \mu^\pm \nu_\mu$ and $K^\pm \rightarrow \pi^\pm \mu \nu_\mu$. The different detectors that comprise the NDC BLM are described in detail in Volume 3 of this CDR.

The following subsections describe the three techniques LBNE will use to obtain accurate simulations of its neutrino flux. The LBNE NDC plans to combine data from the NuMI beamline experiments such as MINOS and MINERνA with updated target hadron-production data and muon flux measurements from the LBNE BLM systems. Based on experience with current measurements from NuMI/MINOS, NA49 and expected updated hadron-production measurements from the NA61/Shine and MIPP experiments, it is expected that the LBNE unoscillated neutrino fluxes can be conservatively predicted to $\sim$10%. In-situ LBNE BLM measurements of the muon flux are expected to further improve the beamline simulation and predictions. For the $\nu_\mu \rightarrow \nu_e$ oscillation analysis, the oscillated ν_μ spectrum observed in the Far Detector can be used to further reduce the beam uncertainty on the ν_e appearance signal to $\sim$5%.

6.2.1.1 Beamline Simulation Tuning using NuMI Experiments

The LBNE beamline (described in Volume 2 of this CDR) is very similar to the NuMI beamline in design. The target and focusing horns are identical and in fact the only major difference is in the dimensions of the hadron decay pipe. (The length and diameter of the NuMI decay pipe are 675 m and 2 m, respectively, whereas LBNE's will be 204 m and 4 m.) The LBNE beamline simulation is therefore based on NuMI's, which has been tuned using MINOS near detector data at different beam energies, as shown in Figure 6–7.

The tuning involves reweighing the p_t, p_z distribution of the parent hadrons from the proton beam target and varying the production ratios of the different hadrons from the target as shown in Figure 6–8 [18]. In addition, the horn focusing and some cross section parameters are allowed to vary within modeling uncertainties.

As a result of the tuning, the NuMI simulation is able to model the MINOS near detector ν_μ and $\bar{\nu}_\mu$ spectra to better than 10% in the energy region from 0.5 to 10 GeV. The more finely segmented MINERνA detector [21], located upstream of the MINOS near detector, will carry out even more precise measurements of the unoscillated NuMI beam flux and is expected to further constrain the simulation of the NuMI beam. MINERνA data will also provide information on the ν_e component of the beam.

6.2.1.2 External Target Hadron Production Data

Measurements of hadron production from graphite targets in other experiments are critical to achieve a high-precision simulation of the neutrino flux from the LBNE beamline. In Figure 6–8, hadron-production data from the NA49 experiment [24] are compared to the tuned NuMI MC and found to be in good agreement. In fact the NuMI beamline tune revealed that the majority of the discrepancy between the MC and near detector neutrino data could be attributed to the inaccuracy of the hadron-production models in the 2005 version of the FLUKA MC [22,23]. For LBNE, additional data from the NA61/Shine experiment [25] and the MIPP experiment [26] will be used to further improve the accuracy and precision of the LBNE beamline MC. These improvements in the beamline simulations can be benchmarked with the NuMI beam simulation.

6.2.1.3 In-situ Muon Flux Measurements

NuMI employs a beamline measurement system to (indirectly) measure the neutrino flux independently of its near neutrino detector. The technique involves extrapolating the neutrino flux from muon data collected by a system that monitors the muon flux in the tertiary beam downstream of the decay pipe. The charge in the NuMI muon monitors is measured using different beam tunes and horn currents as shown in Figure 6–9. LBNE's BLM design is based on NuMI's and uses the same technique [20], but provides significant improvements and is expected to validate and enhance the tuned simulations discussed above.

The NuMI muon monitors [27] are placed in alcoves at three separate locations downstream of the NuMI absorber to sample different portions of the muon spectrum (see Figure 6–10). Each monitor consists of a 9×9 pad ion-chamber array and samples the muon-beam profile to a radius of approximately 1 m. The alcoves are separated by layers of rock to range out muons so that the monitors in each alcove sample different portions of the muon spectrum. The muons must have initial momenta of 5, 12 and 24 GeV, respectively, to be detected at the three locations.

The LBNE BLM will sample the muon flux at six different locations downstream of the LBNE absorber. The locations are separated by walls of steel "blue blocks" that provide several depths at which to monitor the muons as they range out. The BLM employs three

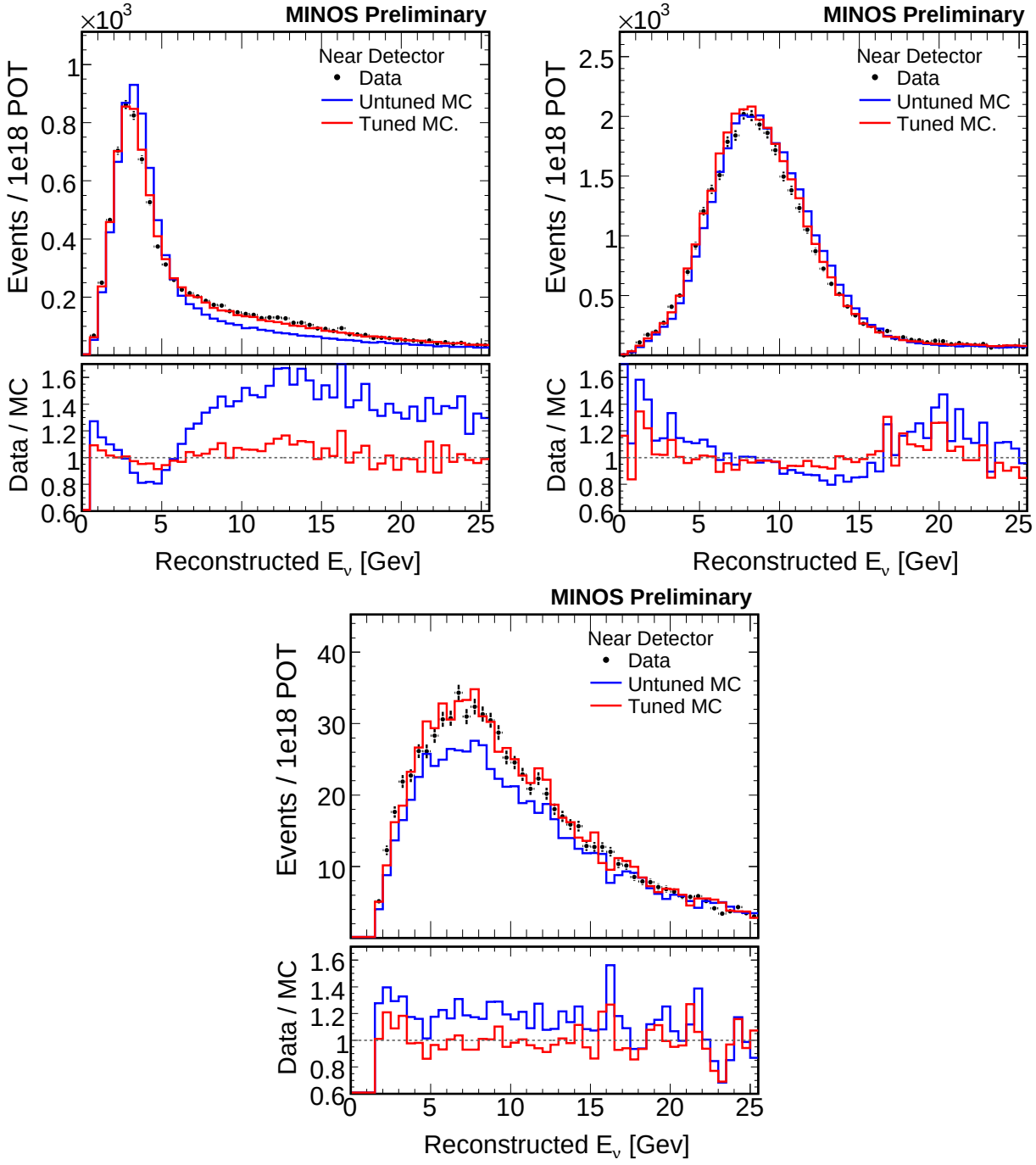

Figure 6–7: The MINOS near detector event spectra and the tuned MC predictions for the ν_μ CC signal from the low-energy tune (top left), the high-energy tune (top right) and $\bar{\nu}_\mu$ CC signal from the low-energy tune (bottom). The black data points with error bars represent experimental data from the MINOS near neutrino detector; the blue histogram shows the default FLUKA 2008 [22,23] MC and the red histogram shows the tuned MC.

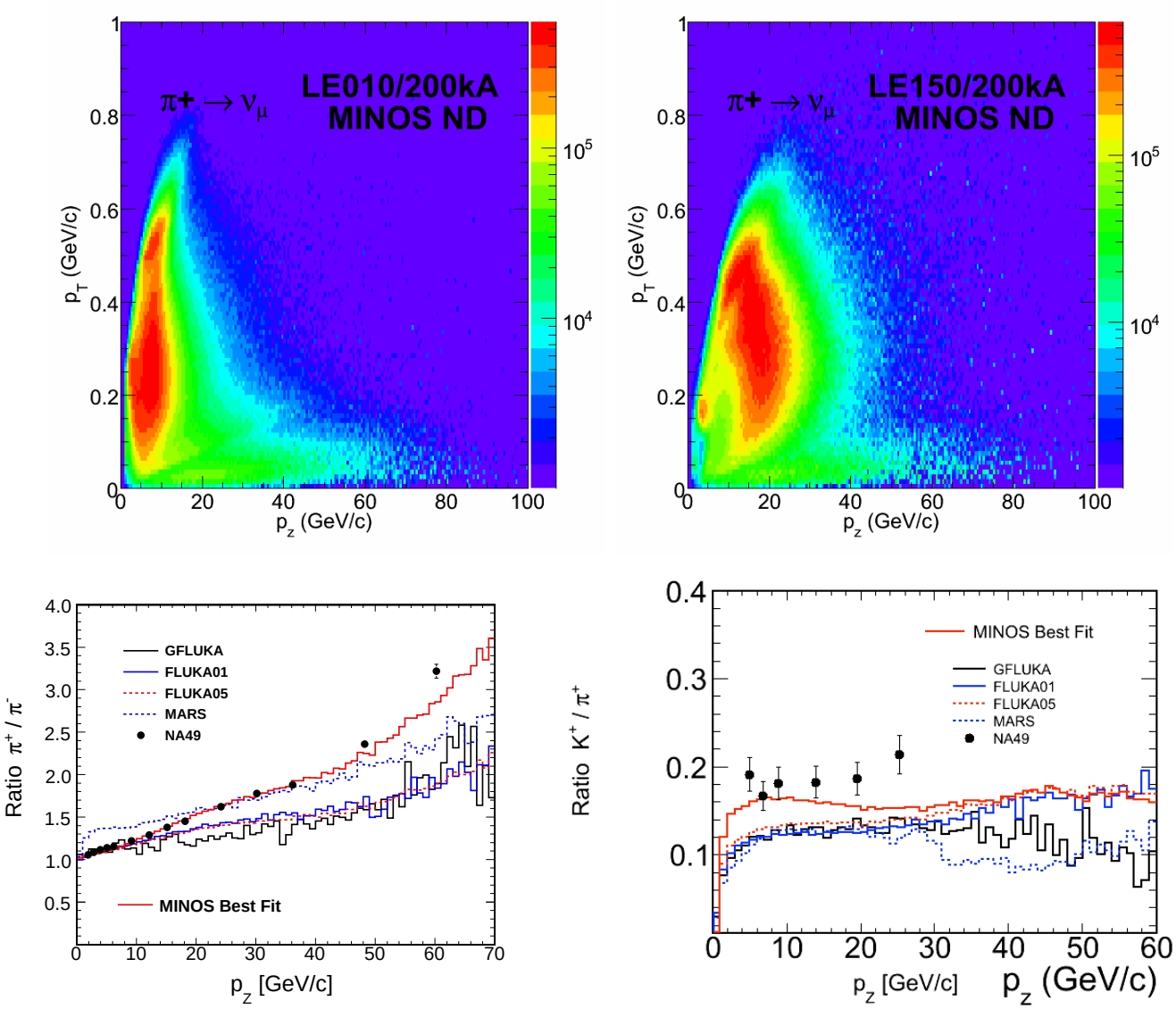

Figure 6–8: Tuning the MINOS MC to agree with the MINOS near detector and muon monitor data involves reweighing the p_t, p_z distribution of different beam tunes (top) of the hadrons produced from the target, varying the relative amount of different hadrons produced like the π^+/π^- ratio (bottom left) and the K^+/π^+ ratio (bottom right) to agree with the data from the near detector measurements. The tuned MC fit shown here (solid red line) is obtained by fitting the near neutrino detector data. Hadron production data from the NA49 experiment are shown as black points with error bars overlaid with the predictions from different simulation models, shown as colored histograms.

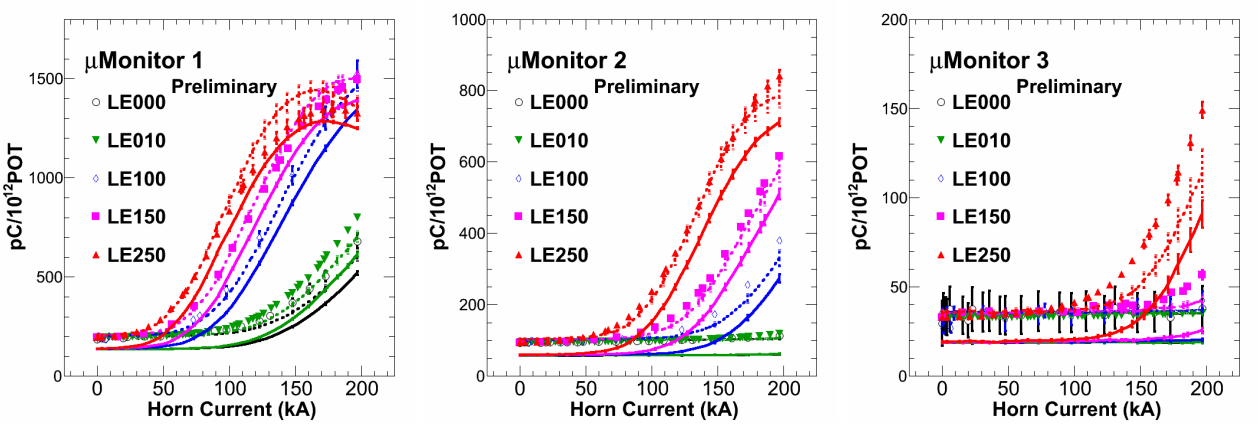

Figure 6–9: The NuMI muon monitor data [20] obtained by varying the beam tunes and varying the horn current. The data is shown as the solid colored points and the default MC prediction is shown as solid lines. The tuned MC prediction is shown as dashed lines and points. The different beam tunes are obtained by moving the target with respect to Horn 1. The tunes are target at -35cm (LE000), -45cm (LE010), -100cm (LE100), -150cm (LE150), and -250cm (LE250).

different detector technologies; the different detectors are distributed among the locations as shown in Figure 6–10. The technologies consist of:

- variable-pressure gas Cherenkov counters
- 5×5 ion-chamber array
- stopped-muon counters

NuMI uses a FLUKA05/GEANT3 simulation of its beamline to predict both the muon flux in each alcove and the neutrino beam spectrum in the neutrino detector. The simulation is tuned using the charge measurements in the muon monitors and utilizes the technique described in Figure 6–8, which is very similar to that used to tune the MC to the MINOS near detector data, described in Section 6.2.1.1.

The NuMI muon-monitor data and the corresponding simulation predictions are shown in Figure 6–9 [20]. The neutrino flux measurements obtained from the NuMI muon monitors and the systematic uncertainties are shown in Figure 6–11. The tuning of the NuMI beamline simulation using the NuMI muon-monitor measurements was limited by the lack of both accurate calibration data and estimates of the neutron and delta ray backgrounds in the ion chambers [20]. This is reflected in the estimate of the neutrino flux uncertainty, which is dominated primarily by background uncertainties. Target hadron-production uncertainties also contribute significantly to this uncertainty since reliable target hadron-production data were not available at the time.

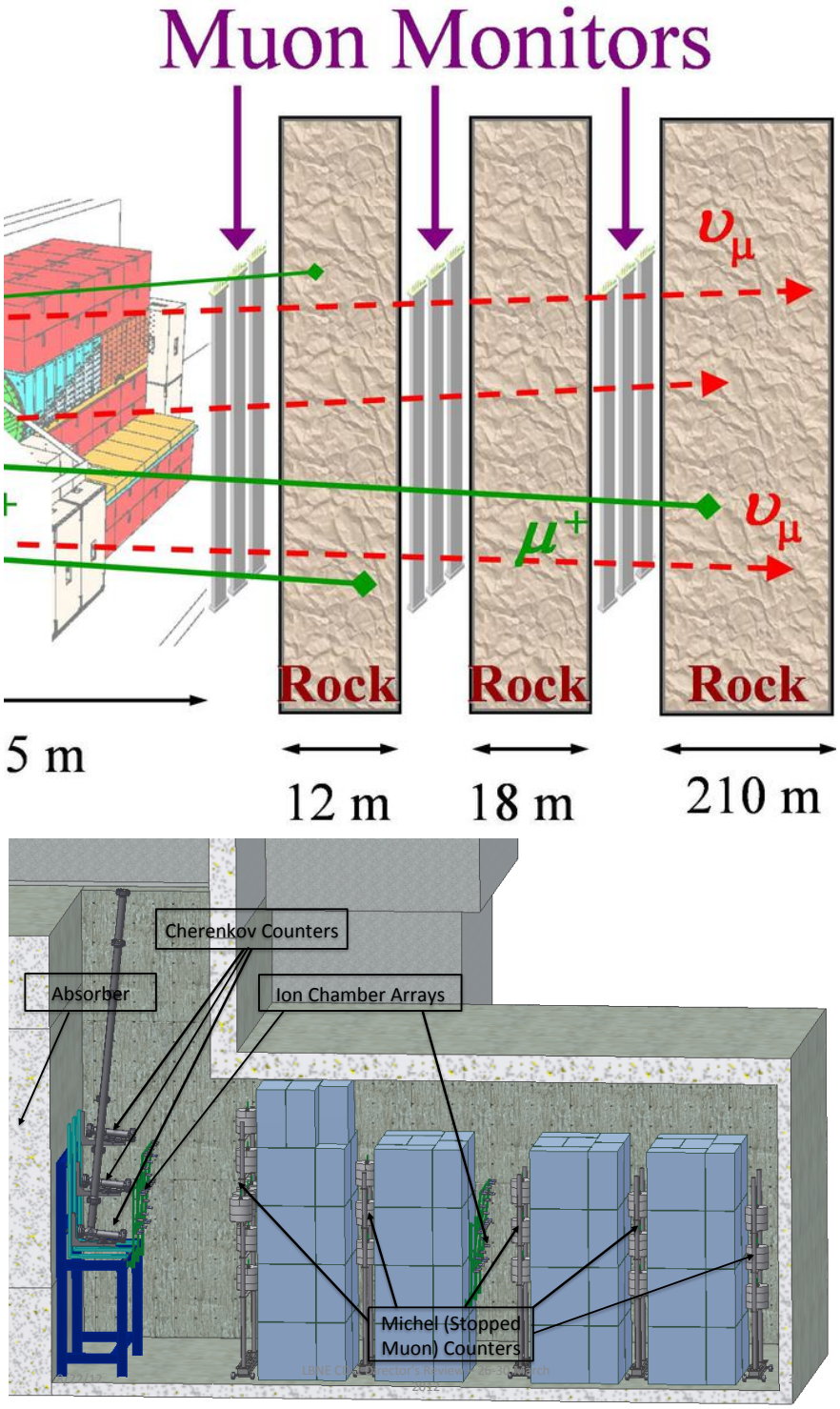

Figure 6–10: The NuMI muon beam measurement system (top) and LBNE BLM systems (bottom). The NuMI system comprises three detector alcoves each containing one array of 9×9 pad ionization chambers. The LBNE BLM system includes three different detector technologies distributed in six locations downstream of the absorber.

The LBNE BLM consists of a variety of detector technologies that improve on the ion-chamber arrays used by NuMI. The system will provide redundant measurements and will include more accurate calibration of the chamber responses. Prototypes of the LBNE muon chambers are scheduled for installation in the NuMI beamline in 2013 in order to carry out simultaneous measurement of the muon and muon-neutrino fluxes and to better understand background estimates.

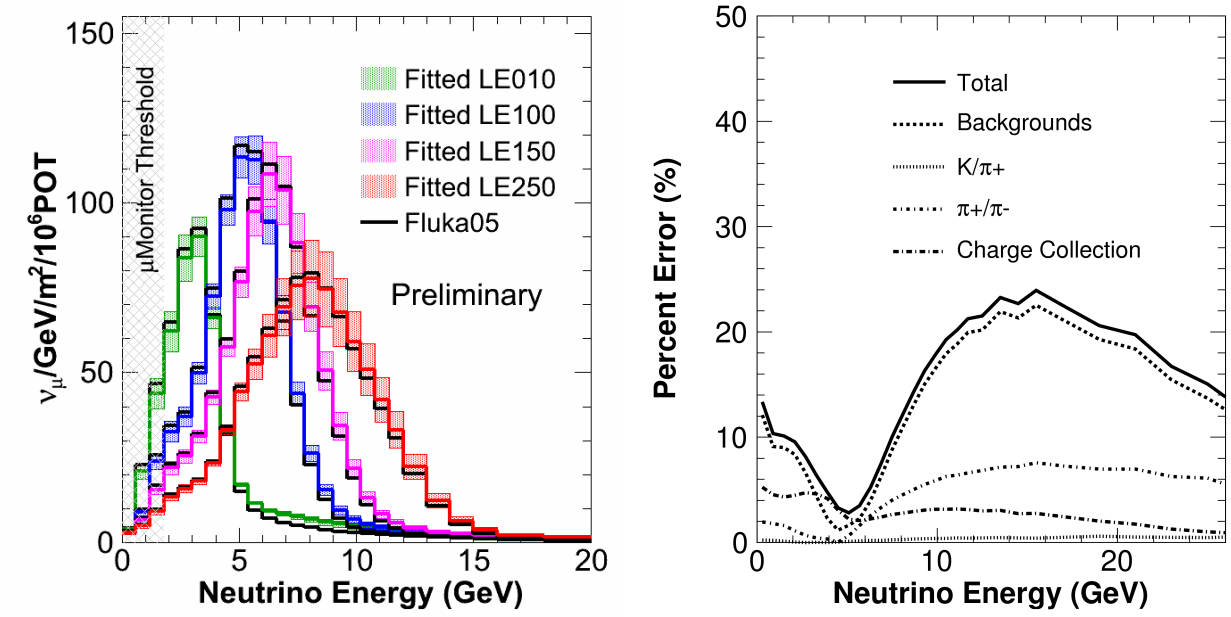

Figure 6–11: The NuMI flux prediction for 3 different beam tunes obtained by fitting the data in the 3 muon monitors is shown as the solid colored histograms (left). The black histogram is the untuned FLUKA 2005 MC prediction. The colored bands represent the uncertainty on the flux prediction from the muon monitors. The shaded gray area represents the region of the NuMI flux that is not sampled by the muon monitors. The plot on the right shows the breakdown of the uncertainties on the flux prediction of the low energy beam.

6.2.2 Measurements of Mass Hierarchy and the CP-Violating Phase

A primary science objective of LBNE is to make precise measurements of the parameters that govern $\nu_\mu \rightarrow \nu_e$ oscillations. These parameters probe CP violation in the neutrino sector and determine the neutrino mass hierarchy. The sensitivity of the LAr-FD for ν_e appearance physics is primarily dependent on the signal efficiency for detecting electron-neutrino interactions and the background rejection of neutral current (NC) events and ν_μ charged current (CC) events in the range of 500 MeV to 5 GeV. NC events containing π^0s are the dominant source of background from NC interactions. The π^0 decays to two photons which convert to e^+e^- pairs and initiate an electromagnetic shower that can be difficult to distinguish from an electron shower. High particle-identification efficiency and e/γ separation with high purity

Table 6–3: Description of the LAr-TPC simulations used to determine the performance for beam neutrino interactions.

Study	TPC geometry	Analysis technique
T2K 2km proposal [29] (2005)	140 tons, 4.5m(w)x4.5m(h)x5m(l) 2 readout chambers, 2 planes/chamber 3mm/6.4m wire pitch/length 2.21m/1.1ms max drift distance/time	Fully automated reconstruction, event topology, $\mu/\pi^{\pm}/K/p^{+}$ dE/dX and event kinematics included in a Random Forest analysis
Tufts Visual Scan [30] (2006)	Unknown	Blind visual scan visible energy precuts topology only
FNAL Visual Scan [31] (2008)	2.5m(w)x2.5m(h)x2.5m(l) 1 readout chamber, 2 planes/chamber 5mm and 10mm wire pitch	Blind visual scan MC truth used in precuts topology and dE/dX included in a log-likelihood analysis
FNAL Visual Scan [32] (2011)	MicroBooNE TPC	Blind visual scan topology only

is required to distinguish ν_e CC from ν NC events. Excellent μ/e separation is also required to enable the distinction of ν_μ and ν_e CC interactions.

In addition to measurements of the CP parameters, LBNE will search for physics beyond the Standard Model with high-precision measurements of the parameters Δm^2_{32} and $\sin^2 2\theta_{23}$ in ν_μ and $\bar{\nu}_\mu$ long-baseline oscillations. These measurements require high-purity identification of ν_μ CC interactions, which requires high-precision separation of $\mu/\pi/p^{+}$. The strength of the LAr-FD is the ability to use detailed event topology, particle kinematics and dE/dx to differentiate ν_e, ν_μ CC and NC π^0 event classes with high purity and efficiency as illustrated in Figure 6–12.

The expected performance of the LAr-FD is extrapolated from the analysis results obtained from four independent studies of massive LArTPCs. The four studies are detailed in references [29], [30], [31] and [32], and are summarized in Table 6–3.

The most detailed LArTPC performance parameters to date were obtained from studies by the ICARUS collaboration [33] and the 2-km detector proposal for the T2K experiment [29]. The simulated geometry of the TPC for the 2-km T2K proposal is summarized in Table 6–3. This study is the only one to use fully automated 3D event reconstruction combined with dE/dx particle id and event kinematics in an automated analysis. The neutrino-event reconstruction and analysis were optimized to separate ν_μ CC and ν_μ NC events, but did not include e/π^0 separation. As a result, the observed rate of 6.9% of NC events misidentified as ν_e CC is an over-estimate. A separate likelihood analysis of single electrons and π^0 interactions

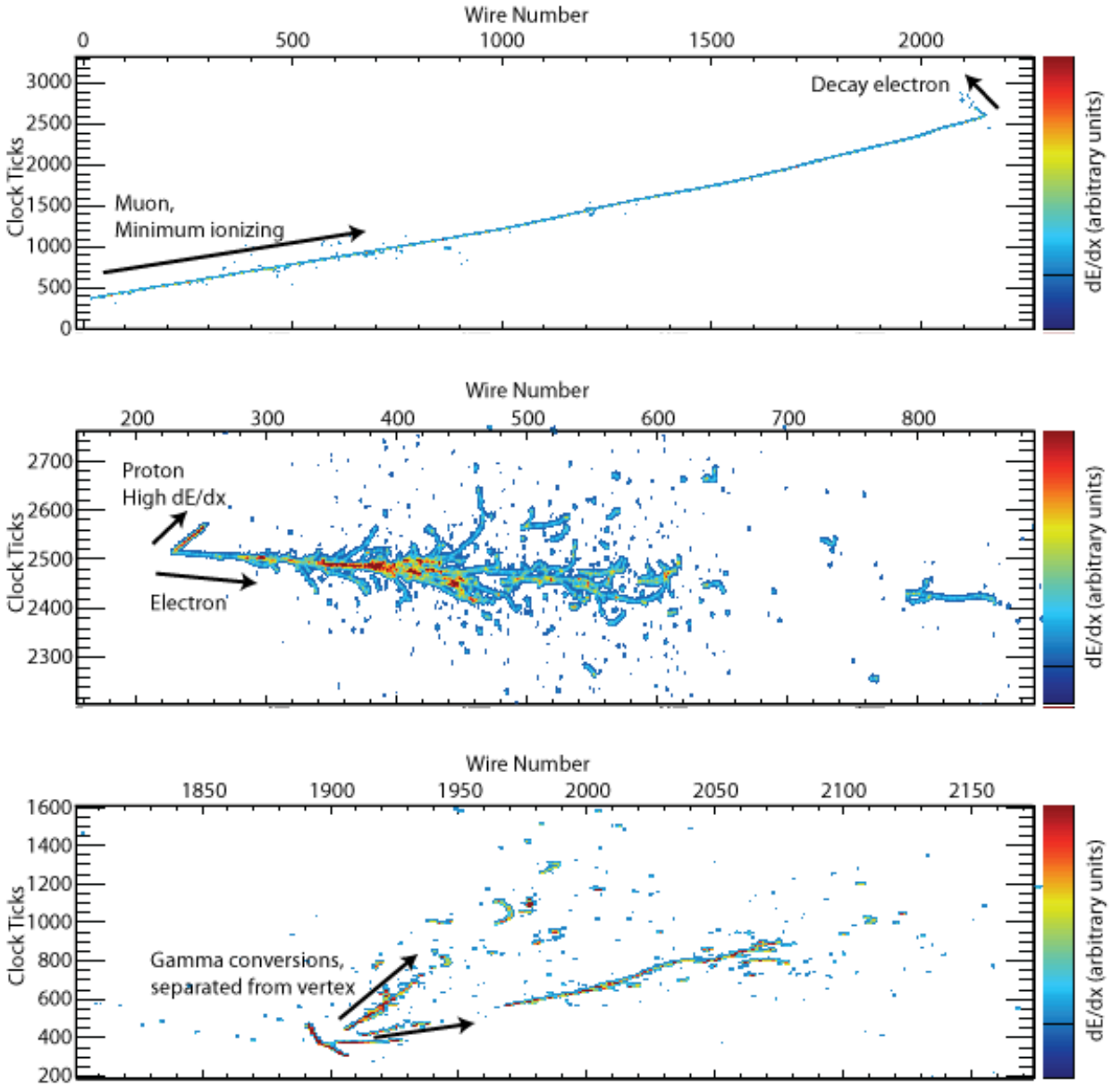

Figure 6–12: Examples of neutrino beam interactions in an LArTPC obtained from a GEANT4 simulation [28]. A CC ν_μ interaction with a stopped μ followed by a decay Michel electron (top), a CCQE ν_e interaction with a single electron and a proton (middle), an NC interaction which produced a π^0 that then decayed into two γ's with separate conversion vertices (bottom)

in the T2K 2-km LArTPC demonstrated that the single π^0 misidentification rate can be reduced to a few % using dE/dx alone, as shown in Figure 6–13. Therefore, the 6.9% NC misidentification rate could be greatly reduced by including e/π^0 separation in the analysis.

The last three studies in Table 6–3 comprise visual scans of simulated events in which

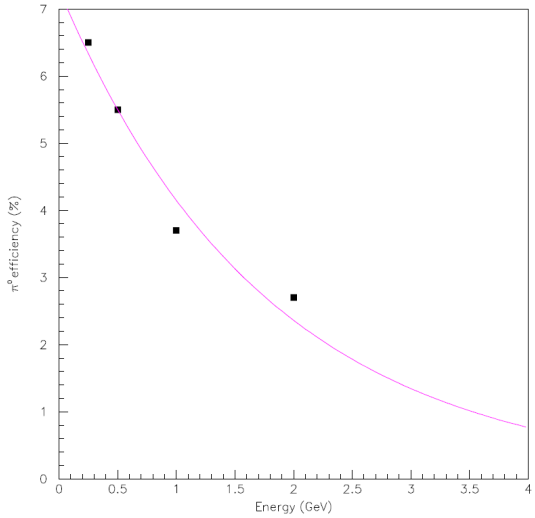

Figure 6–13: The electron mis-identification rate of single π^0 interactions as a function of the incoming π^0 energy [29].

researchers are trained to identify ν_e, ν_μ and NC π^0 interactions by studying event displays on an event-by-event basis. After training, the scanners are presented with a mixed sample of simulated events and asked to categorize them. Efficiencies are determined by comparing the scanners' results to the known event type. The selection efficiencies for signal-neutrino interactions and the rejection efficiencies for NC background, determined by the four studies summarized here, are shown in Table 6–4. There is general agreement between all four studies regarding the efficiency for identifying ν_e CC events in the few-GeV range; they find it to be between 70 and 95%. In addition, the reconstruction efficiency of ν_e CC as a function of neutrino energies has been found to be approximately flat for neutrino energies > 1 GeV, as shown in Figure 6–14. The misidentification rate of ν_μ CC events obtained from these studies is about 2%. Since optimized e/μ separation using dE/dx has not yet been implemented in these studies, the 2% ν_μ misidentification rate will be considered an upper limit.

A large variation is observed in the NC misidentification rate. The lowest rate was obtained by the visual scan study that included a crude dE/dx measurement combined with topology [31]. The estimation of the NC misidentification rate is further complicated by the fact that only the last study in Table 6–4 simulated ν NC interactions with energies >5 GeV. In the search for ν_e appearance by the MINOS experiment [34], which has a beam-neutrino spectrum and ν_e-signal range very similar to LBNE's, it was observed that $\approx$ 50% of the NC background in the 1–5 GeV signal region originated from NC inelastic interactions with neutrino energies >5 GeV. An example of the complicated topology of deep inelastic NC interactions is shown in Figure 6–15. Reliable estimates of the NC misidentification rate of such events are not available. Given the current knowledge of LArTPC performance from these studies, the LBNE NC misidentification rate is estimated to be between 2% (conservative) to 0.4% (aggressive), depending on how well e/π^0 separation techniques will perform in more complicated topologies.

Table 6–4: Selection efficiencies for ν_e CC candidates and ν_e misidentification rates for ν_μ CC and ν_μ NC determined by various studies. The / symbol indicates samples where the event size was too small to draw meaningful conclusions.

Study	**Average** ν energy	**# events** studied	ν_e **CC** ϵ_{select}	ν_μ **CC** $\epsilon_{\text{mis-id}}$	ν_μ **NC** $\epsilon_{\text{mis-id}}$
T2K 2km proposal (2005)	0.25-4.0 GeV	2000	94.5%	2%	6.9%
Tufts Visual Scan (2006)	NOνA beam 1.5-4.5 GeV	450	$72 \pm 5\%$	/	$1.3 \pm 0.4\%$
FNAL Visual Scan (2008)	NOνA beam 0.5-3.5 GeV	4997	$92 \pm 9\%$	/	$0.6 \pm 0.1\%$
FNAL Visual Scan (2011)	Uniform 0.5-15 GeV	1501	$90 \pm 1\%$	$2.0 \pm 0.6\%$	$5 \pm 1\%$

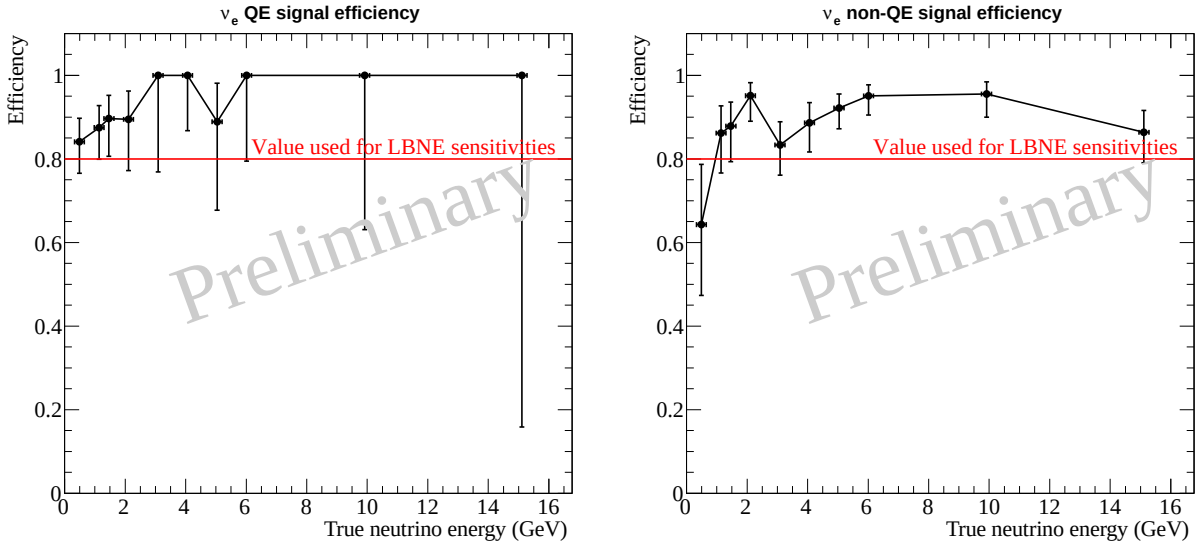

Figure 6–14: The efficiency, as determined by the 2011 Fermilab hand scan study [32] , of selecting ν_e CC quasi-elastic (left) and non-quasi-elastic(right) events.

For the neutrino-oscillation sensitivity calculations, information from the hand scans in Table 6–4 is used to set the detector-signal efficiencies and background-rejection efficiencies. Table 6–5 shows the range of ν_e selection efficiencies, background levels and neutrino energy resolutions from these hand scans, along with the specific values chosen for the long-baseline oscillation-sensitivity projections.

Studies from ICARUS have estimated and measured single-particle energy resolutions in LAr. Below 50 MeV, the energy resolution of electrons is $11\%/\sqrt{E[MeV]} + 2\%$. As shown

Table 6–5: Estimated range of the LAr-TPC detector performance parameters for the primary oscillation physics. Signal efficiencies, background levels, and resolutions are obtained from the studies described in this chapter (middle column) and the value chosen for the baseline LBNE neutrino-oscillation sensitivity calculations (right column). * For atmospheric neutrinos this is the mis-identification rate for < 2 GeV events, the mis-identification rate is taken to be 0 for > 2 GeV.

Parameter	**Range of Values**	**Value Used for LBNE Sensitivities**
For ν_e CC appearance studies		
ν_e CC efficiency	70-95%	80%
ν_μ NC mis-identification rate	0.4-2.0%	1%
ν_μ CC mis-identification rate	0.5-2.0%	1%
Other background	0%	0%
Signal normalization error	1-5%	1-5%
Background normalization error	2-15%	5-15%
For ν_μ CC disappearance studies		
ν_μ CC efficiency	80-95%	85%
ν_μ NC mis-identification rate	0.5–10%	0.5%
Other background	0%	0%
Signal normalization error	1-10%	5–10%
Background normalization error	2-20%	10-20%
For ν NC disappearance studies		
ν NC efficiency	70-95%	90%
ν_μ CC mis-identification rate	2-10%	10% *
ν_e CC mis-identification rate	1-10%	10% *
Other background	0%	0%
Signal normalization error	1-5%	under study
Background normalization error	2-10%	under study
Neutrino energy resolutions		
ν_e CC energy resolution	$15\%/\sqrt{E(GeV)}$	$15\%/\sqrt{E(GeV)}$
ν_μ CC energy resolution	$20\%/\sqrt{E(GeV)}$	$20\%/\sqrt{E(GeV)}$
E_{ν_e} scale uncertainty	under study	under study
E_{ν_μ} scale uncertainty	1-5%	2%

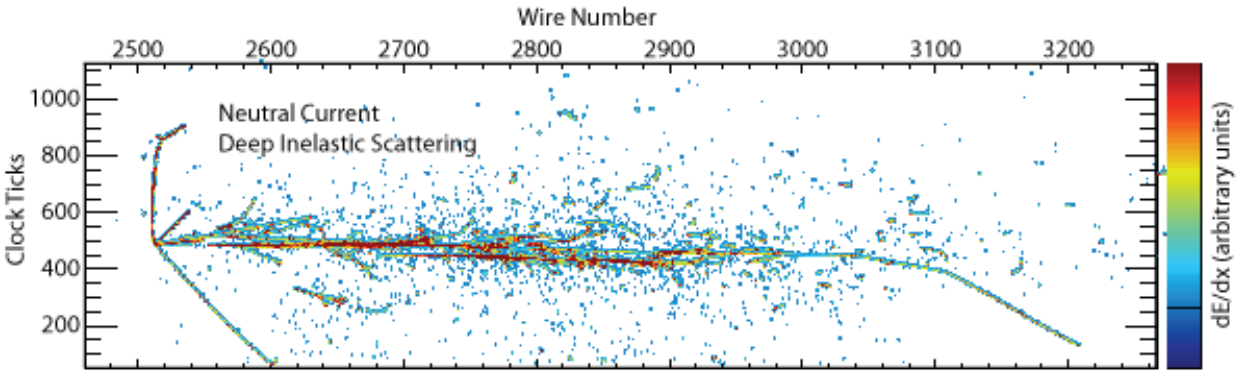

Figure 6–15: An example of a deep inelastic NC interaction in a LAr-TPC.

in Figure 6–16, the energy resolution of an electromagnetic shower with energy in the range (50–5000) MeV is $33\%/\sqrt{E(MeV)} + 1\%$ [35]. The energy resolution of hadronic showers in an LArTPC is $\approx 30\%/\sqrt{E(GeV)}$. A significant fraction of the ν_e CC signal in LBNE in the range of 1–6 GeV is non-quasi-elastic CC interactions with a large component of the visible energy in the hadronic system. From recent simulations of neutrino interactions in the region of 1–6 GeV it has been determined that $< E_{\rm lepton}/E_\nu > \approx 0.6$. For this reason, the total electron-neutrino energy resolution for the neutrino-oscillation sensitivity calculation is chosen to be $15\%/\sqrt{E(GeV)}$. In a non-magnetized LArTPC the muon momentum can be obtained from range and multiple scattering. The muon-momentum resolution is found to be in the range $10 - 15\%$ [29] [36] for muons in the 0.5–3 GeV range. Therefore the total muon-neutrino energy resolution in LBNE is assumed to be $20\%/\sqrt{E(GeV)}$.

In five years of neutrino (antineutrino) running, assuming $\sin^2(2\theta_{13}) = 0.1$, $\delta_{CP} = 0$, and normal mass hierarchy, a total of about 180 (62) selected $\nu_e(\overline{\nu}_e)$ signal events in a 10 kton LAr-FD are expected with a 708-kW beam. Table 6–6 is a summary of the expected number of signal and beam background events for ν_e and $\overline{\nu}_e$ running for normal and inverted hierarchy. The spectrum of expected signal and background events is shown in Figure 6–17.

A preliminary study of the expected non-beam background events expected from cosmic rays in the 10-kton LAr-FD located near the surface at SURF is detailed in [37]. The study simulated cosmic-ray interactions in the LAr-FD and focused on cosmic-ray induced signals from neutrons and muons that mimic electron-neutrino interactions, such as electromagnetic cascades from knock-on electrons, muon Bremstrahlung, and hadronic cascades with electromagnetic components from photons and π^0s. Backgrounds from decays of neutral hadrons into electrons such as $K^0_L \rightarrow \pi e \nu$ were also studied. The energy of the cascades was required to be > 0.1 GeV.

Initial studies indicate that a combination of simple kinematic and beam timing cuts will help in significantly reducing the cosmic-ray background event rate in the 10-kton LAr-FD.

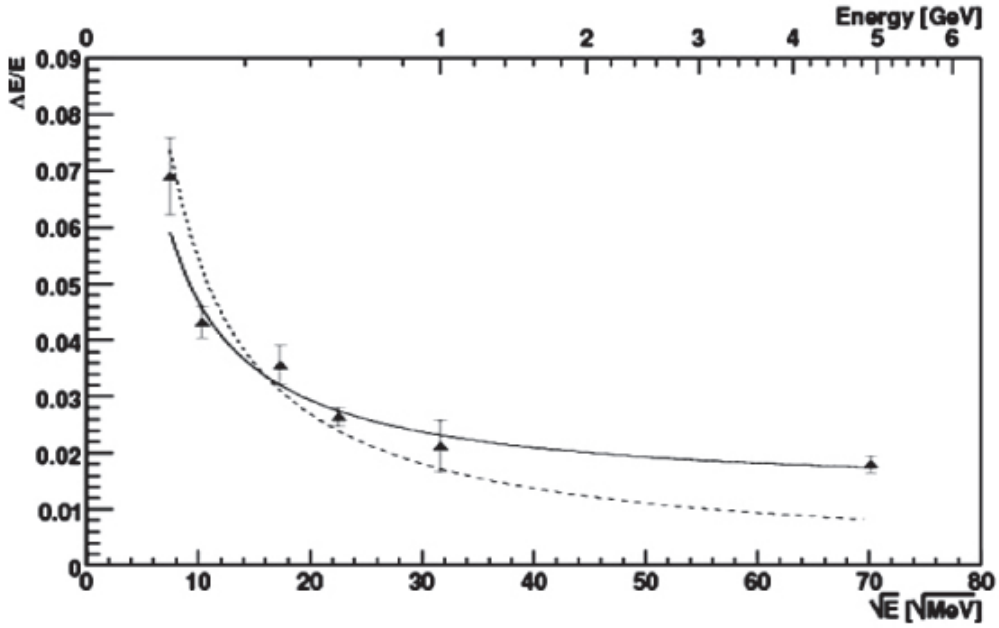

Figure 6–16: Resolution of electromagnetic showers from ICARUS [35]

In particular:

1. Only electromagnetic cascades with energies greater than 0.25 GeV are considered background (for the neutrino oscillation sensitivity calculations, only neutrino energies ≥ 0.5 GeV were considered)

2. $e^{\pm}$ background candidates are tracked back to the parent muon; the distance between the muon track and the point-of-closest-approach (PoCA) to the muon track is required to be > 10 cm

3. the vertex of the $e^{\pm}$ shower is required to be within the fiducial volume of the detector (defined as 30 cm from the edge of the active detector volume)

4. the $e^{\pm}$ cascade is required to be within a cone around the beam direction (determined from the angular distribution of the beam signal $e^{\pm}$ and the incoming neutrino beam)

5. it is assumed that em showers initiated by γ's and $\pi^0 \rightarrow \gamma\gamma$ can be effectively distinghuished from primary electron interactions using particle ID techniques such as dE/dX and the reconstructed event topology as shown in Figure 6–13

6. events are timed with a precision of ≤ 1 μ seconds using the photon detection system which limits backgrounds to events occuring within the 10μ seconds of the beam spill.

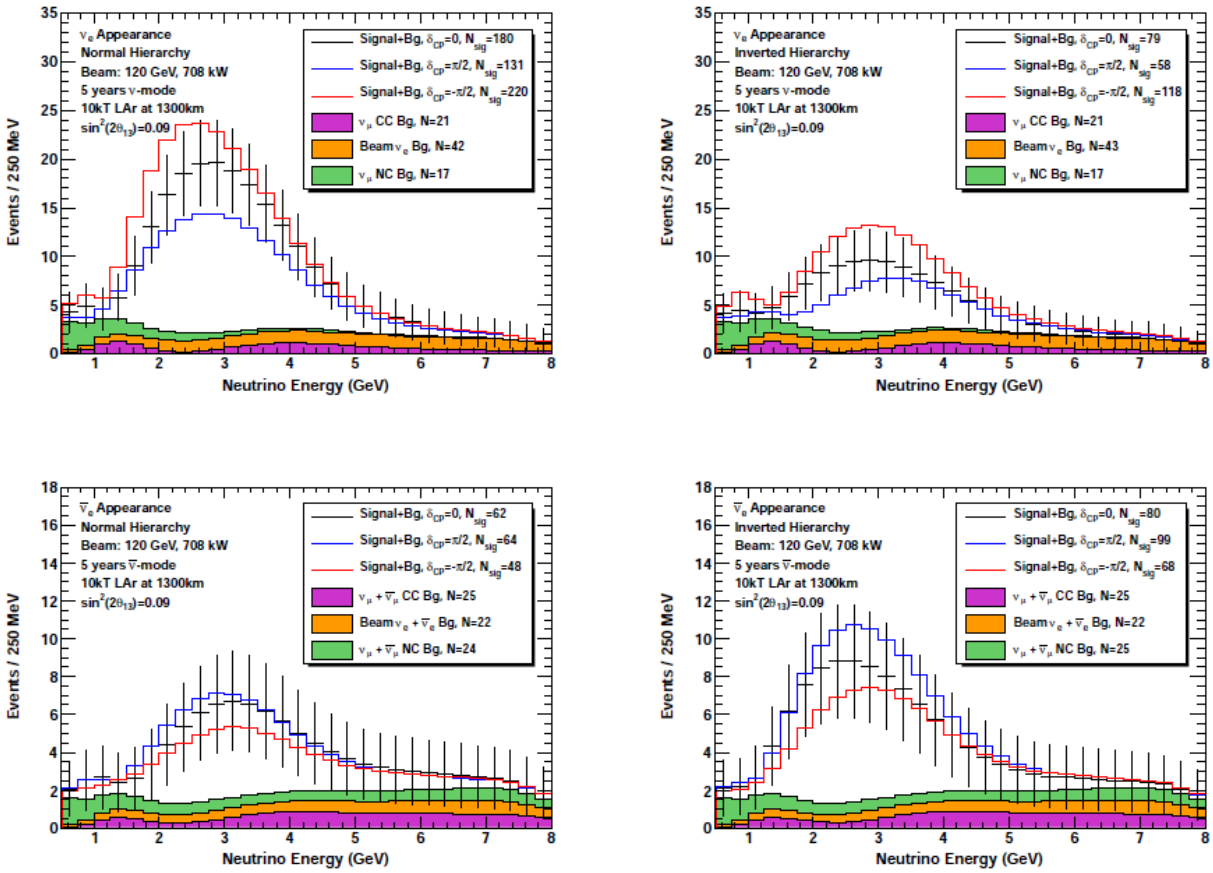

Figure 6–17: The expected spectrum of ν_e or $\overline{\nu}_e$ oscillation events in a 10 kton LArTPC for 5 years of neutrino (left) and antineutrino (right) running with a 708 kW beam assuming $\sin^2(2\theta_{13}) = 0.09$ for normal hierarchy (top) and inverted hierarchy (bottom). Backgrounds are displayed as stacked histograms.

The result of applying these selection criteria to the electromagnetic showers initiated by cosmics are summarized in Table 6–7.

The studies indicate that application of these selection critiria can potentially reduce the background from cosmic rays to a few events per year – mostly in the energy region < 1 GeV.

Although the preliminary studies outlined above indicate that it is feasible to reduce the cosmic-ray-induced background to a level below that of the beam background, a full simulation of the LAr-FD combined with advanced reconstruction techniques is needed for an accurate estimation of this background. Any such background will be accurately measured using off-spill data. It is assumed to be negligible when calculating sensitivities to neutrino-oscillation physics.

Table 6–6: Expected number of neutrino oscillation signal and background events in the energy range (0.5 – 8.0) GeV at the LAr-FD, assuming $\sin^2(2\theta_{13}) = 0.1$ and $\delta_{CP} = 0$, 10kt LAr-FD and 5 years of running with 6.5×10^{20} protons-on-target/year. The background from $\nu_\mu \rightarrow \nu_\tau \rightarrow \tau X \rightarrow e\bar{\nu}_e\nu_\tau X$ is estimated to be 2-3 events and is considered to be negligible.

	Signal Events	**Background Events**			
	ν_e	ν_μ CC	ν_μ NC	ν_e Beam	Total
Neutrino Normal Hierarchy	180	21	17	42	80
Neutrino Inverted Hierarchy	79	21	17	43	81
Anti-neutrino Normal Hierarchy	62	25	24	22	71
Anti-neutrino Inverted Hierarchy	80	25	25	22	72

Table 6–7: Cosmic ray backgrounds that produce electromagnetic showers in the detector and the expected event rate/yr after various selection critiria are applied from left to right. The initial background event rate is calculated assumning a 1.4 ms drift time per beam pulse, a beam pulse every 1.33 seconds and 2×10^7s of running/yr. The detector is assumed to be on the surface with 3m of rock overburden. Outer γ events are γ events that originate outside the detector and migrate into the active detector volume.

Background	$E_e > 0.25$ GeV	PoCA > 10cm	Fid > 30cm	Beam angle	e/γ PID	Beam timing
Muons in the detector						
$\mu^\pm \rightarrow e^\pm$	3.3×10^7	64	0	0	0	0
$\pi^0, K^0_L \rightarrow e^\pm$	940	170	170	68	68	0.5
$\pi^\pm, K^\pm, ... \rightarrow e^\pm$	7.4×10^5	2.7×10^3	43	17	17	0.12
$\pi^0 \rightarrow \gamma \rightarrow e^\pm$	1.6×10^5	2.0×10^4	1.9×10^4	7.5×10^3	150	1.1
$\mu \rightarrow \gamma \rightarrow e^\pm$	1.3×10^6	8.7×10^4	21	0	0	0
Outer $\gamma \rightarrow e^\pm$	4.7×10^5	4.6×10^3	530	210	4	0.03
Muons outside the detector						
Outer $\gamma \rightarrow e^\pm$	3.5×10^4	N/A	360	152	3	0.02
$\pi^0 \rightarrow \gamma \rightarrow e^\pm$	43	N/A	43	18	0.4	0.003
Cosmic neutrons from the surface						
Outer $\gamma \rightarrow e^\pm$	1.5×10^3	N/A	230	81	1.6	0.01
$\pi^0 \rightarrow \gamma \rightarrow e^\pm$	3.4×10^3	N/A	2.4×10^3	890	18	0.13
$n, \eta, \Sigma \rightarrow \gamma \rightarrow e^\pm$	140	N/A	110	37	0.75	0.05
Total $e^\pm$ background events/yr						
	3.7×10^7	2.2×10^5	2.2×10^4	9.0×10^3	270	2.0

The uncertainty on the ν_e signal prediction at the Far Detector is estimated to be around 1% with a high precision near detector, and 5% without a near detector as discussed in Section 6.2.1.1. The background uncertainties for the ν_e appearance signal is estimated to be 15% without a high-precision near detector. The background uncertainties are driven by the flux uncertainties, estimated to be around 10%, and the detector particle-identification and cross section uncertainties. With a 10-kton LAr-FD, the statistical uncertainties on the signal – especially in the anti-neutrino mode – are expected to dominate the sensitivity.

Figure 6–18 shows the significance with which the mass hierarchy can be resolved and the determination of whether CP is violated ($\delta_{cp} \neq 0$ or π) as a function of the value of δ_{cp}. The bands indicate the sensitivity range corresponding to different assumptions on background and signal normalization uncertainties. The range of assumptions covers the estimates of background and signal uncertainties that could be achieved with the currently planned tertiary muon detectors monitoring the beam or with a high-accuracy near neutrino detector.

For values of $\sin^2 2\theta_{13} = 0.092$, LBNE with a 10-kton LAr-FD can alone determine the mass hierarchy at the 3σ level for 75% of all values of δ_{cp} and will determine whether CP is violated for 25% of all δ_{cp} values at 2.5σ level [7]. A combination of the results from the LAr-FD with six years of NOνA running and the expected T2K data up to 2021 (5×10^{21} protons-on-target) [7] would enable a determination of both the mass hierarchy at $> 3.5\sigma$ for all values of δ_{cp} and the CP-violation at $\geq 3\sigma$ for 40% of all δ_{cp} values.

The precision on the simultaneous measurements of $\sin^2 2\theta_{13}$ and δ_{cp} that can be achieved with a 10-kton detector is shown in Figure 6–19 using different assumptions on signal and background normalization uncertainties. LBNE will be able to measure $\delta_{cp} = 0, \pi/2$ with a precision of $21^\circ, 34^\circ$ assuming $\sin^2 2\theta_{13}$ is externally constrained with an accuracy of 5%, which is the current systematic uncertainty from the Daya Bay experiment. LBNE can also independently measure $\sin^2 2\theta_{13}$ with a precision $\sim 10\%$, which is comparable to the current precision from the reactor experiments.

6.2.3 Precision Measurements of the Oscillation Parameters in $\nu_\mu \rightarrow \nu_x$ Oscillations

In addition to measurements of ν_e appearance, LBNE can make precise measurements of θ_{23} and $|\Delta m^2_{32}|$ using the $\nu_\mu/\bar{\nu}_\nu$-disappearance channel. Differences in the measured values of $|\Delta m^2_{32}|$ and $|\Delta \bar{m}^2_{32}|$ are sensitive to new physics arising from NC-like non-standard interactions [38] as described in Section 6.2.6.

The expected range of detector performance parameters for the ν_μ-disappearance channel are summarized in Table 6–5. The precision of the measurements of the oscillation parameters and searches for new physics using the $\nu_\mu/\bar{\nu}_\nu$-disappearance channel depends on the accuracy with which the unoscillated spectrum can be estimated using measurements from the near detector complex as well as external measurements and beam simulations.

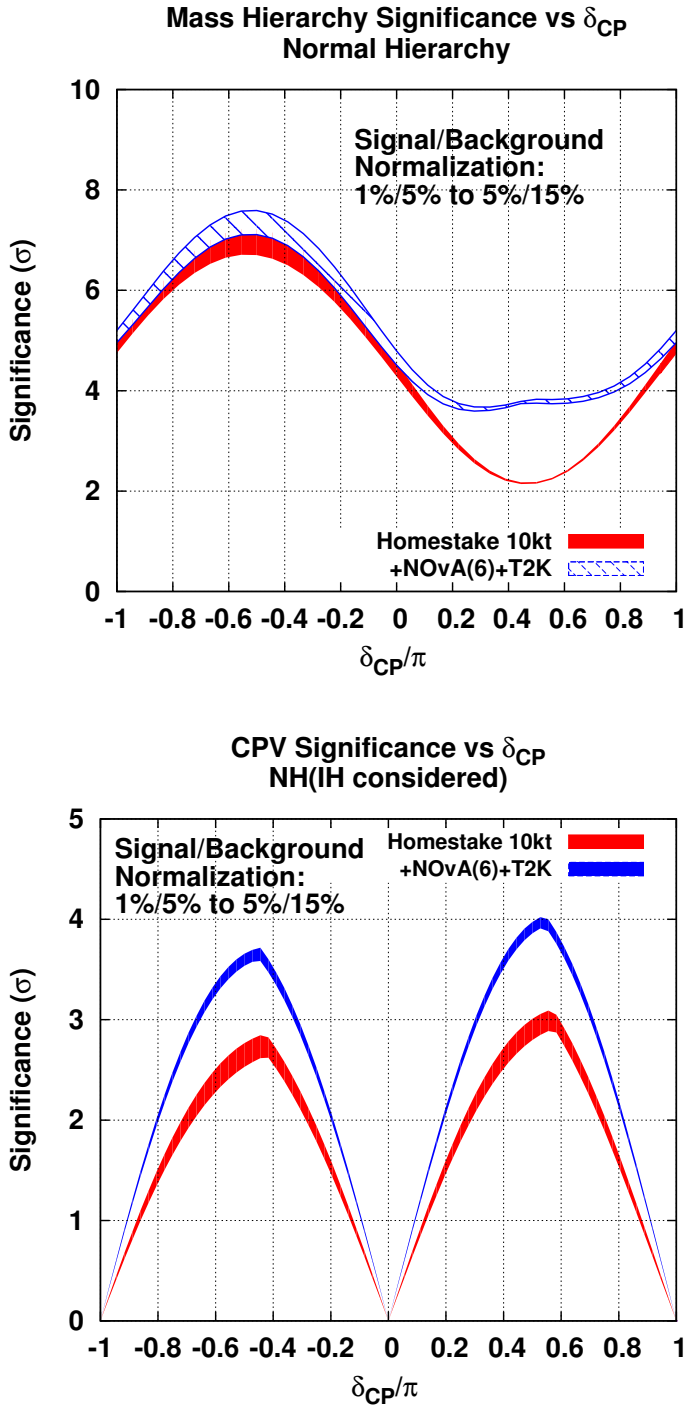

Figure 6–18: The significance with which the mass hierarchy (top) and CP-violation - $\delta_{cp} \neq 0$ or π - (bottom) can be determination as a function of the value of δ_{cp}. The significance is indicated for a 10-kton fiducial volume LAr-FD forfor 5+5 yrs ($\nu + \bar{\nu}$) running in a 708kW beam (6.5×10^{20} protons-on-target/yr). The curves in red show the sensitivity that is achieved by LBNE 10 kton alone. The curves in blue show the sensitivity obtained by combining LBNE 10 kton with T2K and NOνA. The bands indicate the sensitivity range corresponding to different assumptions on background and signal normalization uncertainties.

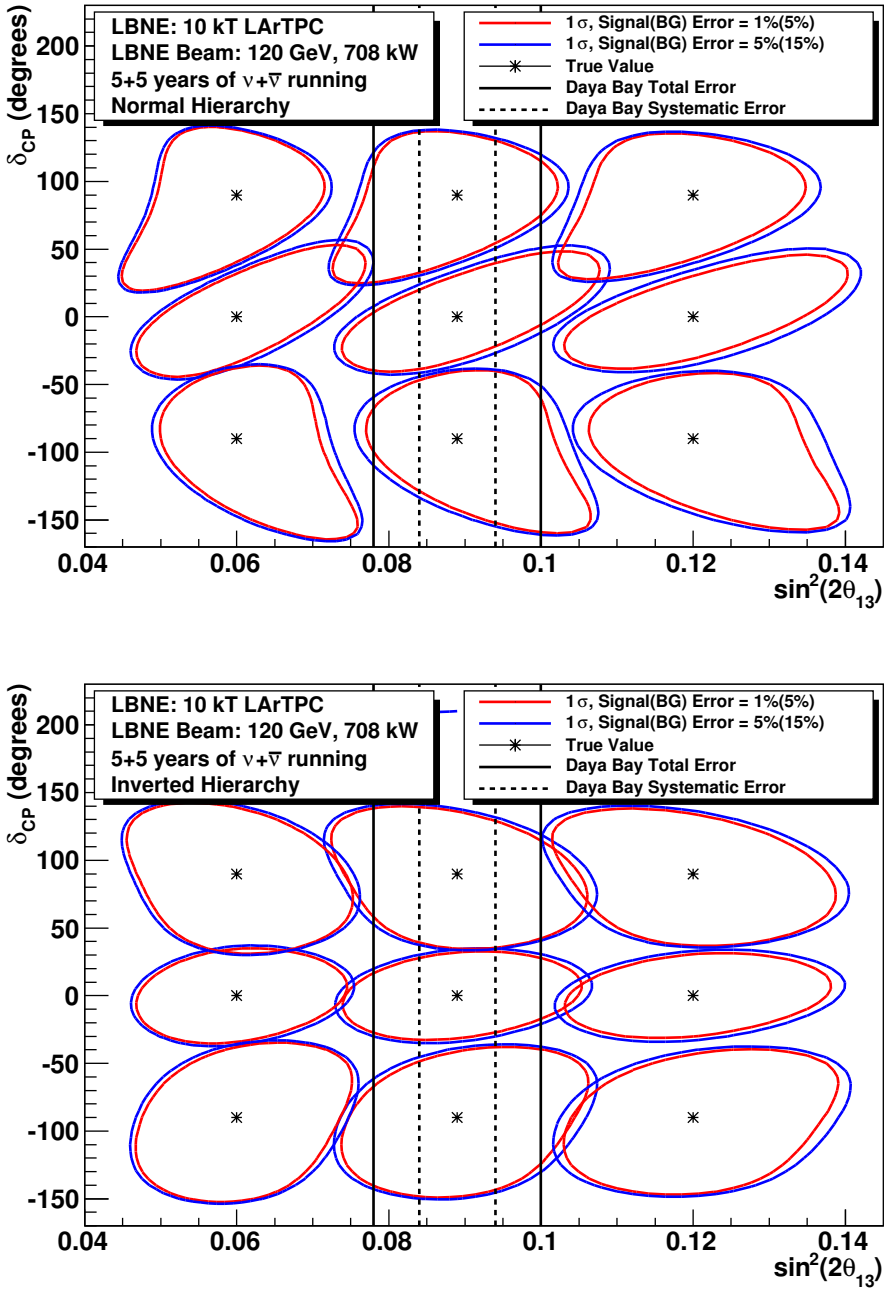

Figure 6–19: Fits to the values of $\sin^2 2\theta_{13}$ and δ_{cp} as a function of $\sin^2 2\theta_{13}$ for normal hierarchy (top) and inverted hierarchy (bottom). The LAr-FD detector mass is assumed to be 10 kton. The uncertainties on the signal/background are varied from 1%/5% (red) to 5%/15% (blue). The dotted and dashed lines represent the current 1σ bounds (dashed = systematics only, dashed = total) on the measurement of $\sin^2 2\theta_{13}$ from the Daya Bay experiment.

The predicted spectrum of oscillated ν_μ and $\bar{\nu}_\mu$ CC events in LBNE is shown in Figure 6–20.

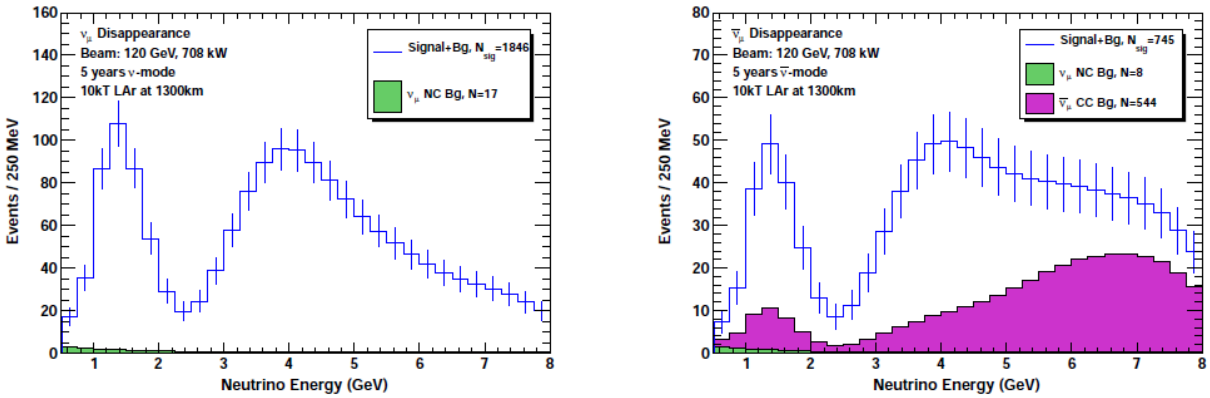

Figure 6–20: The expected spectrum of ν_μ or $\overline{\nu}_\mu$ events in a 10 kton LArTPC for five years of neutrino (left) and antineutrino (right) running with a 700 kW beam, with and without neutrino oscillation.

In Figure 6–21, the result from fits of the expected spectrum of $\nu_\mu/\bar{\nu_\mu}$ CC in the LBNE LAr-FD is shown for different values of Δm^2_{32} and $\sin^2 2\theta_{23}$ for neutrinos and antineutrinos. A $\nu_\mu/\bar{\nu_\mu}$ CC-reconstruction efficiency of 85% and a NC-contamination rate of 0.5% is assumed for these measurements. The signal and background normalization uncertainties are varied from 5–10% for the signal and 10–20% for the background. The larger uncertainties on the absolute normalization of the signal and background are to chosen to reflect a conservative estimate for how well the absolute flux could be determined using only the muon detectors at the near site. The 10-kton LAr-FD can achieve <2% precision on these parameters assuming the unoscillated ν_μ flux at the Far Detector can be estimated with a precision of 10% or better.

6.2.4 Observation of ν_τ Appearance

The LBNE baseline at 1,300 km will be longer than any long-baseline experiment currently in operation. As a result, ν_μ oscillations occur at higher energy and in particular the energy range is favorable to $\nu_\mu \rightarrow \nu_\tau$ appearance above the τ CC production threshold of 3.2 GeV, as shown in Figure 6–22. In this respect LBNE offers a unique ability compared to current long-baseline experiments in that oscillation between all three flavors of neutrinos could be explicitly observed in a single experiment. To increase the ν_τ CC appearance signal, several high-energy beam tunes produced by moving the target further upstream of LBNE Horn 1 are being considered.

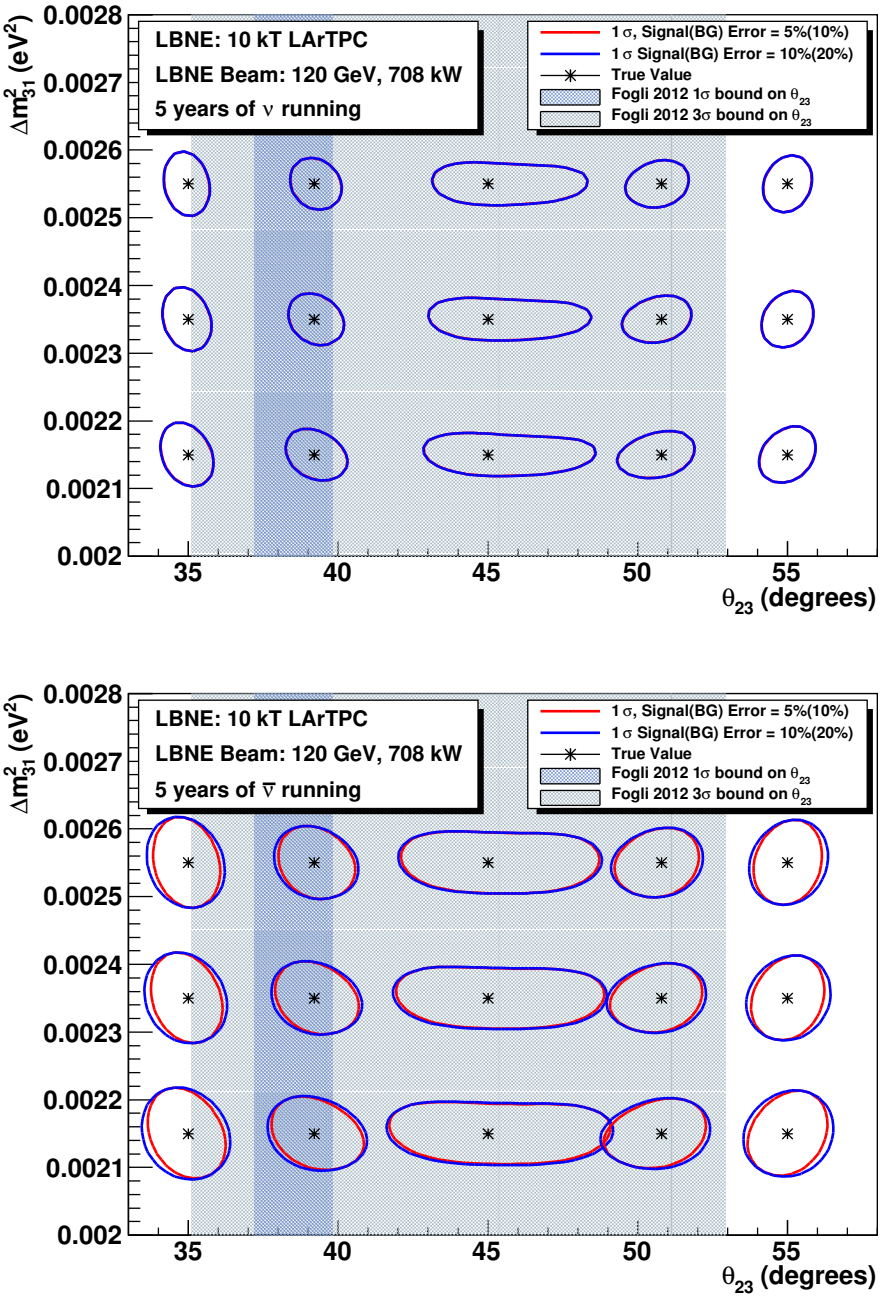

Figure 6–21: Fit to different values of Δm^2_{32} and θ_{23}, for neutrino running (top) and anti-neutrino running (bottom). The LAr-FD detector mass is assumed to be 10 kton. The signal/background normalization uncertainties are assumed to be 5%/10% (red) and 10%/20% (blue). The shaded bands reflect the current 1 and 2 σ uncertainties on θ_{23} obtained from a global fit [15].

In Table 6–2, ν_τ CC appearance rates for several LBNE beam tunes are shown. The first row in Table 6–2 corresponds to the low-energy beam tune used for the primary oscillation physics

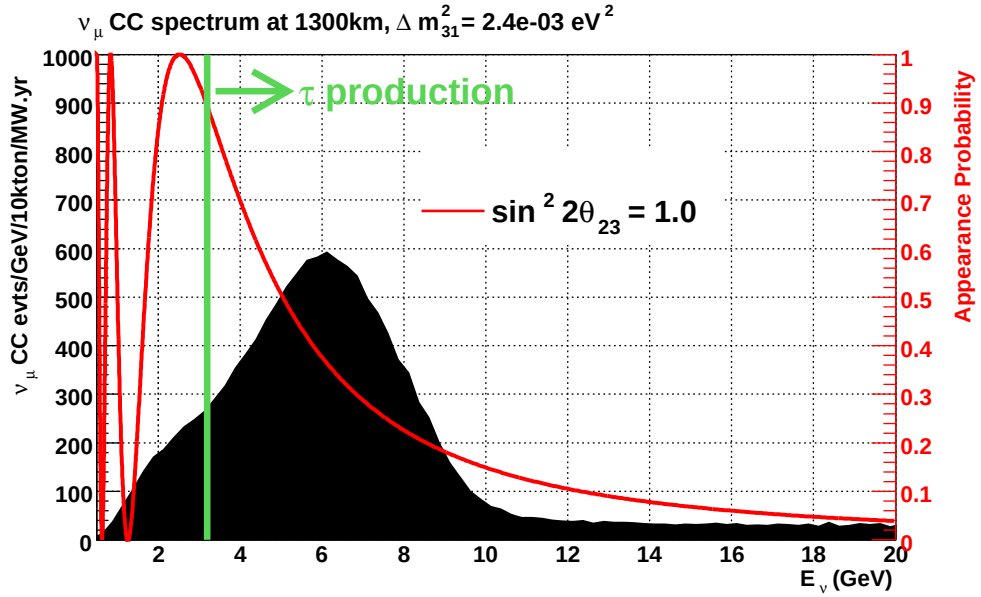

Figure 6–22: The $\nu_\mu \rightarrow \nu_\tau$ oscillation probability (red curve) at 1300 km for $\sin^2 2\theta_{23} = 1.0$. The shaded histogram is the unoscillated ν_μ CC spectrum at 1300 km from the medium-energy (ME) beam tune.

analysis. The last two rows correspond to two proposed high-energy beam tunes produced by pulling the target back by 1.5 m and 2.5 m, respectively, from a double parabolic Horn 1. The higher-energy beam tunes can be used to greatly enhance the ν_τ appearance rate. In particular, the medium-energy (ME) tune has high appearance rates for ν_e and ν_τ. It is to be noted that the OPERA experiment which has observed $\nu_\mu \rightarrow \nu_\tau$ appearance in the ν_τ CC mode [39] expects an interaction rate of 2 ν_τ events/1.25 kton/year compared to LBNE which would record a rate of ~ 30 ν_τ events/10 kton/year in the ME beam.

6.2.5 Resolving the θ_{23} Octant

Current experimental results indicate that $\sin^2 2\theta_{23}$ is near maximal ($\sin^2 \theta_{23} = 0.95 \pm 0.02$ [15]), however there exist two solutions of θ_{23} for a given set of measured oscillation parameters, known as the θ_{23} *octant ambiguity*. If the oscillation associated with ν_μ disappearance is not maximal, then it will be important to determine whether θ_{23} is greater than or less than $\pi/4$. This in turn will help show whether the third neutrino mass eigenstate couples more strongly to ν_μ or ν_τ. The value of θ_{23} varies the $\nu_\mu \rightarrow \nu_e$ appearance spectrum as shown in Figure 6–23. The impact of the θ_{23} octant in the energy regions around the second oscillation maximum is very small compared to the effect of δ_{cp} – which is much larger at lower energies – and is the same for neutrinos and antineutrinos, which helps to resolve the degeneracy with the mass hierarchy and δ_{cp} in the region of the first oscillation maximum.

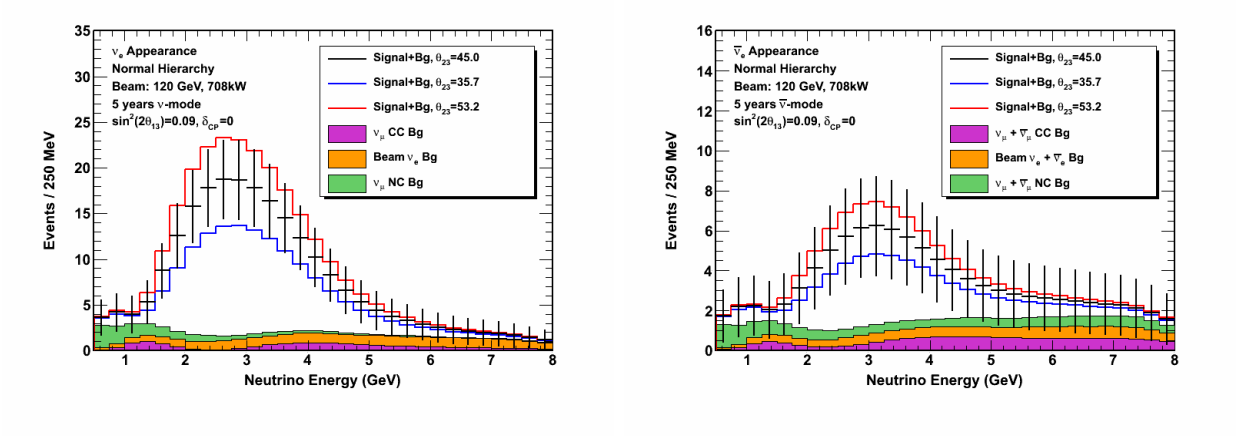

Figure 6–23: The expected spectrum of ν_e or $\overline{\nu}_e$ oscillation events in a 10 kton LArTPC for 5 years of neutrino (left) and antineutrino (right) running with a 708-kW beam, assuming normal hierarchy, $\sin^2(2\theta_{13}) = 0.09, \delta_{cp} = 0$ and varying the value of θ_{23} within the current range of allowed values. Backgrounds are displayed as stacked histograms.

Figure 6–24 displays the capability of LBNE to resolve the θ_{23} octant with a 34-kton LAr-FD running in a 708-kW beam for 10 years or a 10-kton detector running in a 2.3-MW beam for 10 years. The exposure (detector mass $\times$ beam power) assumed for this study is triple that of the LBNE Project design. For the current best-fit value of $\sin^2 2\theta_{13} = 0.09$, tripling the exposure of LBNE will resolve the θ_{23} octant degeneracy for θ_{23} values less than 41° or greater than 49° at 90% C.L. for 90% of δ_{CP} values. Further improvements in the resolving power of LBNE could be achieved by optimizing the target and focusing in order to produce a greater neutrino flux at lower energies to break degeneracies with δ_{cp} values.

6.2.6 Searches for New Physics in Long-baseline Oscillations

In addition to precision measurements of the standard three-flavor neutrino-oscillation parameters, the design of LBNE provides the best potential for discoveries of physics beyond the standard three-flavor oscillation model. This section discusses some examples of new physics that the LBNE design is well suited to pursue. It is to be noted that to fully exploit the sensitivity of the LBNE design to new physics will require higher precision predictions of the unoscillated neutrino flux at the Far Detector and larger exposures (detector mass $\times$ beam power) than currently proposed.

6.2.6.1 Non-standard Interactions

NC non-standard interactions (NSI) can be understood as non-standard matter effects that are visible only in a Far Detector at a sufficiently long baseline. LBNE has a unique advantage

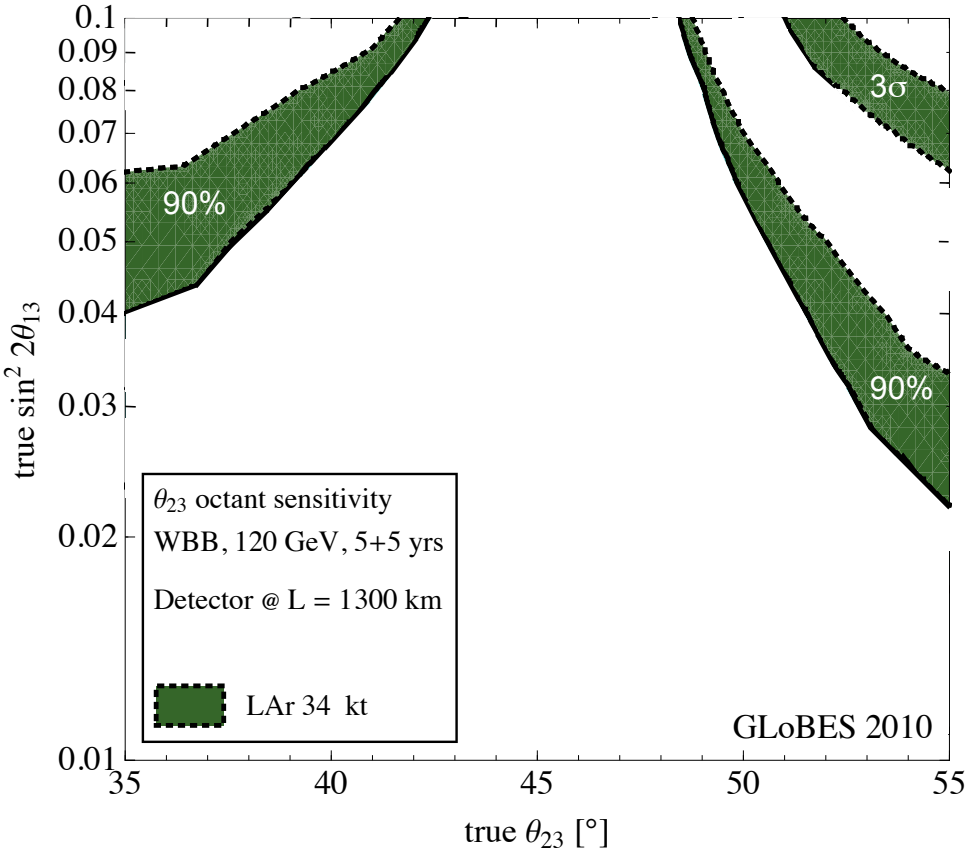

Figure 6–24: Sensitivity of LBNE to resolve the θ_{23} octant degeneracy for 5+5 years of ν+$\bar{\nu}$ running at 700 kW and normal mass hierarchy. The green band shows the results for 34 kton LAr. The width of the bands corresponds to the impact of different true values for δ_{CP}, ranging from a 10% to 90% fraction of δ_{CP}. In the region above the bands, the determination of the θ_{23} octant is possible at 90% CL (lower bands) and 3σ (upper bands).

in this area compared to other long-baseline experiments (except atmospheric-neutrino experiments, which are, however, limited by systematic effects). NC NSI can be parameterized as new contributions to the MSW matrix in the neutrino-propagation Hamiltonian:

$$H = U \begin{pmatrix} 0 & & \\ & \Delta m^2_{21}/2E & \\ & & \Delta m^2_{31}/2E \end{pmatrix} U^\dagger + \tilde{V}_{\rm MSW}\,, \tag{6.1}$$

with

$$\tilde{V}_{\rm MSW} = \sqrt{2} G_F N_e \begin{pmatrix} 1+\epsilon^m_{ee} & \epsilon^m_{e\mu} & \epsilon^m_{e\tau} \\ \epsilon^{m*}_{e\mu} & \epsilon^m_{\mu\mu} & \epsilon^m_{\mu\tau} \\ \epsilon^{m*}_{e\tau} & \epsilon^{m*}_{\mu\tau} & \epsilon^m_{\tau\tau} \end{pmatrix} \tag{6.2}$$

Here, U is the leptonic mixing matrix, and the ϵ-parameters give the magnitude of the NSI

relative to standard weak interactions. For new physics scales of few $\times$ 100 GeV, $|\epsilon| \lesssim 0.01$ is expected.

To assess the sensitivity of LBNE to NC NSI, the NSI discovery reach is defined in the following way: After simulating the expected event spectra, assuming given "true" values for the NSI parameters, one attempts a fit assuming no NSI. If the fit is incompatible with the simulated data at a given confidence level, one would say that the chosen "true" values of the NSI parameters are within the experimental discovery reach. Figure 6–25 shows the NSI discovery reach of LBNE for the case where only one of the $\epsilon^m_{\alpha\beta}$ parameters at a time is non-negligible [40]. This calculation assumed a Far Detector mass of 34 kton. With the smaller 10-kton detector, the limits will be less sensitive. Scaling roughly by the expected statistics, LBNE with a 10 kton detector can produce competitive model-independent bounds on NSI in the e–μ sector and significantly improve the bounds in the e–τ sectors by a factor of 2 or 3.

6.2.6.2 Long-range Interactions

The small scale of neutrino-mass differences implies that minute differences in the interactions of neutrinos and antineutrinos with background sources can be detected through perturbations to the time evolution of the flavor eigenstates. The longer the experimental baseline, the higher the sensitivity to a new long-distance potential acting on neutrinos. For example, some of the models for such long-range interactions (LRI) as described in [43] (see Figure 6–26) could contain discrete symmetries that stabilize the proton and a dark matter particle and thus provide new connections between neutrino, proton decay and dark matter experiments. The longer baseline of LBNE improves the sensitivity to LRI beyond that possible by the current generation of long-baseline neutrino experiments. The sensitivity will be determined by the amount of $\nu_\mu/\bar{\nu_\mu}$ CC statistics accumulated and the accuracy with which the unoscillated and oscillated ν_μ spectra can be determined. Studies are underway to estimate the sensitivity of the LBNE project to long-range interactions.

6.2.6.3 Search for Active-sterile Neutrino Mixing

Searches for evidence of active-sterile neutrino mixing at LBNE can be conducted by examining the NC event rate at the Far Detector and comparing it to a precision estimate of the expected rate extrapolated from ν_μ flux measurements from the Near Detector Complex and beam and detector simulations. Observed deficits in the NC rate could be evidence for active-sterile neutrino mixing. The latest such search in a long-baseline experiment was conducted by the MINOS experiment [44]. The expected rate of NC interactions with visible energy > 0.5 GeV in LBNE is approximately 1,000 events over five years (see Table 6–2) in the LE beam tune and 3,000 events over five years in the ME beam tune. The NC identification efficiency is high, with a low rate of ν_μ CC background misidentification as shown

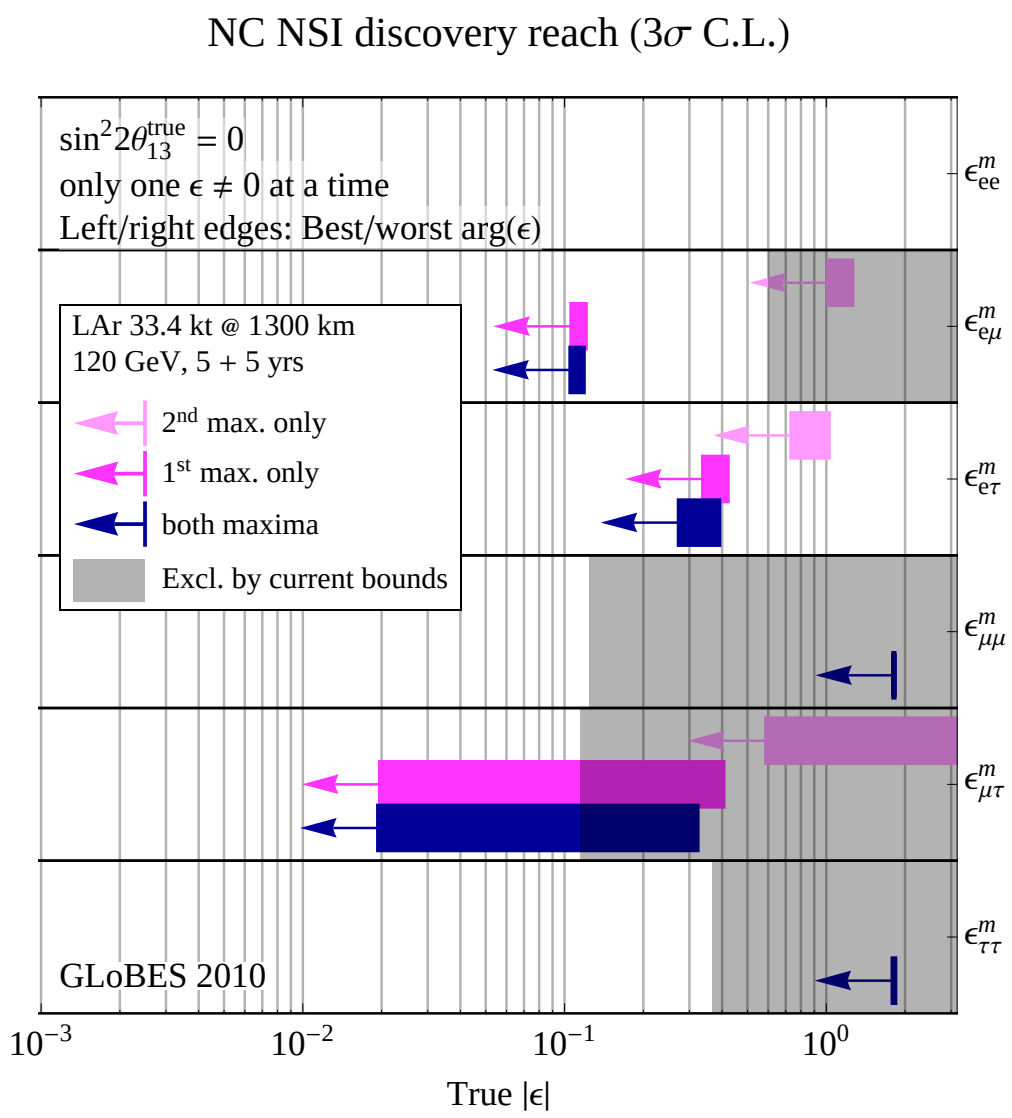

Figure 6–25: Non-standard interaction discovery reach in LBNE with a 34 kton LAr-TPC. The left and right edges of the error bars correspond to the most favorable and the most unfavorable values for the complex phase of the respective NSI parameters. The gray shaded regions indicate the current model-independent limits on the different parameters at 3 σ [41] and [42].For this study the value of $\sin^2 2\theta_{13}$ was assumed to be 0.

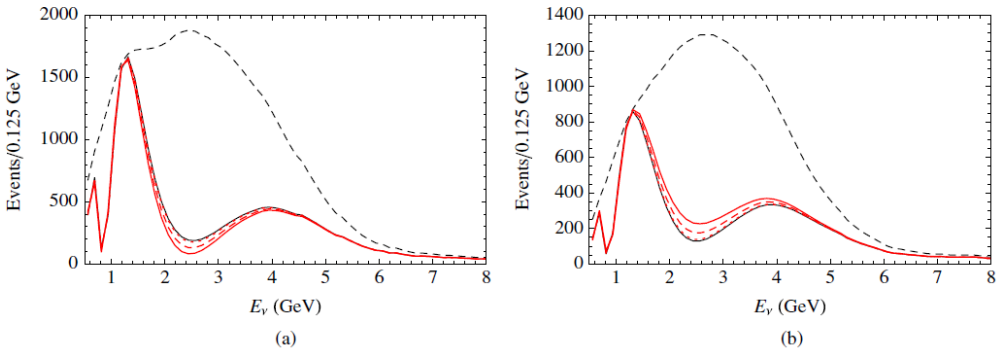

Figure 6–26: Long-range Interactions in LBNE. The number of (a) neutrino and (b) antineutrino events versus E_ν, in a long-baseline experiment with a 1,300-km baseline. The unoscillated case (top black dashed curves) and the case of no new physics (thin black solid curves) are displayed, as well as the cases with $\alpha' = 1.0, 0.5, 0.1 \times 10^{-52}$ corresponding to thick solid, dashed, and dotted curves, respectively. α' is the "fine structure constant" of such interactions which is constrained to be $\alpha' \leq 10^{-47}$ [43].

in Table 6–5. LBNE will provide a unique opportunity to revisit this search with higher precision over a large range of neutrino energies and a longer baseline.

6.2.7 Summary of Accelerator-based Long-Baseline Neutrino Oscillation Measurements

The primary scientific objectives of the LBNE Project are the following:

1. precision measurements of the parameters that govern $\nu_\mu \rightarrow \nu_e$ oscillations, including precision measurements of θ_{13}, measurement of the CP-violating phase δ_{CP} and determination of the mass ordering (the sign of Δm^2_{32})
2. precision measurements of θ_{23} and $|\Delta m^2_{32}|$ in the ν_μ-disappearance channel

Table 6–8 summarizes the expected sensitivity of the LBNE Project to CP-violation in the lepton sector and the neutrino mass ordering and the precision with which θ_{23} and $|\Delta m^2_{32}|$ can be measured. LBNE will significantly improve the sensitivity to CP violation in the neutrino sector beyond that possible by the current generation of experiments (T2K, NOνA). The longer baseline of LBNE will allow an unambiguous determination of the neutrino mass ordering with a $\geq 3\sigma$ significance over 75% of δ_{cp} values. In the small parameter space where CP violating effects and the mass hierarchy are difficult to disentangle in LBNE ($\sim \delta_{cp} = \pi/2(-\pi/2)$ for normal (inverted) hierarchy), combining the measurements of LBNE with the data accumulated by the NOνA and T2K experiment will resolve the degeneracy. LBNE will produce the most competitive measurement of the value of $\sin^2 2\theta_{13}$ from a

$\nu_\mu \rightarrow \nu_e$ appearance experiment with a precision comparable to that of the current generation of reactor experiments which measure the parameter using $\bar{\nu_e}$ disappearance. Measurements of θ_{13} with similar precision in both accelerator and reactor experiments over-constrains the three-flavor neutrino oscillation model. LBNE will also measure θ_{23} and $|\Delta m^2_{32}|$ in the ν_μ-disappearance channel with a precision of 1-2% - assuming the unoscillated ν_μ flux can be estimated with an accuracy of 10%. The accuracy of these measurements is comparable to the accuracy expected from the current generation experiments with much shorter baselines. Comparison of oscillation parameter measurements over different baselines will improve sensitivity to new physics that manifests through matter interactions of neutrinos.

The fundamental design of LBNE, with an optimal baseline, a wide-band tunable beam and a high-precision Far Detector, provides a platform for expanding this program in subsequent phases to enable a truly comprehensive investigation of neutrino-oscillation phenomena, which will provide the best potential for discoveries of physics beyond the three-flavor oscillation model. Increasing the detector mass to 34 kton or more, as is allowed by the scalable design of the Far Detector, and increasing the beam power to at least 2.3 MW, as is allowed by the LBNE beam design, will allow full exploitation of this potential.

Table 6–8: Summary of LBNE accelerator-based neutrino oscillation measurements with a 10 kton LAr-FD, running for 5+5 $(\nu + \bar{\nu})$ years in a 708 kW beam. The results summarized here are obtained using the detector performance assumptions listed in the third column of Table 6–5. The mass hierarchy and CP violation sensitivities listed correspond to $\sin^2 2\theta_{13} = 0.092$.

Measurement	Precision
Mass Hierarchy (LBNE 10 kton only)	$> 3\sigma$ for 75% of δ_{cp} values
Mass Hierarchy (with T2K)	$> 3.5\sigma$ all phase space
CP violation (LBNE 10 kton only)	$> 2.5\sigma$ for 25% of δ_{cp} values
CP violation (with T2K/NoνA)	$> 3\sigma$ for 40% of δ_{cp} values
δ_{cp} resolution (with external θ_{13} constraint)	$21^\circ(\delta_{cp} = 0),\ 35^\circ(\delta_{cp} = 90^\circ)$
$\sin^2 2\theta_{13}$ resolution	0.01
$\lvert\Delta m^2_{31}\rvert$ resolution	$0.024(\nu),\ 0.034(\bar{\nu}) \times 10^{-3}\mathrm{eV}^2$
θ_{23} resolution	$0.7^\circ(\nu), 1.0^\circ(\bar{\nu})$

6.3 Non-Accelerator Physics that would be Enabled by an Underground Far Detector

A 10 kiloton-scale LArTPC sited deep underground would offer significant opportunities for addressing physics topics inaccessible for a surface detector, such as proton decay, and atmospheric and supernova neutrinos. LArTPC capabilities are described in detail in reference [1]. The expected performance of the LBNE LAr-FD design would enable a substantially expanded scientific program should it become possible to place it deep underground, either by obtaining external resources beyond those assumed in the current LBNE Project, or in a later phase of the LBNE program.

No external trigger would be available for non-beam physics, therefore, assuming that suitable triggering can be implemented, selection of signal from background becomes a key issue. The photon-detection system included in the LAr-FD design, which detects scintillation light produced by ionizing events, will be a key element of the trigger for non-beam events. Since backgrounds are dominated by cosmic rays, physics reach for a given detector size depends primarily on depth. Table 6–9 summarizes expected signal rates. Proton decay and atmospheric neutrino events are, like beam events, ∼GeV scale, and should in principle be quite cleanly identifiable in an LArTPC; see Figures 6–27 and 6–28. Proton-decay events, although distinctive, would be extremely rare, and hence highly intolerant of background; in contrast, atmospheric neutrinos (which are background for proton decay) have a higher rate and could tolerate some background. The signatures of individual supernova-burst neutrino interaction events are much less clean. With only a few tens of MeV of energy, these neutrinos will create small tracks involving only a few adjacent wires; see Figure 6–29. For diffuse "relic" supernova events which arrive singly, the very low expected signal rate makes their selection overwhelmingly difficult, and they are not considered further here. A nearby core collapse is more promising; it will provide a pulse of low-energy events all arriving within ∼30 seconds, so that LBNE can hope to make a meaningful measurement of signal over a (well-known) background.

Table 6–9: Expected signal rates of non-beam processes whose detection would be enabled by placing the LBNE Far Detector underground. The supernova-burst event rate is the average over the ≈ 30second interval of the occurrence for a supernova at 10 kpc.

Physics	Energy range	Expected signal rate (events kton^{-1}s^{-1})
Proton decay	$\sim$ GeV	$< 2 \times 10^{-9}$
Atmospheric neutrinos	$0.1 - 10$ GeV	$\sim 10^{-5}$
Supernova burst neutrinos	few-50 MeV	~ 3
Diffuse supernova neutrinos	20-50 MeV	$< 2 \times 10^{-9}$

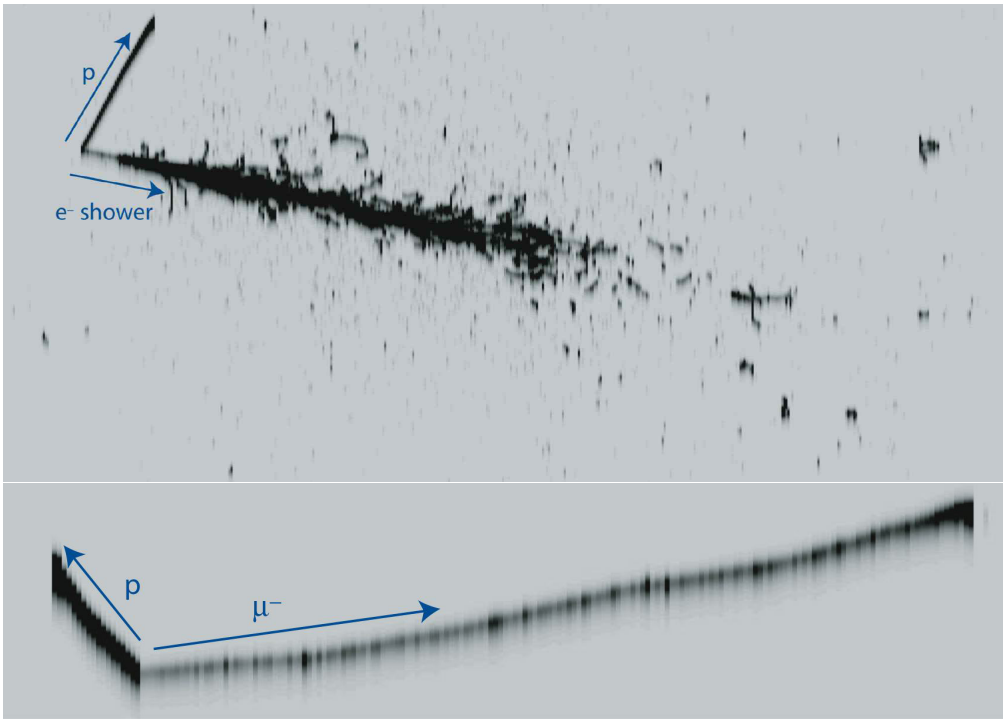

Figure 6–27: Simulated ν_e and ν_μ CC atmospheric neutrino events in liquid argon from reference [45].

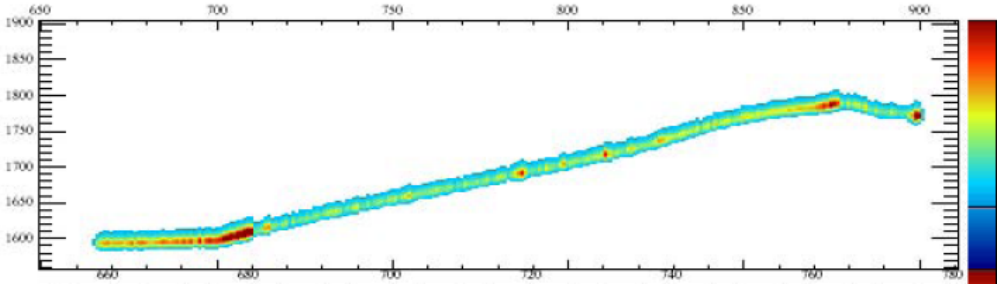

Figure 6–28: LArSoft simulation of $p \to K^+\bar{\nu}$ decay with $K^+ \to \mu^+ \to e^+$ in the MicroBooNE geometry. The drift time is along the vertical axis. The wire number is along the horizontal axis (3-mm wire spacing). The color indicates amount of charge deposited (red is larger, blue smaller).

The physics reach will be considered as a function of detector mass and depth for proton decay, supernova bursts and atmospheric neutrinos. (Solar neutrinos will not be considered; with mostly <10 MeV energies, they require stringent control of background. Other than providing a ν_e calibration in argon for supernova neutrinos, they are not likely to indicate anything not already known in the detectors under consideration.)

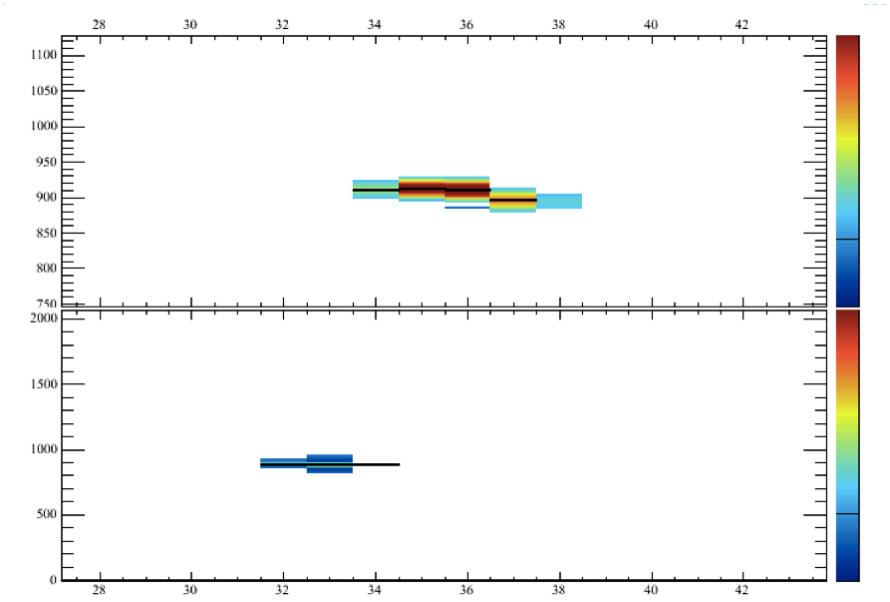

Figure 6–29: LArSoft simulation of a 10 MeV electron (which would resemble a supernova-neutrino event) in the MicroBooNE geometry (3-mm wire spacing). There are four reconstructed hits (black bands) on five adjacent wires. This event would create signals on about four wires with 5-mm spacing. The drift time is on the vertical axis, and the wire number is on the horizontal axis.

6.3.1 Searches for Baryon Number Non-conservation

Searches for baryon-number-violating processes are highly motivated by grand unified theories. Even a single event could be evidence of physics beyond the Standard Model. Current limits are dominated by Super–Kamiokande [46]; however for some predicted modes, most prominently $p \to K^+\bar{\nu}$, efficiency for water Cherenkov detectors is low, and detectors that can cleanly reconstruct kaon decay products have a substantial efficiency advantage. Other modes for which LArTPCs have an edge include $n \to e^- K^+$ and $p \to e^+\gamma$. Figure 6–30 shows the expected limit as a function of time for $p \to K^+\bar{\nu}$. According to this plot, approximately 10 kton of LAr is required to improve the limits significantly beyond continued Super–Kamiokande running.

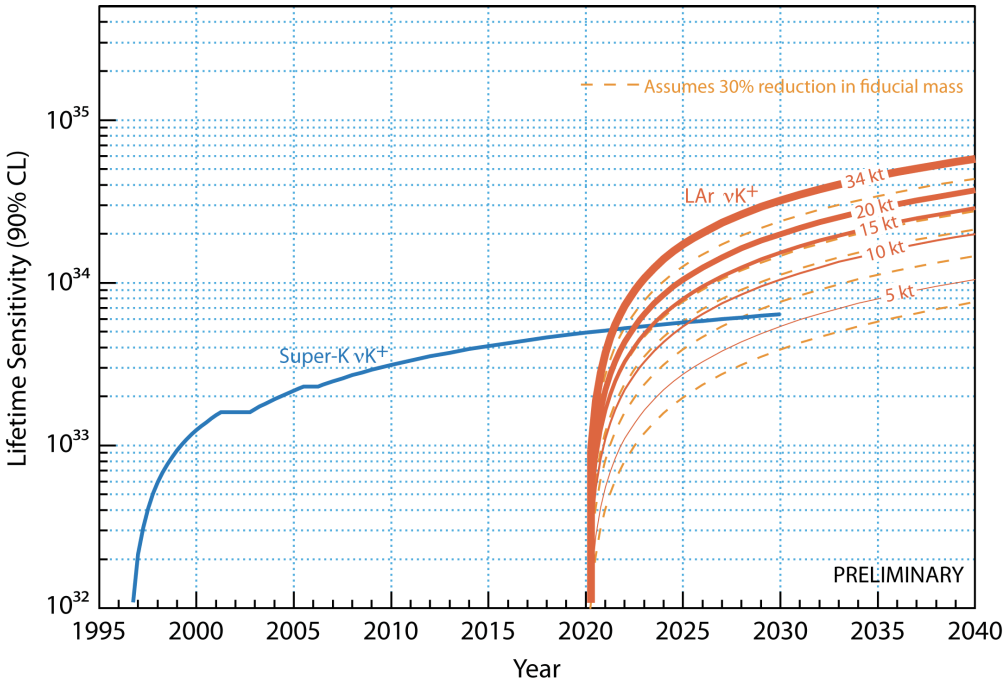

Figure 6–30: Proton decay lifetime limit for $p \to K^+\bar{\nu}$ as a function of time for Super–Kamiokande compared to different LAr masses at the 4850 level SURF starting in 2020. The dashed lines show the effect of a 30% reduction of fiducial mass, conservatively assumed for a shallower depth of 2300 feet. The limits are at 90% C.L., calculated for a Poisson process including background assuming that the detected events equal the expected background. (Figure from J. Raaf.)

In LAr, the most pernicious background for proton decay with kaon final states comes from cosmic rays that produce entering kaons in photonuclear interactions in the rock near the detector. Backgrounds as a function of depth have been studied for LAr in references [45,12,47]. These studies show that proton decay searches can be successful at moderate depth at the expense of a reduction of fiducial mass or in conjunction with a high-quality veto, but cannot be done at the surface. The 4850L at SURF would be an excellent location and would not

require an external veto system.

6.3.2 Atmospheric Neutrinos

Atmospheric neutrinos are unique among sources used to study oscillations: the oscillated flux contains neutrinos and antineutrinos of all flavors, and matter effects play a significant role. The expected interaction rate is about 285 events per kiloton-year. The excellent CC/NC separation and the ability to fully reconstruct the hadronic final state in CC interactions in an LArTPC would enable the atmospheric neutrino 4-momentum to be fully reconstructed. This would enable a higher-resolution measurement of L/E to be extracted from atmospheric-neutrino events in an LArTPC compared to the measurements obtained from Super–Kamiokande, and would provide good sensitivity to mass hierarchy and to the octant of θ_{23}. Since the oscillation phenomenology plays out over several decades in energy and path length, atmospheric neutrinos are very sensitive to alternative explanations or subdominant new physics effects that predict something other than the characteristic L/E dependence predicted by oscillations in the presence of matter.

Because atmospheric neutrinos are somewhat more tolerant of background than proton decay, a depth that is sufficient for a proton decay search should also be suitable for atmospheric neutrinos. For the SURF 4850L depth, a veto should not be necessary, and one can assume full fiducial mass; at depths around 2,700 feet, a one-meter fiducial cut should be adequate. Figure 6–31 shows expected sensitivity to mass hierarchy; for ten years of running, even a 10-kton detector would add to world knowledge.

6.3.3 Core-Collapse Supernova Neutrinos

A nearby core-collapse supernova will provide a wealth of information via its neutrino signal (see [48,49] for reviews). The neutrinos are emitted in a burst of a few tens of seconds duration. Energies are in the few tens of MeV range, and luminosity is divided roughly equally between flavors. Ability to measure and tag the different flavor components of the spectrum is essential for extraction of physics and astrophysics from the signal. Currently, world-wide sensitivity is primarily to electron anti-neutrinos, via inverse beta decay on free protons, which dominates the interaction rate in water and liquid-scintillator detectors. LAr has a unique sensitivity to the *electron neutrino* component of the flux, via the absorption interaction on ^{40}Ar, $\nu_e + {}^{40}\mathrm{Ar} \rightarrow e^- + {}^{40}\mathrm{K}^*$. In principle, this interaction can be tagged via the de-excitation gamma cascade. About 900 events would be expected in the 10-kton fiducial mass of the LAr-FD for a supernova at 10 kpc; the number of signal events scales with mass and the inverse square of distance as shown in Figure 6–32. For a collapse in the Andromeda galaxy, a 34-kton detector would expect about one event. This sensitivity would be lost for the smaller 10-kton detector. However the 10-kton detector would gather a unique ν_e signal from within the Milky Way.

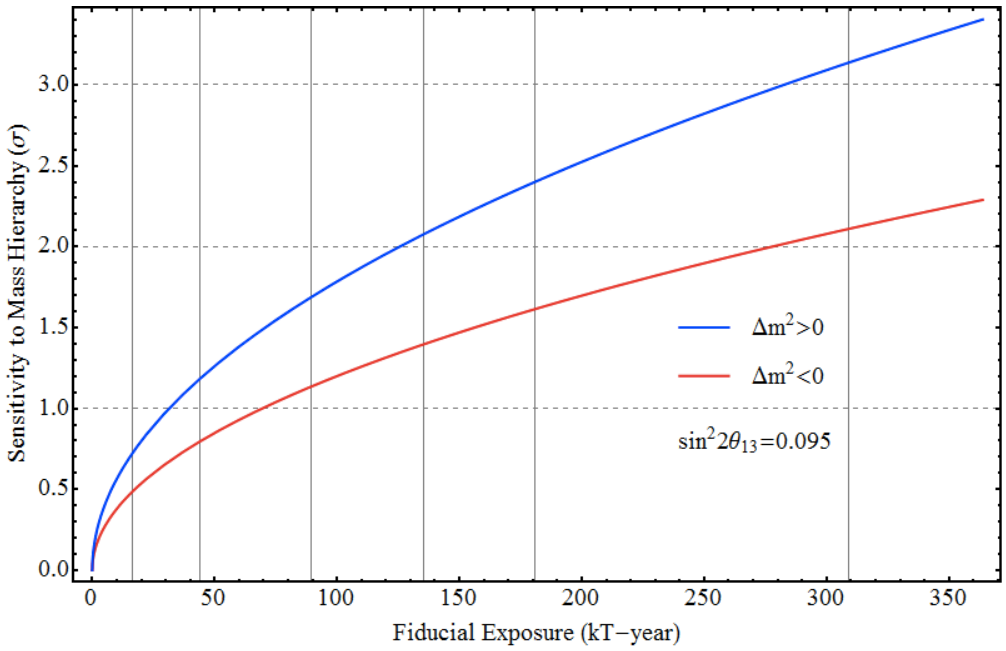

Figure 6–31: Sensitivity to mass hierarchy using atmospheric neutrinos as a function of fiducial exposure in a LAr detector. (Figure from H. Gallagher, J. Coelho, A. Blake.)

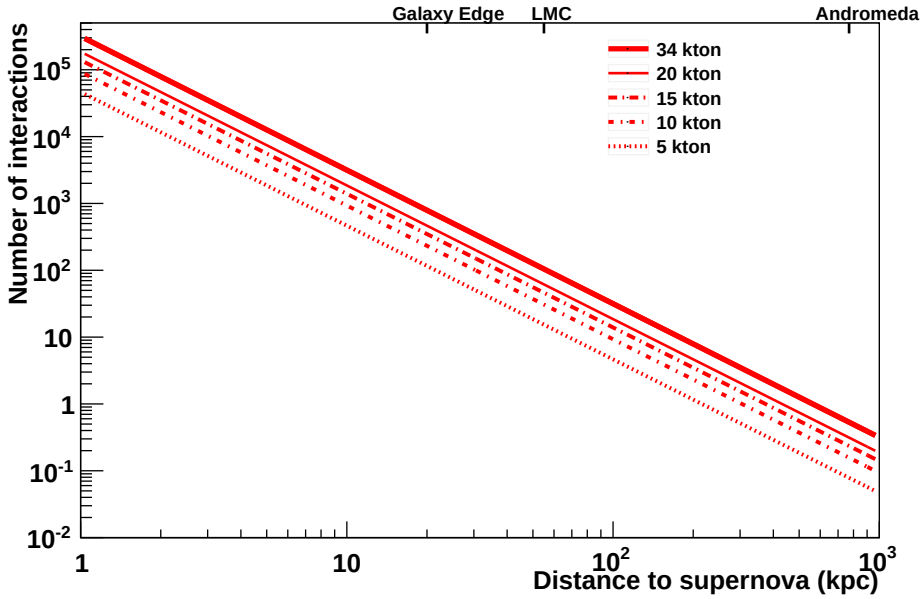

Figure 6–32: Number of supernova neutrino interactions in an LAr detector as a function of distance to the supernova, for different detector masses. Core collapses are expected to occur a few times per century, at a most-likely distance of about 10–15 kpc.

As noted above, due to their low energy, supernova events are subject to background, although the short-timescale-burst nature of the signal means that the background can be well known and subtracted. Muons and their associated Michel electrons can in principle be removed. Radioactive decays, including cosmogenic spallation products, tend to make <10 MeV signals. They lie below the main supernova signal range, but inhabit a potential region of interest for physics signatures. Preliminary studies from reference [37], extended for cosmic-ray rates on the surface, suggest that while the 4850L depth is acceptable, the surface cosmic-ray-associated signal rates are daunting. It will require at least a few orders of magnitude of background rejection to pull the signal from background. While more work needs to be done to determine the extent to which the background can be mitigated, a surface option is highly unfavorable for supernova-neutrino physics.

6.3.4 Summary

Although more work needs to be done to understand backgrounds at shallow depth, the following findings are fairly robust:

- Proton decay capabilities as a function of depth are quite well documented, and a search at the surface seems impossible. A detector mass of at least 10 kton would be needed for competitiveness.
- For atmospheric neutrinos, less is known about signal selection on the surface; however separation of signal is probably extremely difficult. The 4850L depth at SURF is highly acceptable. Underground, a 20-kton detector would be needed for competitiveness, although a 10-kton detector could still provide useful information.
- For supernova-burst neutrinos, selection of signal events over background at the surface will be a daunting task, and information will be highly degraded even in the best case. The 4850L depth at SURF is acceptable. More mass is always better, but even a 5-kton detector would provide a unique ν_e-flavor supernova signal.

In summary, a reasonably-sized LAr detector $\geq$ 10 kton sited at the 4850L at SURF would provide excellent opportunities for a diverse range of physics topics. At the current shallow location for the LBNE LAr-FD, capabilities for non-beam physics are extremely poor.

7 Supporting Documents

Additional information related to the CDR is available in a set of supporting documents. Detailed information on risk analysis and mitigation, value engineering, ES&H, costing, project management and other topics not directly in the design scope can be found in these documents, listed in Table 7–1. Each document is numbered and stored in LBNE's document database, accessible via a username/password combination provided by the Project. Project documents stored in this database are made available to internal and external review committees through Web sites developed to support individual reviews.

Table 7–1: LBNE CD-1 Documents

Title	**LBNE Doc Number(s)**
Alternatives Analysis	4382
Case Study Report; Liquid Argon TPC Detector	3600
Configuration Management Plan	5452
DOE Acquisition Strategy for LBNE	5442
DOE Preliminary Project Execution Plan	5443
Integrated Environment, Safety and Health Management Plan	4514
LAr-FD Preliminary ODH Analysis	2478
LBNE Reconfiguration Final Report	Linked from LBNE web site (lbne.fnal.gov) under "Reports and Documents"
Global Science Objectives, Science Requirements and Traceback Reports	4772
Muon-induced Background for Beam Neutrinos on the Surface	6159
Parameter Tables, Far Detector	3383
Preliminary Hazard Analysis Report	4513
Preliminary Security Vulnerability Assessment Report	4826

Procurement Plan	5329
Project Management Plan	2453
Project Organization Chart	5449
Quality Assurance Plan	2449
Report on the Depth Requirements for a Massive Detector at Homestake	0034
Requirements, Beamline	4835
Requirements, Far Detector	3747
Requirements, Far Site Conventional Facilities	4958
Requirements, Near Detectors	5579
Requirements, Near Site Conventional Facilities	5437
Risk Management Plan	5749
The Science and Strategy for a Long-Baseline Neutrino Experiment Near Detector	8625
Value Engineering Report	3082
Work Breakdown Structure (WBS)	4219

References

[1] T. Akiri *et al.*, "The 2010 Interim Report of the Long Baseline Neutrino Experiment Collaboration Physics Working Groups." arXiv:1110.6249.

[2] Y. K. Kim *et al.*, "LBNE Reconfiguration: Steering Committee Report," 2012. `http://www.fnal.gov/directorate/lbne_reconfiguration/index.shtml`.

[3] R. N. Mohapatra *et al.*, "Theory of Neutrinos: A White Paper," 2005. arXiv:hep-ph/0510213v2.

[4] F. An *et al.*, "Observation of electron-antineutrino disappearance at Daya Bay," *Phys.Rev.Lett.*, vol. 108, p. 171803, 2012. arXiv:1203.1669 [hep-ex].

[5] Particle Physics Project Prioritization Panel, "US Particle Physics: Scientific Opportunities; A Strategic Plan for the Next Ten Years," 2008. `http://science.energy.gov/~/media/hep/pdf/files/pdfs/p5_report_06022008.pdf`.

[6] DOE Office of High Energy Physics, "Mission Need Statement for a Long-Baseline Neutrino Experiment (LBNE)," tech. rep., DOE, 2009. LBNE-doc-6259.

[7] J. Appel *et al.*, "Physics Working Group Report to the LBNE Reconfiguration Steering Committee," 2012. `http://www.fnal.gov/directorate/lbne_reconfiguration/files/LBNE-Reconfiguration-PhysicsWG-Report-August2012.pdf`.

[8] LBNE Project Office, "LBNE Project Management Plan," tech. rep., FNAL, 2011. LBNE Doc 2453.

[9] LBNE Project Office, "Physics Research Goals before Reconfiguration," tech. rep., FNAL, 2012. LBNE Doc 3056v5.

[10] LBNE Science Collaboration, "LBNE Case Study Report, Liquid Argon TPC Far Detector, Draft Version 1.2," 2011.

[11] LBNE Project Office, "Key Assumptions: Physics Research Goals of the LBNE Project," tech. rep., FNAL, 2010. LBNE Doc 3056v1.

[12] A. Bernstein *et al.*, "Report on the Depth Requirements for a Massive Detector at Homestake (LBNE:DocDB-34)," 2009. arXiv:0907.4183 [hep-ex].

[13] T. Katori, "MicroBooNE, A Liquid Argon Time Projection Chamber (LArTPC) Neutrino Experiment." arXiv:1107.5112 [hep-ex], 2011.

[14] J. Beringer *et al.*, "Review of Particle Physics," *Phys.Rev.D.*, vol. 86, p. 010001, 2012.

[15] G. Fogli *et al.*, "Global analysis of neutrino masses, mixings and phases: entering the era of leptonic CP violation searches," *Phys.Rev.D.*, vol. 86, p. 013012, 2012.

[16] S. Agostinelli *et al.*, "GEANT4 — A Simulation Toolkit," *Nucl. Instrum. Methods*, vol. A, no. 506, pp. 250–303, 2003.

[17] M.Bishai *et al.*, "The Science and Strategy for a Long-Baseline Neutrino Experiment," 2012. `http://www.fnal.gov/directorate/lbne_reconfiguration/index.shtml`.

[18] P. Adamson *et al.*, "Improved search for muon-neutrino to electron-neutrino oscillations in MINOS," *Phys. Rev. D.*, vol. 77, p. 072002, 2008.

[19] `http://www-boone.fnal.gov/`.

[20] L. Loiacono, *Measurement of the muon neutrino inclusive charged current cross section on iron using the MINOS detector*. PhD thesis, University of Texas, Austin, 2010.

[21] B. Osmanov, "MINERvA Detector: Description and Performance." arXiv:1109.2855 [hep-ex], 2011.

[22] A. Ferrari *et al.*, "FLUKA: a multi-particle transport code," 2005.

[23] G. Battistoni *et al.*, "The FLUKA code: Description and benchmarking," *AIP Conference Proceeding*, vol. 896, p. 31, 2007.

[24] M. Makariev, "Pion production in p + C collisions at 158-GeV/c beam momentum.," *AIP Conf.Proc.*, vol. 899, p. 203, 2007.

[25] N. Abgrall *et al.*, "Measurements of Cross Sections and Charged Pion Spectra in Proton-Carbon Interactions at 31 GeV/c," *Phys.Rev.*, vol. C84, p. 034604, 2011.

[26] R. Raja, "The main injector particle production experiment (MIPP) at Fermilab," *Nucl. Instrum. Meth.*, vol. A553, pp. 225–230, 2005.

[27] S. Kopp *et al.*, "Secondary beam monitors for the NuMI facility at FNAL," *Nucl. Instrum. Meth. A*, vol. 568, p. 503, 2006.

[28] The LArSoft Collaboration. `https://plone4.fnal.gov:4430/P1/Main/wiki/LArSoft/LArSoft`.

[29] T2K Collaboration, "Proposal to Extend T2K with a detector 2km Away from the JPARC Neutrino Source," 2007. `http://neutrino.cgi.phy.duke.edu/2km/wiki/index.cgi/`.

[30] "A Large Liquid Argon Time Projection Chamber for Long-baseline Off-Axis Neutrino Oscillation Physics with the NuMI Beam," tech. rep., 2005. Submitted to the NuSAG committee; inspirehep.net FERMILAB-FN-0776-E.

[31] B. Baller *et al.* tech. rep. LBNE-doc-266-v1, LBNE-doc-3414-v2.

[32] J. Raaf *et al.*, "LAr Hand Scan," tech. rep., FNAL, IMsA, 2012. LBNE-doc-5446.

[33] `http://icarus.lngs.infn.it/`.

[34] P. Adamson *et al.*, "Improved search for muon-neutrino to electron-neutrino oscillations in MINOS," *Phys. Rev. Lett.*, vol. 107, p. 181802, 2011.

[35] S.Amoruso *et al. Eur. Phys. J.*, vol. C33, p. 233, 2004.

[36] A. Ankowski *et al.*, "Measurement of through-going particle momentum by means of multiple scattering with the icarus t600 tpc.," *Eur. Phys. J.*, vol. C48, p. 667, 2006.

[37] D. Barker *et al.*, "Muon-induced background for beam neutrinos at the surface," 2012. LBNE-doc-6232.

[38] W. A. Mann *et al.*, "Apparent multiple Δm^2_{32} in muon anti-neutrino and muon neutrino survival oscillations from non-standard interaction matter effect," *Phys. Rev. D.*, vol. 82, p. 113010, 2010.

[39] U. Kose, "Search for $\nu_\mu \to \nu_\tau$ oscillations in appearance mode in the OPERA experiment.." arXiv:1106.3871 [hep-ex], 2011.

[40] P. Huber and J. Kopp, "Two experiments for the price of one? The role of the second oscillation maximum in long baseline neutrino experiments." arXiv:1010.3706, 2011.

[41] S. Davidson, C. Pena-Garay, N. Rius, and A. Santamaria hep-ph/0302093, 2003.

[42] M.C. Gonzalez-Garcia, and M. Maltoni, "Phenomenology with Massive Neutrinos," *Phys. Rept.*, vol. 460, p. 1, 2008. arXiv:0704.1800 [hep-ph].

[43] H. Davoudiasl *et al.*, "Long-Range Lepton Flavor Interactions and Neutrino Oscillations.," *Phys. Rev. D.*, vol. 84, p. 013009, 2011. arXiv:1102.5352 [hep-ph].

[44] P. Adamson *et al.*, "Search for sterile neutrino mixing in the MINOS long baseline experiment," *Phys. Rev. D.*, vol. 81, p. 052004, 2010. arXiv:1001.0336 [hep-ex].

[45] A. Bueno, A. J. Melgarejo, S. Navas, Z. D. ai, Y. Ge, M. Laffranchi, A. M. Meregaglia, and A. Rubbia, "Nucleon decay searches with large liquid Argon TPC detectors at shallow depths: atmospheric neutrinos and cosmogenic backgrounds," *Journal of High Energy Physics*, vol. 2007, no. 04, p. 041, 2007.

[46] H. Nishino, S. Clark, *et al.*, "Search for Proton Decay via $p \to e^+\pi^0$ and $p \to \mu^+\pi^0$ in a Large Water Cherenkov Detector," *Phys. Rev. Lett.*, no. 102:141801, 2009. arXiv:0903.0676 [hep-ex].

[47] V. Kudryavtsev *et al.*, "Cosmic rays and cosmogenics. report to the lbne collaboration.," tech. rep., 2012. LBNE-doc-5904.

[48] K. Scholberg, "Supernova neutrino detection," *Nucl.Phys.Proc.Suppl.*, vol. 221, p. 248, 2011. astro-ph/0701081.

[49] A. Dighe, "Physics potential of future supernova neutrino observations," *J.Phys.Conf.Ser.*, vol. 136, p. 022041, 2008. arXiv:0809.2977 [hep-ph].